REDOX-ACTIVE CONJUGATED POLYMERS FOR ELECTROCHROMIC AND SUPERCAPACITIVE APPLICATIONS

A Dissertation
Presented to
The Academic Faculty

by

Rayford Huseyin Bulloch

In Partial Fulfillment
of the Requirements for the Degree
Doctor of Philosophy in the
School of Chemistry and Biochemistry

Georgia Institute of Technology
December 2015

REDOX-ACTIVE CONJUGATED POLYMERS FOR ELECTROCHROMIC AND SUPERCAPACITIVE APPLICATIONS

Approved by:

Dr. John R. Reynolds, Advisor
Schools of Chemistry and Biochemistry, Materials Science and Engineering
Georgia Institute of Technology

Dr. Lawrence Bottomley
School of Chemistry and Biochemistry
Georgia Institute of Technology

Dr. Jiri Janata
School of Chemistry and Biochemistry
Georgia Institute of Technology

Dr. Dong Qin
Schools Chemistry and Biochemistry, Materials Science and Engineering
Georgia Institute of Technology

Dr. Paul Russo
School of Materials Science and Engineering
Georgia Institute of Technology

Date Approved: July 29th, 2015

“We are here to help each other get through this thing, whatever it is.”

-Mark Vonnegut, via Kurt Vonnegut

“...he had a tremendous propensity for getting lost when driving. This was largely because of his "Zen" method of navigation, which was simply to find any car that looked as if it knew where it was going and follow it. The results were more often surprising than successful, but he felt it was worth it for the sake of the few occasions when it was both.”

-Douglas Adams

To Nell, Berin, the rest of my family, and Gianna.

ACKNOWLEDGEMENTS

There are, as seems to be common in this situation, quite literally too many people to reasonably thank without writing an additional dozen pages of text. Following that realization, I feel that the writing advice of Kurt Vonnegut, namely to "Pity the reader" is best applied, and I'll make an effort to keep this short not for lack of gratitude or sentimentality, but rather so as to avoid altering the table of contents listings. The following is written with no particular regard for chronology or depth of gratitude.

First, I'd like to thank Dr. Reynolds, initially for inviting me into his research group, and later for his seemingly unending patience. Much of my frustration in learning of our impending move to Georgia was not in the reality of the move itself, but rather because of the sudden realization that I didn't have the luxury of pretending to make up my mind; it was always made to stay on with the group. There is no one I would rather have worked with and for, and your commitment to your research and your students is largely to blame for my enduring gratitude.

I also would like to express my gratitude to my research advisors during my undergraduate years, Drs. Ed Hilinski and Michael Roper. The prior for showing me what I didn't want to do, and the latter for showing me what I really did want to do. I'd like to further thank Dr. Roper for encouraging my pursuit of independent research, and for (hopefully successfully) attempting to cultivate and mold me as a scientist. This simply would never have happened without your help.

Further into an academic vein, I would like to thank the many collaborators I've worked with in my time at both the University of Florida and the Georgia Institute of

Technology. One of the most reassuring aspects of pursuing an advanced degree is knowing that I myself don't have to know everything, but I should learn to find people that, collectively, do.

Having joined the Reynolds group when I did, I had the chance to interact with one of the largest pools of people the group has ever seen, and following the move to Atlanta, the smallest pool it had seen in years. I want to thank David Liu and Ken Graham especially, as well as Jared Lynch, for inviting a young, dumb kid into their home, and always being available to demonstrate just how to make it through grad school in the happiest state possible. Thank you to all the graduate students and post-doctoral researchers I've had the pleasure of working and interacting with throughout my time with the group and the following in particular: Frank Arroyave, Pengjie Shi, Egle Puodziukynaite, Leandro Estrada, Chad Amb, and finally Mike Craig for working a similarly odd set of hours and his appreciation of Lemon Jelly. I'd also like to thank the undergraduate researchers I've had the pleasure of interacting with, namely Emily Thompson, Eric Knott, Suhas Rao, Brenda Calderon, Matt Nelson, Andy Chilton and Keith Thompson. I also want to thank Drs. Aubrey Dyer and Anna Österholm, for shouldering much of the burden I would otherwise have been saddled with, making my time with the group that much more enjoyable.

Not to go unmentioned, I would like to thank Eric Shen, Coralie Richard, and Caroline Grand for making the most of a strange living situation, and helping to create a happy sanctuary so close to and yet so far from the lab. Thanks to the students and researchers joining the group following our move to Georgia Tech for accepting a group of people full of stories of people you've never met, and in particular James Ponder, Kin

Lo, and Rylan Wolfe. I also want to thank the friends I left behind in Gainesville: Mike Costanzo, Andrew Mowson, Russ Winkle, Corey Gros, Michelle Bousquet, Andrew Powers, Richard Farley and Brendan Sweeney. A man could consider himself lucky to feel at home in a single town, and through your friendship I've had two homes.

On a deeply personal level, there are a few more statements gratitude I feel I should make. Three men in particular conspired without their knowledge to steer me towards chemistry: my father, Steve, my scoutmaster Clovis Linkous, and my chemistry teacher Thomas Vaughan. Each of you shares the blame for this equally. I want to thank Justin Kerzsulis for seeming to know which way he was going, and therefore leading me in a great direction. Working alongside of him, frequently at the expense of every single person in our vicinity, is an experience I will never forget, and will always be grateful for. In a similar vein, I want to thank Amber Vercesi. You, along with Justin serve as a constant reminder that some friendships are worth any amount of effort to preserve, and that the science behind the seven-day chili dog cleanse is irrefutable. I hope it'll be many long years before we're all free of each other. I want to thank Gianna, from the bottom of my heart, for her patience, intelligence, caring, and her selfless faith in me. I'll never be able to repay you fully for those, but I would certainly like to try. Finally, I want to thank my family, and in particular my parents Steve and Fusun. Your support has been unwavering and the examples you've set have, in various circuitous ways, brought me to where I am today. If I never find any other way to repay you for those things, I'll always remember that pine is the material of choice, and encourage you to finally leave for Çeşme.

TABLE OF CONTENTS

LIST OF TABLES

LIST OF FIGURES

LIST OF EQUATIONS

LIST OF SYMBOLS AND ABBREVIATIONS

CIE	International Commission on Illumination (Commission Internationale de l'Eclairage)
CMY	Cyan-Magenta-Yellow
ECP	Electrochromic Polymer
E_g	Band Gap Energy
HOMO	Highest Occupied Molecular Orbital
LUMO	Lowest Unoccupied Molecular Orbital
PPy	Polypyrrole
PT	Polythiophene
λ_{max}	Wavelength of Maximum Absorption
EDOT	3,4-ethylenedioxythiophene
PEDOT	Poly(3,4-ethylenedioxythiophene)
NIR	Near-infrared
E_{ox}	Oxidation Potential
DOT	Dioxythiophene
D-A	Donor-Acceptor
DOP	Dioxypyrrole
MCCP	Minimally Color Changing Polymer
ECD	Electrochromic Device
UV	Ultraviolet
ITO	Indium tin oxide
EC	Electrochromic

CNT	Carbon nanotube
ECDL	Electrochemical double layer
EDLC	Electrochemical double layer capacitor
PANI	Polyaniline
PTFE	Poly(tetrafluoroethylene)
psi	pounds per square inch
PC	Propylene Carbonate
PMMA	Poly(methyl methacrylate)
$TBAPF_6$	Tetrabutylammonium Hexafluorophosphate
LiBTI	Lithium bis(trifluoromethane)sulfonamide
pTSA	p-toluenesulfonic acid
PEIE	Poly(ethylenimine ethoxylate)
PDPP3T	Poly(diketopyrrolopyrrole-terthiophene)
PCBM	Phenyl-C61-butyric acid methyl ester
PEDOT:PSS	poly(3,4-ethylenedioxythiophene):Poly(styrene sulfonate)
OPV	Organic Photovoltaic
DMSO	Dimethyl sulfoxide
ECP-M	ECP-Magenta
ECP-C	ECP-Cyan
ECP-Y	ECP-Yellow
CV	Cyclic voltammetry (voltammogram)
WE	Working Electrode
CE	Counter Electrode
RE	Reference Electrode
AU	Absorbance (Arbitrary) Units

a*	Red-Green Balance
b*	Yellow-Blue Balance
L*	White-Black Balance
PIB	Poly(isobutylene)
ASTM	American Society of Testing and Materials
AM	Air Mass
XPS	X-ray Photoelectron Spectroscopy
HKEA	Hemispherical Kinetic Energy Analyzer
UHV	Ultra-high Vacuum

SUMMARY

The study of conducting, redox-active polymers has rarely wanted for potential applications, ranging from modulation of optical properties, charge storage, drug release, and more. This subset of redox-active polymers stands in contrast with many of the oft-cited applications for conducting polymers, such as in photovoltaics and transistor technologies, in that the redox-active polymers often take on a much more dynamic or active role in the operation of a device or technology. It is notable that, if care is taken in the design of a redox-active polymer, the same materials may be utilized for both optical and charge storage applications. As a result, this dissertation primarily focuses on the application of a family of redox-active polymers in both electrochromic or charge storage devices, solution processing strategies for modulating optical properties of polymer mixtures, and the stability of these materials with regards to photo-oxidative stress.

The presentation of research in this document begins first with the application of conjugated polymers to charge storage applications. Detailed in Chapter 3, a water-processable polymer with a broad electroactive window resembling that of PEDOT is used to modify a non-woven CNT textile via drop casting. Cyclic voltammetry was used to probe supercapacitor devices fabricated using the hybrid CNT-conjugated polymer electrodes, and the capacitive performance was observed to more than double when compared to devices fabricated using the unmodified CNT substrate. Subsequently, efforts made to study color mixing in electrochromic polymers are detailed in Chapters 4 and 5. Mixed color stimuli were produced using various combinations of ECPs following on the cyan-magenta-yellow subtractive color mixing system, first through the use of a "dual active" electrochromic device, and later through the co-processing of ECP mixtures into visually homogenous films. The colorimetric values of the resultant electrochromic films were assessed spectroscopically, and quantified in the CIE L*a*b* color space. The

access of a broad color gamut using polymers representative of the CMY system is demonstrated, as is the ability to "dial in" a color state using the dual active ECD configuration, as is the ability to predict the colorimetric properties of a co-processed ECP mixture via quantification of a mass extinction coefficient for the component ECPs. Finally, the photostability of select ECPs is assessed in Chapter 6. Thin films of two ECPs were encapsulated in both air and argon atmospheres, and exposed to a solar simulator for durations ranging from 24 hours to 1 month. Characterization of these films following irradiation through both spectroelectrochemical and x-ray photoelectron spectroscopic techniques demonstrate that while photo-oxidation is observed to occur under an air environment, encapsulation in an inert atmosphere precludes photo-oxidation and no deleterious effects stemming from long term irradiation are observed. The research detailed in this dissertation demonstrates the varied routes to redox-active, conjugated polymer application.

CHAPTER 1

INTRODUCTION – CONJUGATED, REDOX-ACTIVE POLYMERS

Redox-active, π-conjugated polymers have lent themselves to a number of applications. The work discussed herein focuses primarily on two of these applications, namely electrochromism, and the utilization of redox-activity for the purposes of charge storage. However, to properly discuss those applications, one should first have an understanding of how each of these properties emerge from the physical characteristics of conjugated polymers. The following chapter will hopefully serve as an introduction to the field of conjugated polymers in general, and the concepts behind their applications.

1.1 Introduction to Conjugated Polymers and Electrochromism

The study of conjugated polymers as redox dopable conductors largely originated with the discovery of two materials: polypyrrole and polyacetylene[1-3]. The properties observed in these materials served to lay the groundwork of understanding necessary for the work discussed within this dissertation, and while the structures of the polymers under study have changed, the physical principles behind their properties remain the same. Due to the connection between the properties leading to both charge storage and electrochromic (EC) applications, it serves us well to begin with a general discussion of conjugated polymers.

1.1.1.Theory of Conjugated Polymers

Any discussion of the fundamental properties behind conjugated, conductive polymers would do well to begin with the model of polyacetylene, the discovery and study of which led to Hideki Shirakawa, Alan Heeger, and Alan MacDiarmid receiving the Nobel Prize in Chemistry in 2000[4]. The chemical structure of polyacetylene, consisting of alternating double and single carbon-carbon bonds, leads to the creation of

its band structure, which in turn leads to its unique properties. In general, as the number of π bonds along a polymer backbone increases, numerous new, discrete energy levels are formed, and this process is stabilized by the delocalization of electrons throughout the conjugated system. As the number of conjugated π bonds increases, hybridization of the newly created energy levels into energy bands occurs at some extent of conjugation. This process is illustrated for the polyacetylene repeat unit structure in Figure 1.1.1.1.

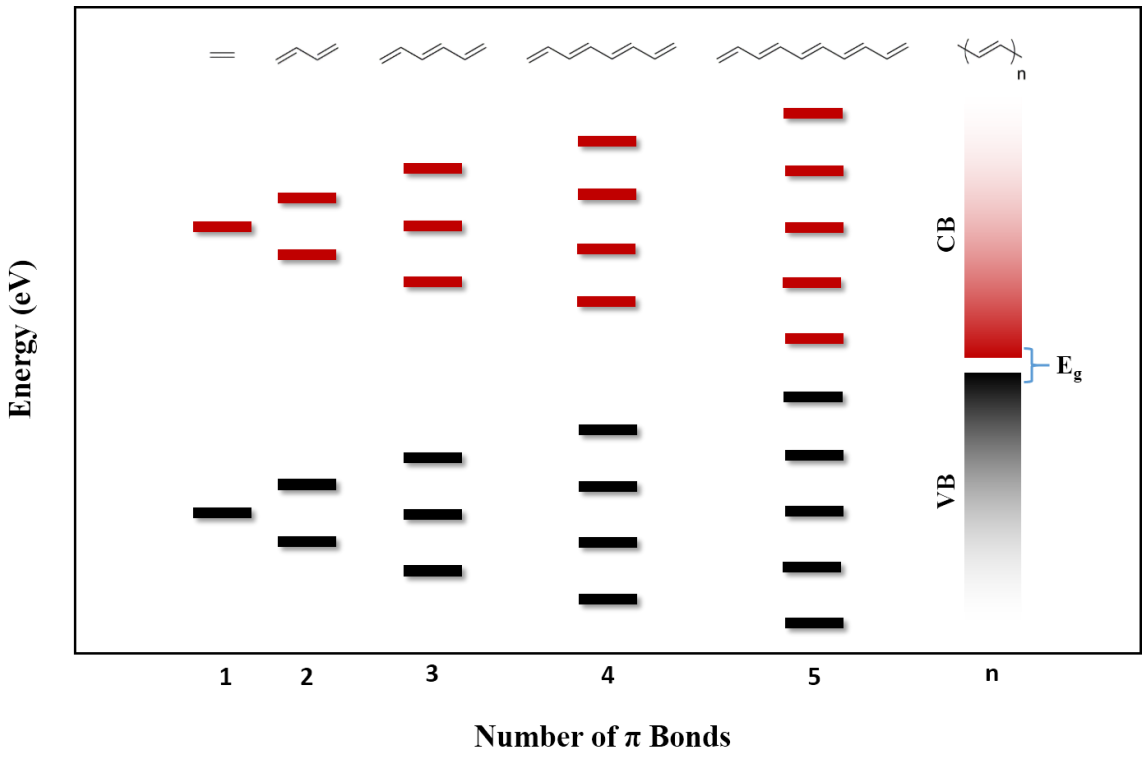

Figure 1.1.1.1. Representation of the shift from discrete energy levels to creation of energy bands as the conjugation along the polyacetylene backbone increases. The "filled" or "HOMO" energy levels/bands are represented in black, while "empty" or "LUMO" levels/bands are shown in red. Adapted from Salzner *et al*[5].

When the "band gap" or the "energy gap" (commonly given the symbol E_g) of a polymer material is discussed, it is the energy differential between the newly formed valance and conduction bands (or HOMO and LUMO levels) that is being referred to. Many of the properties commonly studied in conjugated polymers are directly related to the energy corresponding to this gap. The hybridization of π bonds into non-discrete band structures is arrested somewhere within a "semi-conductor" regime, prior to further hybridization

creating an overlap in the valance and conduction bands (a null value for the term E_g) and producing a polymer with a metal-like band structure. For better or worse, the effects of Jahn-Teller distortion (if one is concerned with specially separated degenerate energy levels created in conjugated polymers) or alternatively Peierls distortion (if one is concerned with the spacing of electrons along the conjugated axis of a polymer), prevent this metallic state from being attained[6-7]. The distortion prevents the alternating single and double carbon-carbon bonds in polyacetylene from becoming fully degenerate, where each bond would have a bond order of 1.5, and rather the formation of shorter (though not as short as double bonds) and longer (though not as long as single bonds) is observed[8]. While this scenario is unfortunate for the design of polymers with a truly metal-like band structure, the developing understanding of structure-property relationships to has been used to tune the energy of the interband of π to π* transition, resulting in the diverse family of conductive, electrochromic polymers (ECPs) discussed later in this chapter and throughout the rest of this dissertation. Briefly, steric interactions along the polymer backbone, particularly those effecting the angle of twisting between adjacent heterocycles and subsequently the extent of π orbital overlap, plays a role in dictating the energy associated with the π to π* transitions observed in conjugated polymers. Should the heterocycles of the backbone be twisted to a further extent out of plane, the energy associated with the π to π* transition will be higher, and through this higher energy photon absorption materials which appear yellow, orange, and even red have been produced. Low degrees of twisting between backbone heterocycles correspond with lower energy π to π* transitions, yielding materials which appear blue or violet. Materials which reflect or transmit light in the middle of the visible region (variations of green) require a material to absorb light in both the high and lower energy portions of the visible spectrum simultaneously.

While the band gap energy of conjugated polymers is intrinsically linked to the backbone structure, through doping, the structure of the backbone can be altered, eliminating one structure (and its E_g) in favor of a new structure with a new value of E_g. In the case of oxidation, as more and more portions of the backbone are oxidized, new geometries are adopted to maintain an equilibrium. Throughout oxidization as radical cations are formed (which can be thought of as polarons in the case of conjugated polymers), twisting strain along the backbone is relieved[9-11]. As oxidation of the material continues, dicationic or bipolaronic states are formed, due to the relaxation in the twisting strain along the backbone being greater for a pair of charges localized at one point than it is for two uncoupled charges separated at two points. This process is illustrated, using the structure of polythiophene, in Figure 1.1.1.2.

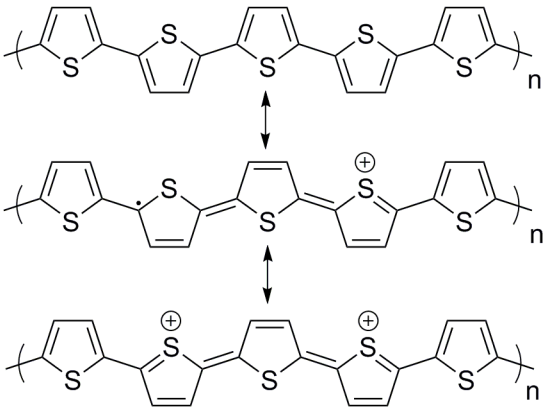

Figure 1.1.1.2. Formation of radical cation (polaron) and dication (bipolaron) states in polythiophene upon oxidation. Adapted from Beverina *et al*[12].

The formation of these bipolaronic states creates structures which are more planar in comparison with their undoped states, reducing the energy of any photons absorbed[13]. In this fashion the trend emerges that the more twisting strain is relieved (the more "relaxed" a system becomes), the more planar the bipolaron units can become, which in turn is able to absorb photons of lower and lower energy having the net effect of making the oxidized state of an electrochromic material more transmissive in the visible region. While this section has largely used polyacetylene as a model to discuss conjugated

polymers at large, nearly all the systems discussed in this dissertation are composed of aromatic heterocycles similar to the polythiophene seen in Figure 1.1.1.2., which will be examined in the following section.

1.1.2.Recognizing Polythiophene and PEDOT

Roughly contemporaneously with the discovery and study of polyacetylene, similar properties were noted in polyaromatic materials, such as polypyrrole (PPy) and polythiophene (PT). Polypyrrole in particular served as a system of choice in the study of many properties of conjugated polyaromatics, including doping and electrochromism[14-16]. The electrochromic transition observed in PPy is from a yellow-green neutral state, with a λ_{max} around 420 nm, to a blue-purple state with a λ_{max} at around 670 nm[17]. While this sort of transition might find utility in particular applications, the electrochromic properties of unmodified polypyrrole are not particularly useful for display or window applications.. Alternatively however, efforts to utilize PPy in charge storage applications have been ongoing for years, in part due to the low cost of the pyrrole monomer, and its solubility in aqueous systems[18-20]. Additionally, the electron-rich nature of PPy was a possible contributing factor to instability over repeated switching, leading to a research interest in the study of PT, which is less electron rich. As can be seen for PT in Figure 1.1.1.2. (and indeed for PPy as well) the 3 and 4 positions are not protected from participating in the coupling reactions used in polymerization, which led to mixtures of materials produced through α-β and β-β coupling which reduce the effective conjugation lengths within the polymer. To circumvent the formation of these structures, these positions were protected from coupling via the addition of various alkyl groups, the simplest of which is a methyl group[21]. The reduction in the α-β couplings formed through this protection scheme extends the effective conjugation lengths along the backbone, lowering the bandgap energy in the undoped form and also stabilizing polaronic and bipolaronic states formed upon oxidation. This motif was expanded further

by using groups that bridged the 3 and 4 positions of thiophene, a notable example of which was the synthesis and characterization of 3,4-ethylenedioxythiophene (EDOT), which after polymerization is referred to as PEDOT[22-23]. While the structural protection against non-conjugative couplings through the 3 and 4 positions was an important aspect of this discovery the electrochromic properties of PEDOT were, with particular regard to the history of the materials discussed in the remainder of this document, a turning point. In its undoped state, PEDOT exhibited a λ_{max} at 621 nm, showing a blue film when deposited electrochemically and upon oxidation this absorption was nearly eliminated, coinciding with the emergence of an absorption in the near-infrared (NIR) portion of the spectrum. While the NIR absorption tails into the visible, giving the oxidized state of PEDOT a slight blue coloration, the electrochromic behavior of a visibly colored-to-clear behavior is one that stoked interest for future practical application[24-25]. The dioxyethylene bridge appended to the core thiophene unit came with benefits beyond blocking coupling defects. Donation of electron density into the thiophene π systems made the conjugated system as a whole more electron rich. Through this added electron density, the HOMO levels of polymers produced using dioxythiophene (DOT) units are raised to some degree, which in turn lowers their potential of oxidation (E_{ox}), a property which becomes particularly important in the consideration of charge storage applications for conjugated polymers discussed in a subsequent section. The following section, however, will focus more on the tuning of the value of E_g by design of repeat unit structures in order to produce the family of ECP materials spanning the visible spectrum that are the focus of much of this document.

1.1.3. History of ECP Development – Completing the Color Palette

As previously mentioned, an intrinsic link might be drawn between the E_g of a conjugated polymer and the color of its undoped state. Over the previous decades, much effort has been directed at elucidating the relationships between repeat unit structures and

the properties of polymers created using structures, often referred to simply as "structure-property relationships". The conjugated polymers used throughout the work presented in this dissertation are no exception to this, and the general system for the design of ECP band gaps is shown in Figure 1.1.3.1.

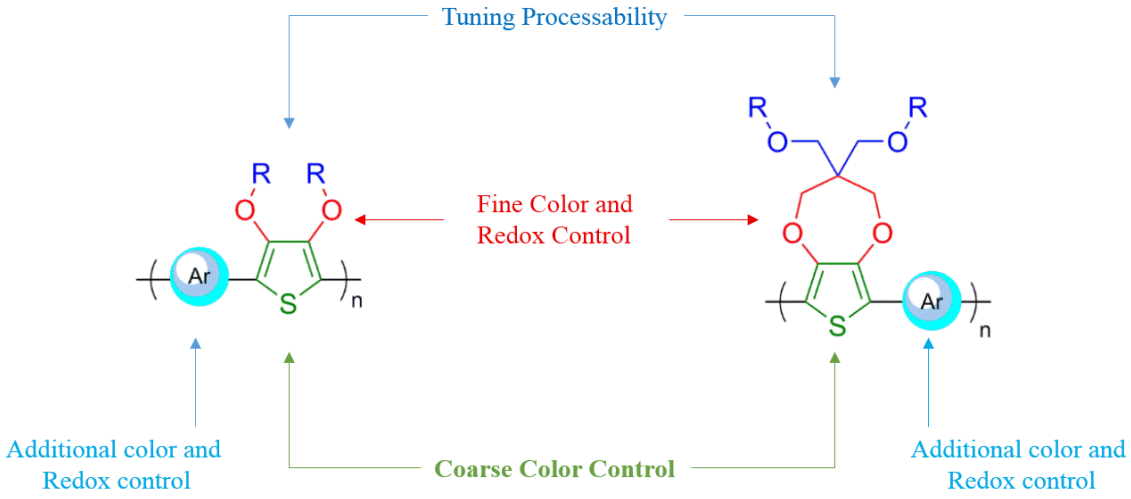

Figure 1.1.3.1. Schematic representation of the general structure-property relationships used to tune the color of the undoped state of an ECP. Adapted from the dissertation of Justin Kerszulis[26].

The general principles outlined in Figure 1.1.3.1. have allowed synthetic efforts in the Reynolds group to create a family of ECPs, wherein the values of E_g touch either end of the visible spectrum, and a variety of colors in between[27-28]. While this family of polymers has expanded to include multiple iterations for many of the color states, an illustration of the first full ECP "family" is shown in Figure 1.1.3.2. Many of the polymers represented in this family are "tuned" via steric interactions in repeat unit structures, causing twisting along the polymer backbone and shifting the energy of the π to π* transition, as discussed in Section 1.1.1. In the order from highest strain (twist, and consequently E_g) to the lowest, these are ECP-Yellow, ECP-Orange, ECP-Red, and ECP-Magenta[29-32]. As previously mentioned, to produce ECPs which appear green or cyan, dual absorption bands are required to remove both the high and low wavelengths from a visual stimulus. In the family of ECPs shown, this was done through the use of donor-

acceptor (D-A) moieties, wherein the π to π* transitions (absorbing high energy light) are tuned with varying degrees of donor content, and donor-acceptor interactions serve to provide an absorption band at lower energies[33-35]. This D-A structure also served to produce a blue-to-clear material, in ECP-Blue[36].

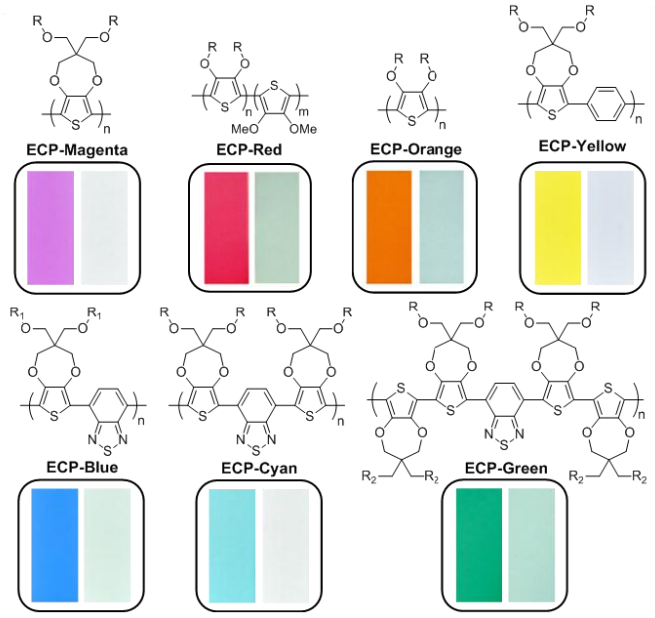

Figure 1.1.3.2. Structures and photographs in both neutral and oxidized states for the first DOT-based ECP family spanning the visible spectrum. Adapted with permission from Dyer et al[27]. Copyright 2011, American Chemical Society.

It is important to remember though that two other ECP systems make up important bookends to this family of materials: MCCP and ECP-Black. The first material, which switches between two nearly colorless states, i.e. with a minimal color change between its redox states, was developed based on a dioxypyrrole (DOP) heterocycle, rather than the DOT systems that make up most of the ECPs in this dissertation. Due to this minimal color change, this material was dubbed a "Minimally Color Changing Polymer", frequently shortened to MCCP[37]. This material in particular has been invaluable in the refinement of window-type electrochromic devices (ECDs), and its utilization can be found throughout Chapters 4 and 6. ECP-Black, while still predicated on DOT moieties in its repeat unit structure, is a random copolymer, rather than a well-defined structure such as those shown in Figure 1.1.3.2. The random nature of ECP-Black copolymer is the

origin of its absorptive properties, which reach from one end of the visible spectrum to the other nearly evenly[38-39]. The structure and spectrum of this unique ECP are shown in Figure 1.1.3.3.

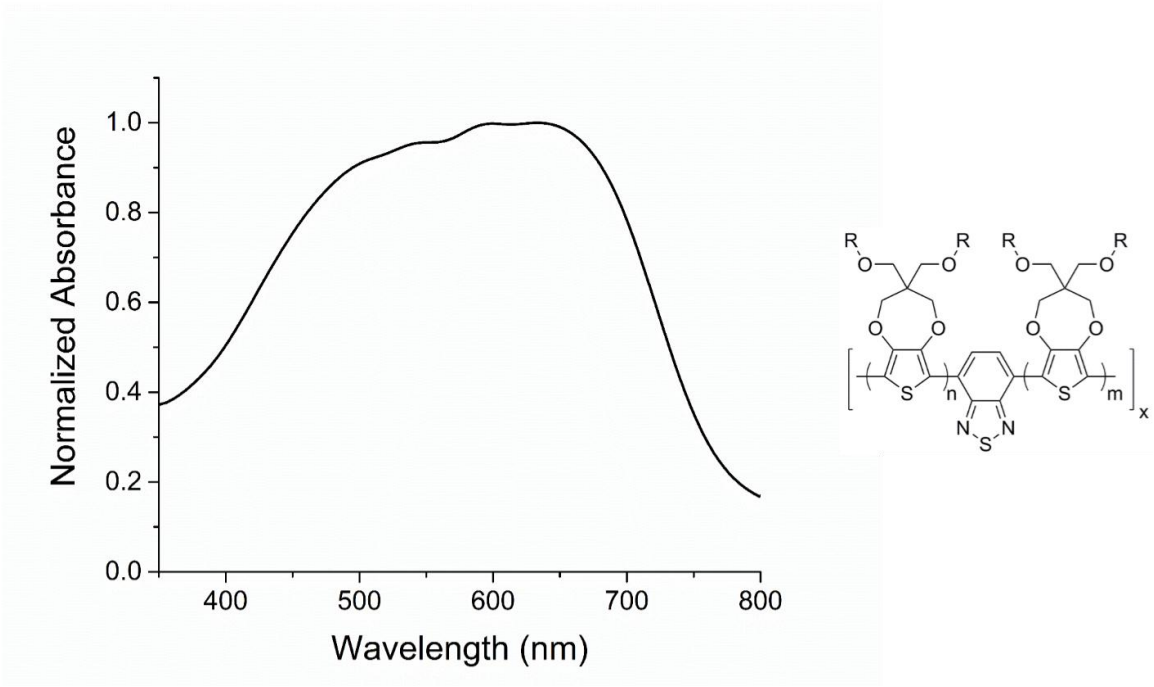

Figure 1.1.3.3. Spectrum and structure of ECP-Black, illustrating the origin of the broad spectral profile of this material from the random nature of its copolymerization. Adapted from the dissertation of Justin Kerszulis[26].

This material was designed to incorporate random lengths of all donor units, enabling the final polymer to absorb light at the lower wavelengths, capturing light in the middle of the visible spectrum towards the ultraviolet (UV). The random incorporation of acceptor moieties, with a varying number of donor units surrounding each acceptor, enables the absorption of low energy light as well. The nearly random formation of both these moieties, all donor and donor-acceptor units, during polymerization allows for the roughly even spectral profile throughout the visible spectrum, and the even attenuation of light across the range of visible light imparts this material with its nearly black chromaticity. With this versatile family of electrochromic polymers available for study,

the following section will describe potential future applications, as well as offer a bit of perspective on the future of development of DOT-based conductive polymers.

1.2. Applications and Perspective for Conjugated Polymers

The field of conducting polymers has matured significantly in the decades following the recognition of polyacetylene and polypyrrole. A major focus in this document is given towards the electrochromic aspects of conductive polymers, and in this area strides are being made to make these materials practically applicable. However, while perhaps less able to catch the eye, efforts to utilize the faradaic processes coinciding with the reversible redox reactions in the DOT-based polymers for charge storage applications have been fruitful as well. The following section will discuss a few of these potential applications, and offer a view towards the future of conducting polymers.

1.2.1. ECP Applications and Electrochromic Devices

The general architecture of electrochromic devices takes two routes towards light modulation: transmission and reflection. These terms are most often applied towards lab-scale devices for either prototyping or performance assessment, however the principles behind the naming convention in describing the general activity of the device as a whole would carry through to the consumer application level. Further, it's worth noting that the nomenclature applied to ECDs utilizing polymer electrochromes is for all intents and purposes identical to the nomenclature applied to devices using non-polymer electrochromic materials[15, 40]. Let's first discuss the design and applications for reflective ECDs. The primary difference in reflective and transmissive ECDs is the presence of some reflective material, whether incorporated between two transmissive electrodes, or as a reflective electrode surface. When the intended application of a reflective ECD is to perform a colored-to-white transition, such as might be used in a

display type application, a diffuse reflecting additive is incorporated into the electrolyte-filled space between electrodes, often making use of passivated titanium dioxide (TiO_2) for this purpose[41-44]. A schematic representation of this form of reflective ECD is shown in Figure 1.2.1.1.

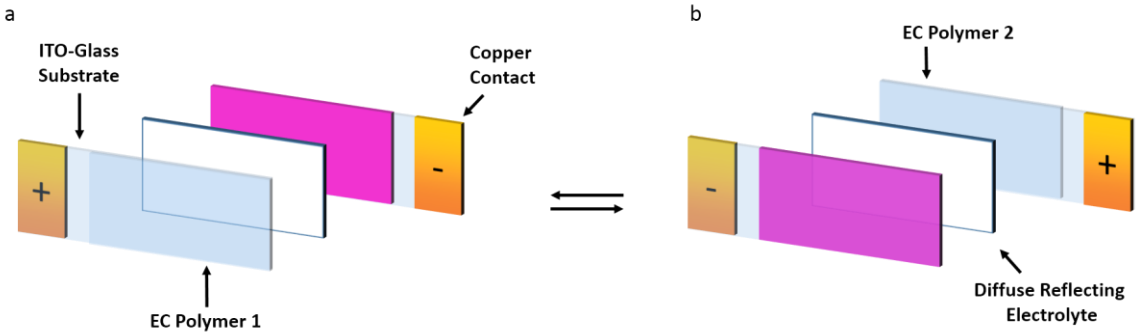

Figure 1.2.1.1. Schematic representation of a reflective-type ECD in the a) white and b) colored states. Shown is a device with a diffusely reflective white electrolyte additive, such as titania. Adapted from the dissertation of Aubrey Dyer[45].

One obvious benefit of this form of reflective ECD is that the same material might be used on both electrode surfaces, ensuring that, provided processing and film thicknesses are relatively uniform, sufficient material will be present for charge compensation to either state of the device. Alternatively, reflective ECDs have been fabricated using reflective, metallic electrode substrates, rather than the transmissive indium tin oxide (ITO) coated glass often employed. In this case, a transmissive electrode is used at the "top" of the device, and upon bleaching of the electrochromic materials within the device, the reflective metallic electrode "underneath" is revealed[46-48]. The most frequently mentioned application of reflective type ECDs is in non-emissive image or data displays. Such applications might be applied to indicators on security cards and banknotes, advertising displays, or even watches and clock faces[49-53]. One application which bridges the transmissive and reflective aspects of electrochromic devices is in the dimming of mirrors. More often than not utilized in an automotive setting, ECDs are placed in front of rear-view mirrors that might be illuminated by the headlights other vehicles. Placing this ECD in a clear state would allow for full reflection, while a

darkened state would attenuate the reflected light, preventing a driver from being dazzled by the headlights of another vehicle[54-56].

The design of transmissive ECDs is nearly identical to that seen in reflective ECDs. Neither are diffusely reflective electrolyte additives present, nor metallic electrode substrates, and instead electrode surfaces are composed of some transmissive material coated onto either glass or plastics. As the goal of this device type is very likely a colored-to-transmissivity clear transition, the selection of electrochromic polymers becomes pivotal. Where in reflective ECDs, should the same polymer be used on both electrodes, one electrode will always be in the fully colored state if the other is to be in the bleached state. However in transmissive ECDs, either very judicious selections of polymers with opposing doping schemes must be made, or one material which exhibits no visible color in both of its oxidation states must be used[57]. In the latter scenario, the DOP material described above in Section 1.1.3., MCCP, is a suitable material for use in transmissive ECDs, and indeed without the lack of visible color in either of its redox states, much of the work presented in Chapter 4 would not have been possible[37, 58-60]. A schematic representation of a transmissive ECD utilizing an MCCP coated electrode is shown in Figure 1.2.1.2.

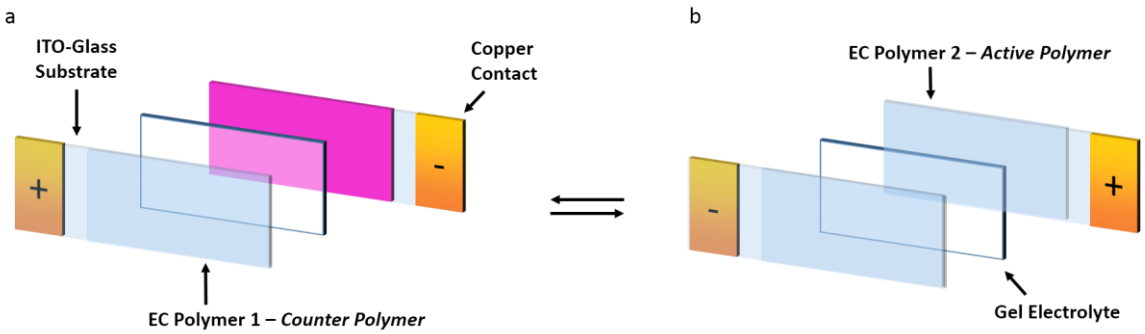

Figure 1.2.1.2. Schematic representation of a transmissive-type ECD in the a) colored and b) clear states. Adapted from the dissertation of Aubrey Dyer[45].

The most obvious application for the transmissive ECD type is its utility in window or eyewear applications. Where architectural windows are primarily concerned the term

"smart glass", coined in 1985, has often been used to describe a window with a tunable transmittance functionality, though examples of this technology in popular media predate the term, such as in the 1982 film *Blade Runner*[61-62]. The primary functionality of transmissive ECDs, and indeed any variation of smart glass technology, is the selective and variable transmission of an otherwise static external window or interior glass wall. Further, it has been suggested that when applied to external windows in buildings, the selectively variable transmission of smart windows will lower cooling or heating requirements, due to the ability of windows to match exterior conditions in a fluid manner[63-67]. While currently not employing electrochromic polymers as active materials, View Inc. and Sage Glass have both been successful in installing EC windows in both public and privately owned buildings[32, 68]. While the maturation in the application of the electrochromic aspects of conducting polymers is an ongoing process, great strides have been made in raising public awareness of both electrochromism and "smart glass" technology. There is however another application for conjugated polymers with great promise. While in the author's opinion considerably less flashy and visually appealing, the utility of conductive polymers for charge storage applications such as in supercapacitors, via utilization of the faradaic currents produced upon their oxidation and reduction, offers just as much promise for successful implementation as any EC technology. This form of implementation, and its direct relevance to supercapacitor devices is discussed in the following section.

1.2.2. Polymer Supercapacitors and High Surface Area Electrodes

To discuss the usage of conducting polymers in supercapacitive devices, the simplest place to begin is likely in the description of supercapacitors in general. While a textbook-style definition could suffice, it seems more often than not, the most successful description of this class of devices comes relative to two other energy storage device types: capacitors and batteries. Capacitors are devices which store electrical energy

electrostatically, often via a pair of polarized plates separated by some dielectric (insulating) material. This form of device construction is able to store only a (relatively speaking) moderate to small quantity of electrical energy per unit volume or mass, meaning a capacitor's energy density is low. On the other hand, a capacitor is able to very quickly accept charge for storage or discharge its stored energy, and this rapid rate of energy transfer being attainable means most capacitors have a high power density. Batteries however (or fuel cells, which will not be discussed here), in a simplistic sense, characteristically display the opposite trends. Batteries are often able to store much larger quantities of energy per unit volume or mass than capacitors (high energy density), but are unable to discharge or accept energy at a high rate (low power density). When plotted, this relationship between energy and power densities (or specific energy and specific power) is referred to as a Ragone chart, named after David V. Ragone[69], and one such plot is shown in Figure 1.2.2.1. Supercapacitors, as can be seen in this chart, are device types that seek to bridge the gap between the high power density of capacitors and the high energy density of batteries.

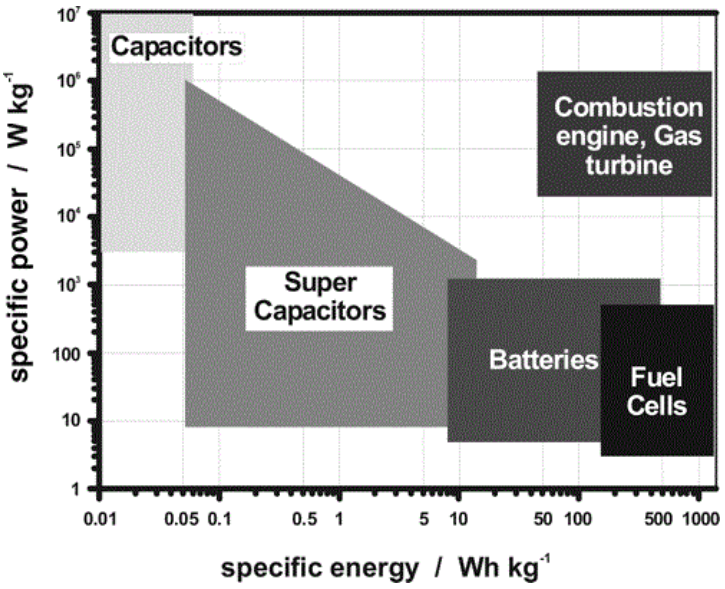

Figure 1.2.2.1. Ragone chart, comparing the specific energies and powers of various energy conversion systems. Reprinted with permission from Winter *et al*[70]. Copyright 2004, American Chemical Society.

Devices that fall within the "supercapacitor" range have been viewed as a promising avenue for energy storage due to the higher power density, higher energy storage densities, and faster charge-discharge cycles, when compared to the Li-ion batteries[71-72]. In recent years, much of the push behind research done in the field of supercapacitor development has been spurred on by the consumer electronics demand for easily portable, light-weight, low form factor, and, if at all possible, flexible energy storage devices[73]. In response to these demands, carbon-based, and specifically carbon nanotube (CNT)-based, devices have been developed in a range of form factors[74-77]. The mechanism of charge storage in many of these carbon-based devices centers around the formation of an electrochemical double layer at the electrode-electrolyte interface, and devices that utilize this route to charge storage are often referred to as electrochemical double layer capacitors, or EDLCs[78]. Part of the success of this mechanism of charge storage is reliant on the carbon materials having a sufficiently large surface area over which this double layer may form upon polarization. It has been suggested in the literature however that the supercapacitive performance of EDLCs is limited by the low specific capacitance inherent to the carbon materials often used to produce these devices[79-81]. In contrast to the ECDL mechanism of charge storage, redox-active materials which store electrical energy faradaically, such as conducting polymers and transition metal oxides, have been found to have much higher specific capacitances than those observed in EDLC materials[82-85]. Among these redox-active materials (frequently referred to as pseudo-capacitors), conductive polymers such as polyaniline (PANI), polypyrrole (PPy), and poly(3,4-ethylenedioxythiophene) (PEDOT) and its derivatives have the greatest potential to display a robust flexibility, along-side the high redox-active capacitances characteristic of pseudocapacitors[73, 86-92]. One of the many strategies for the implementation of conductive polymers for supercapacitor devices has been to form composites with carbon electrode materials, ideally making use of both the high surface area of carbon substrates (and therefore their relatively high double layer capacitance and

power densities) and the high specific capacitance of pseudocapacitive, redox-active polymers[93-98]. Many of these efforts have relied on the electrochemical polymerization of conductive polymer around a carbon substrate, and while successes have been reported via this method, electropolymerization is a process that is difficult to bring to a large scale[90, 99-100]. As discussed in Section 1.1.3., and shown in Figure 1.1.3.1., synthetic design strategies are capable imparting various solubility motifs to conductive polymers, and both aqueous and organic solubilities have been demonstrated for DOT-based polymers[28, 101]. The solubility imparted to these polymers opens the door to a new route of polymer/CNT composite formation, and efforts to examine the capacitive performance of supercapacitive devices utilizing composite electrodes formed via solution processing of a conjugated polymer form the basis for the third chapter of this dissertation.

1.3. Dissertation Thesis

The information contained within this document serves to detail the application and study of conjugated, redox-active polymers, utilizing both pseudocapacitive charge storage properties as well as designed electrochromism. As seen above, Chapter 1 serves as an introduction to the concept of electrochromism, focusing on conjugated polymers and the traits that make them an attractive material for study. Also detailed is the utility of redox-activity for pseudocapacitive applications, polymer-based supercapacitors, and strategies to improve the performance of this technology. Chapter 2 will offer an overview of the experimental techniques used throughout this body of work. Chapter 3 will cover the use of conjugated polymers as a modification to high surface area carbon electrodes intended for super capacitor applications. Chapter 4 will focus on electrochromic devices, including variations in device architecture for specific applications, such as color mixing or self-powering devices. Chapter 5 will detail solution co-processing of polymer mixtures for color mixing applications, based largely on the CMY subtractive color mixing scheme, and deviations from this scheme in order to

optimize specific attributes of mixtures. Chapter 6 will discuss experiments undertaken in order to address the question of photo-stability in pi-conjugated materials in both oxygen containing and oxygen free environments, as well as dry and electrolyte bearing environments.

CHAPTER 2

EXPERIMENTAL AND FABRICATION TECHNIQUES

By and large, the majority of the work presented in this dissertation makes use of a small handful of techniques. Hopefully, this document will be rife with the technical information necessary for similar experiments, in that now that we've discussed the background for studying redox-active conjugated polymers and their applications, a thorough description of the means and methods of that study is in order. The following chapter will discuss topics ranging from the casting of polymer films from solutions and the fabrication of devices using those films, to characterization techniques such as spectral and electrochemical measurements, the derivation of colorimetric information from spectra, photography, and surface-sensitive measurements such as x-ray photoelectron spectroscopy.

2.1 Polymer Processing and Device Fabrication

The technique likely most central to all of the data presented in this work is the processing of polymer films via solution casting methods. Post-synthesis, the physical samples of the materials examined in this dissertation frequently consists of finely dispersed, dark colored powders. The processing of these materials, via solution casting methods, into thin films upon various substrates has opened the door for opto-electronic characterization, well-defined electrochemical behavior where charge storage is concerned, and amenability to surface sensitive techniques. The film producing techniques will be supplemented by details pertaining to the fabrication of devices, both electrochromic and supercapacitive, from cast films.

2.1.1. Spray Casting of Films

The process of casting polymer films begins with the production of a polymer solution. All of the films that were produced and examined to produce data, save that in

Chapter 3, were processed from toluene or chloroform solutions. For the materials discussed in this document, polymer concentrations ranging from 2 to 5 mg per milliliter of solvent are the most common, and those values are well within the solubility limits for the discussed materials. The preparation of solutions rarely requires additional heating to promote dissolution. Should heating be employed however, future students are encouraged to use vials with caps loosely affixed, rather than tightly sealed. Overheating of a loosely sealed sample may cause the evaporation of solvent, but overheating of tightly sealed vials may cause cracked or leaking sample containers. Solution volumes prepared ranged anywhere from 2 mL to 25 mL, though the most common solution volume prepared was 10 mL, at a concentration of 5 mg/mL. That volume, and the concentration stated should be sufficient to cast anywhere from 8 to twelve films from an organic solvent, with an area of roughly 2 cm^2. Your sample mileage may vary, depending on your experience with the casting technique.

Once solutions are prepared, substrates should be prepared for casting. The most common substrate for casting in this document is overwhelmingly ITO-coated glass slides, purchased from Delta Technologies, Ltd, with quoted sheet resistances of 8-12 Ω/sq. These substrates vary in size depending on the final application, with substrates for thin film interrogation having dimensions of 7x 50 x 0.7 mm, and substrates destined for device fabrication measuring 25 x 75 x 0.7 mm, though these are often cut in half along the short axis to produce two electrodes. Prior to casting, substrates are rinsed with wipes wet with acetone. Immediately prior to casting, polymer solutions should be filtered using a 0.45 pore size PTFE syringe filter, to remove insoluble material and polymer aggregates. If the polymer solution has been allowed to sit, and a large degree of aggregation is observed (often a very hazy, albeit translucent liquid), gentle heating may be used to break up these aggregates, though solutions should be at room temperature at the time of filtering. After filtering, solutions are ready to be sprayed, which may be done using an Iwata-Eclipse spray gun, with nitrogen as the carrier gas. Whether toluene,

chloroform, or a mixture of the two was used as the processing solvent, the gas pressure was set at roughly 20 psi, in order to produce a finely dispersed spray. Further, a gun tip to substrate distance of 4-6 inches was maintained throughout casting, with the gun at a 45° angle to the substrate, moving in a continuously fashion both laterally and axially with respect to the substrate during casting.

2.1.2. Device Fabrication and Assembly

Fabrication of simple, window-type electrochromic devices, once films have been cast, is a rather straight-forward proposition, or at least a process which involves several, independently simple steps. After casting, the first of these steps is to place some form of barrier around the active (electrochromic) portion of the substrate being used. Barrier materials used in this document come in the form of either a foamed acrylic tape, coated in adhesive on both sides (3M VHB tape), or a modified polyisobutylene tape that will be discussed in more detail in section 2.6. Frequently, this barrier layer takes the form of a double barrier, as illustrated in Figure 2.1.2.1., and the author strongly encourages this type of barrier for ECD applications when possible.

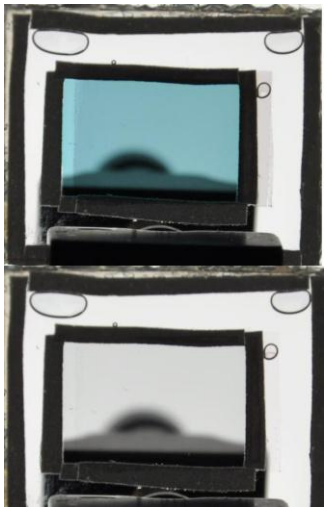

Figure 2.1.2.1. Illustration of the "double barrier" bordering scheme for window-type ECDs, a simple means of keeping bubbles from becoming trapped within the active area.

Putting down this double barrier layer is done for at least two important reasons. First, this provides a physical separation between the two electrode surfaces, preventing them from shorting together and causing adverse effects. Second, the double barrier leaves room for spill-over of the electrolyte added to the device, ideally trapping any bubbles formed during the sealing process outside of the active electrochromic portion of the device. Electrolyte formulations will no doubt change over the years following this document's publication, but all of the devices described herein make use of an electrolyte comprised of propylene carbonate (PC), 8 wt% poly(methyl methacrylate) (PMMA) to increase viscosity, and 0.5 M of a given salt, being either tetrabutylammonium hexafluorophosphate ($TBAPF_6$) or lithium bis(trifluoromethane)sulfonamide (LiBTI). In short, after film casting, the barrier is laid down on one electrode, electrolyte is pipetted into the interior barrier, and the second electrode is laid on top. Once joined, a small weight (~50 grams) is placed atop the device for roughly five minutes to allow for a good contact to be made between the double sided adhesive and both electrode surfaces. After this step, copper tape may be used to facilitate electrode contact at the ends of the ITO electrodes. This methodology can be adapted to ECD fabrication with little regard for the particular features of the substrates being used, which is further demonstrated throughout Chapter 4 of this document.

2.1.3. Drop Casting from Water

Solution processing can be as sophisticated as complex roll-to-roll coating processes carried out on the industrial scale or, at the other extreme, as simple as placing a drop of solution (or suspension) bearing a relevant material onto your substrate of choice. The spray casting described in the previous sections falls somewhere between these two in terms of complexity, and formed the overwhelming majority of techniques used to study electrochromic polymers. Where the study of materials and structures intended for charge storage applications are concerned though, at least as far as this

document will detail, drop casting became the solution processing technique of choice. Further details of the supercapacitive properties formed via this technique may be found in Chapter 3, however this section will provide detailed information on the casting technique and its parameters employed to generate that data.

As mentioned, drop casting is a very simple method of creating a film of a solution-borne material, with very little mystery beyond what's contained in the name. Frequently used to coat button electrodes for electrochemical characterizations, some known volume of a solution with a well-defined concentration is pipetted or otherwise dispensed onto a substrate, and allowed to sit until fully dry. Really, only two considerations are required to undertake drop casting. First, one will have to be able to form a solution of the material for which processing is desired, or otherwise form a well dispersed suspension. Second, one will have to ensure that the substrates onto which the solution is placed is not perturbed throughout the drying, lest solution be knocked off of the substrate or remaining solvent cause smudging of the cast film.

Beyond the consideration of the general method, this technique as used in Chapter 3 was used to cast thin films of a water-soluble conjugated polymer onto a non-woven carbon nanotube (CNT) substrate to increase the charge storage properties of the CNT textile by the addition of pseudocapacitive or faradaic current upon voltage cycling. As received, the conjugated polymer in question was functionalized as a carboxylate salt, rendering it soluble in water. An aqueous solution of this polymer was prepared at a concentration of 5 mg of polymer per mL of water (previously purified to a resistance of 18 MΩ), and was allowed to stir for 24 hours under very gentle (40-60 °C) heating conditions. After fully solvation, the solution was dispensed onto the CNT textile surface in 40 μL aliquots via a mechanical pipette with a maximum volume of 100 μL. One the number of aliquots proportional to the mass of polymer desired to be deposited were dispensed, samples were left on the benchtop over night to dry undisturbed. As roughly no more than a milliliter was dispensed onto any one sample, twelve hours proved

sufficient to allow for film solidification, and no additional heating was used to dry the cast films. After casting and drying, the newly formed polymer-CNT composites were soaked in a 1 M methanol solution of p-toluenesulfonic acid (pTSA) for 30 minutes to protonate the carboxylate functional groups, rendering it insoluble in aqueous environments. This pTSA soak step was followed by a 30-60 minute soak in an additional bath of 18 MΩ water to remove any pTSA left in the sample after removal from that bath.

2.1.4. Fabrication of Supercapacitor Devices

Following the fabrication of polymer-CNT composite electrodes described in the previous section, the composite samples were used to construct capacitive devices. Fabrication of these devices is much simpler than the fabrication of electrochromic devices described above. As capacitive devices require only that the two electrode elements not be in physical contact in order to prevent shorting, a square of cellulose filter paper (Quantitative Grade 5, medium pore style, Fisher Scientific) wet with the appropriate electrolyte (in this case LiBTI at a concentration of 0.5 M in water) is placed between the two polymer-CNT composite electrodes. In turn, the polymer-CNT composites, previously soaked with electrolyte solution, were placed onto the surfaces of stainless steel shims (0.002" thickness, Maudlin Products, part number 316-002-6-50) in order to facilitate electrical contact with the composites. Around this stainless steel-composite-filter paper sandwich, microscope slides were used to provide structural strength to this "device" assembly, and to add a surface across which pressure could be applied in order to keep all of the electrically active components in close contact during operation and characterization.

2.1.5. Fabrication of Photoelectrochromic Device

Initially, ITO-glass substrates (15 Ω/sq, Colorado Concept Coatings, LLC) were rinsed via ultrasonic bath using a detergent, water, acetone and isopropanol. A ZnO solution, prepared from zinc acetate dehydrate and ethanolamine dissolved in 5 mL of 2-methoxyethanol (all chemicals from Aldrich), was spin coated onto the ITO surface (3000 rpm, annealed at 150 °C for 1 hr). Atop this ZnO layer, polyethylenimine ethoxylate (PEIE) was cast via spin coating (5000 rpm, annealed at 100 °C for 10 min.), and samples were transferred into a glove box with a nitrogen atmosphere for photoactive layer coating. In this N2 atmosphere, a layer of PDPP3T:phenyl-C61-butyric acid methyl ester (PCBM) was deposited via spin casting (1000 rpm for 1 min, annealed at 75 °C for 5 min.). PDPP3T was acquired from Solarmer Materials, Inc. and the PCBM was acquired from Nano-C, Inc. The photoactive layer solution was prepared for spin coating through dissolution of the two aforementioned materials in a mixture of dichlorobenzene:chloroform,1,8-diiodooctane (79:16:5, v/v/v) at a total concentration of 18 mg/mL, and allowing this mixture to stir overnight. The PEDOT:PSS suspension, the final layer of the OPV device, was prepared for casting by adding 5% by volume dimethyl sulfoxide (DMSO), and allowing to stir overnight. The PEDOT:PSS suspension was spin coated (1000 rpm, annealed 80 °C for 5 min.), and the resultant OPV devices were tested in a nitrogen atmosphere. Following OPV device assessment, solutions of ECP-Magenta (ECP-M) and MCCP were prepared in toluene to a polymer concentration of 2 mg/mL. Solutions were filtered using a 0.45 μm PTFE syringe filter, and casting using an Iwata-Eclipse HP-BC airbrush with nitrogen as the carrier gas. Thin strips of VHB foamed acrylic tape were used to produce device boundaries. These boundries were filled with a gel electrolyte composed of 0.5 M LiBTI in propylene carbonate, with an added 8 wt% PMMA and sealed with an additional ECP-OPV assembly. Contact to the device was facilitated via strips of copper tape (series 1181, 3M) at the extreme edges of each device.

2.2 Electrochemical Methods

Electrochemical techniques, such as cyclic voltammetry (CV), lend themselves readily to the study of the redox properties of conjugated polymers. The following section will discuss the basic procedure for gathering CV data on a cast polymer film, as it relates to the electrochemical data presented throughout the rest of this document.

2.2.1. Cyclic Voltammetry

Cyclic voltammetry, as a method, can be generally described as a waveform used to apply a bias across an electrochemical cell (likely in relation to some reference potential). The applied bias is swept linearly and at a constant rate between two extreme values, which is then reversed and brought back to its original value in an identical fashion, hence the cyclical description. The term cyclic voltammetry itself refers to the application of this waveform, however it might be applied either to a three electrode cell arrangement, or across a two electrode "device"-type arrangement. Within this document, working electrodes (WE) commonly consisted of polymer-coated ITO-glass slides. Pt wires and flags served as counter electrodes (CE) and, where used, organic reference electrodes (RE) consisted of 10 mM $AgNO_3$ in a 0.5 M electrolyte. In any following figures, where the phrase "vs. Ag/Ag^+" may be used, this refers to this 10 mM $AgNO_3$ reference. Aqueous reference electrodes, containing AgCl, were purchased from Bioanalytical Systems, Inc. (BASi, product number MF-2021). The potential of reference electrodes was periodically calibrated against a 10 mM Fc/Fc^+ solution, making use of whichever electrolyte syem pertained to that electrode couple prior to use[102]. This electrode arrangement can be compact enough to use within a spectrometer cuvette, and a photograph of just this arrangement is shown in Figure 2.2.1.1. The organic electrolyte systems used throughout this document made use of the salts $TBAPF_6$ or LiBTI, almost exclusively dissolved into propylene carbonate (PC), unless otherwise noted. Aqueous electrolytes were composed of 0.5 M LiBTI in water purified to a resistance of 18 MΩ.

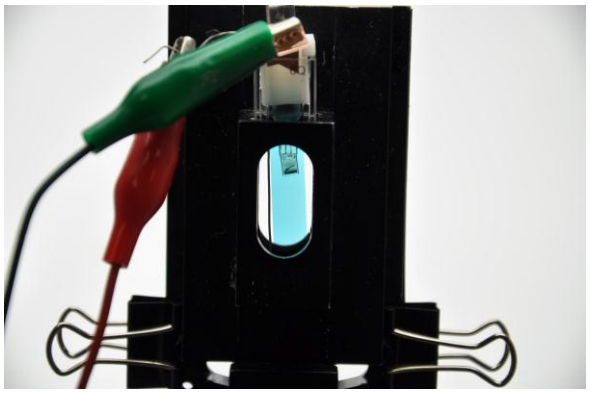

Figure 2.2.1.1. Photograph of the three electrode electrochemical arrangement inside of a spectrometer cuvette.

In practical application, the cyclic voltammetry presented throughout this document was used to fulfill two purposes. First, potential cycling was used to assess the charge storage properties of polymer-CNT composite electrodes at varying scan rates, and additional detail pertaining to those experiments may be found in Chapter 3. Second, but no less important, cyclic voltammetry was used to "break in" electrochromic films. The redox switching behavior of conjugated polymers coincides with the intercalation and expulsion of both solvent and counter ion species, and as a consequence of the this a shift in spectral properties is often reported before and after the initial switches of a film[31, 103-104]. Prior to full spectral characterization, an electrochromic film should be subjected to a number of CV break-in cycles, as after only a few switches, films often enter a steady state in terms of further switching without any shift in their spectral properties. A representation of the break-in cycling, as well as fairly typical cyclic voltammetry traces for an electrochromic polymer, specifically ECP-Cyan, is shown below in Figure 2.2.1.3.

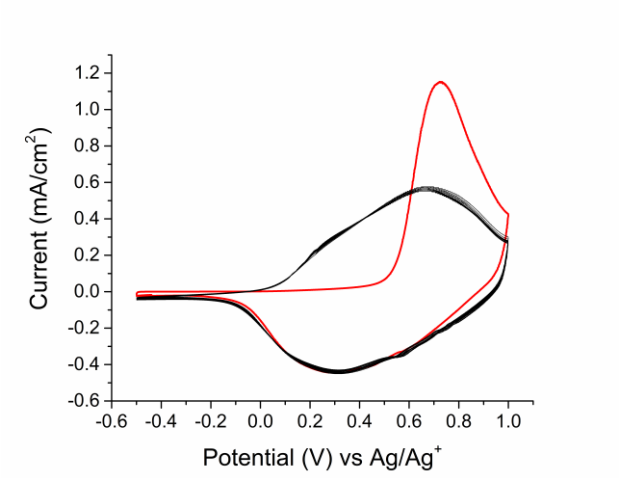

Figure 2.2.1.2. Break-in cyclic voltammogram for a film of ECP-Cyan. The initial cycle is shown in red, and 24 subsequent cycles are plotted in black.

Regarding the application of cyclic voltammetry to two electrode or device type structures, few differences are noted in the voltammograms produced. When performing cyclic voltammetry on a device, the reference and counter electrode leads are shorted together, making the bias applied across the device self-referential, and for this reason the current data collected should not be plotted against a "potential" axis, but rather simply an applied voltage. Beyond the physical augmentation of the connection scheme and the understanding of differences between an applied potential and applied voltage, the procedure and considerations for gathering device CV data are identical to those of the three-electrode electrochemical cell.

2.3 Spectral Techniques

Given the focus on the optical properties of conjugated polymers that makes up the majority of this document, it's only natural that the techniques used to carry out those characterizations be detailed. Rather than simple spectroscopy though, the dependence of each materials optical properties on its redox states necessitates methods than are able to marry both electrochemical and spectral characterization. Two methods of characterization in particular are utilized in this document, spectroelectrochemistry and chronoabsorptometry.

2.3.1. Spectroelectrochemistry

Spectroelectrochemistry is, put simply, the collection of spectrographic data in connection with the application of a steady potential bias across the sample being measured. More specifically though, this technique is used to record the spectral behavior of an ECP at incremental potentials as applied in by a potentiostat, throughout the potential switching window determined for that material. Unless otherwise noted, spectral data throughout this document was recorded on a Varian Cary 5000 UV-Vis-NIR spectrophotometer. The exception to this are portions of data presented in Chapter 4.3, which utilized either an Ocean Optics USB2000+ fiber optic spectrometer or an Optronix OL770 spectroradiometer, which will be noted as such. The spectral window accessible for recording for the Cary 5000 ranges from 175 to 3300 nm, however a range of 300-2000 nm allows for the observation of the polaron and bipolaron states formed upon oxidation of most electrochromic polymers, though an even narrower window (such as 350-1600 nm) may be used to focus on the shift observed within the visible region.

The common procedure for recording spectroelectrochemical data is fairly simple, and as with most methods described in this chapter, is more or less a collection of fairly simple individual steps. The cell arrangement should be established within a spectrometer cuvette, as shown in Figure 2.2.1.2. First, photographs of the unswitched film should be collected (further description found in Section 2.5). Films should then be switched via cyclic voltammetry as described in Section 2.2. As few as 5 cycles is often enough to ensure no further drift in spectral properties is observed, but additional information on a film's stability to repeated cycling may be gather with more cycling. Following this cycling and after ensuring that the thin film in question is within the beam path of the spectrometer and unobstructed by wires, counter electrode wires, or reference electrode tips, a potential which fully neutralizes the film should be applied potentiostatically. After allowing 25-30 seconds for the system to equilibrate, a spectrum is recorded. Following this, the doping potential should be increased in fairly small, regular steps, such as at 50

or 100 mV intervals, throughout the potential window determined for that material during initial characterization, and a spectrum should be recorded at every potential after allowing 30 seconds for the system to re-equilibrate at each new potential. After the maximum potential for that system has been reached, the traces recorded at each potential may be plotted together to form a spectroelectrochemical series. An example of such a series is shown in Figure 2.3.1.1. for a film of ECP-Magenta, illustrating the full series at left, and highlighting the traces produced by potentials dominated by the neutral state absorbance (red), polaron absorbance (blue) and final bipolaron absorbance (black).

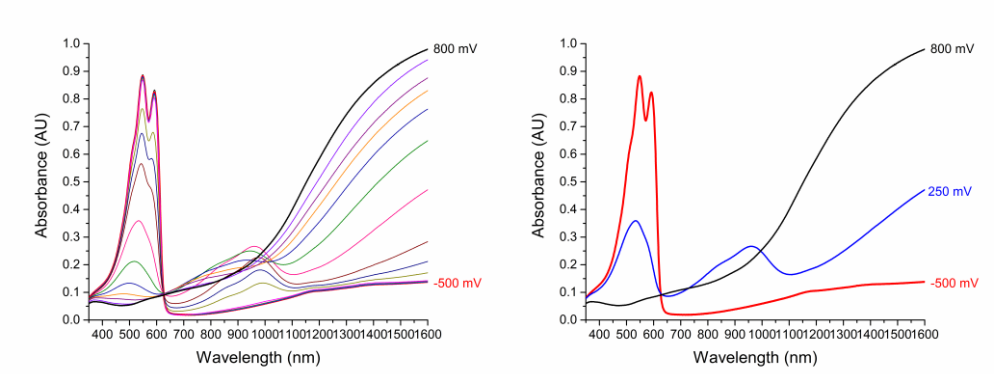

Figure 2.3.1.1. Full spectroelectrochemical series for a film of ECP-Magenta (left) and isolated spectra of the neutral, polaron, and bipolaron states for that film (right).

2.3.2. Chronoabsorptometry

Chronoabsorptometry, as used in this document, is fairly similar to spectroelectrochemistry, in that the data recorded describes the optical properties of an electrochromic polymer film, as they shift with a varying applied bias. A notable difference is made between the two methods however. While spectroelectrochemistry is a fairly static technique, allowing the electrochemical system to reach some steady state prior to data acquisition, chronoabsorptometry is by definition a dynamic method, recording data from a film actively throughout its electrochromic shift. Further, where spectroelectrochemistry records data across a range of wavelengths (most frequently the dominant wavelength, or λ_{max}), the physical demands of performing chronoabsorptometry dictate that a single wavelength be measured throughout the experiment. Through this

method, the time required for a "full" electrochromic switch might be assessed, and colloquially, the data gathered via chronoabsorptometry is referred to as electrochromic "switching kinetics". Chronoabsorptometry makes use of a cell arrangement identical to that used in spectroelectrochemistry, and is primarily performed using the "Kinetics" program written for the Cary 5000 spectrophotometer. A potentiostat is used to apply a varying potential using a potential square-wave program, with fully neutralizing and fully bleaching potentials entered as the potential values for this square-wave. The duration each potential is applied is varied throughout the collection of data, with the longest hold duration commonly being 60 seconds, and the shortest being 0.5 or 0.25 seconds. Through continued monitoring of a single wavelength throughout this potential cycling, a data set similar to that shown in Figure 2.3.1.1. is produced.

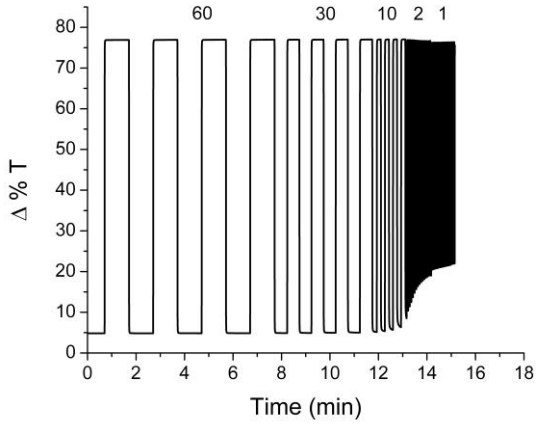

Figure 2.3.2.1. Chronoabsorptometry (kinetic switching) data gathered for a film of ECP-Magenta, cast to 1.0 AU prior to switching, and monitored at the λmax of 608 nm. The duration of potential hold is displayed above the data pertaining to that switching time.

The contrast attained at various switching speeds may be determined by subtracting the transmittance values attained at either end of a switch for that time regime. Indicated by the data shown in Figure 2.3.1.1., for this particular film the re-coloration process appears to be the contrast limiting step, as values of high %T are maintained throughout the

course of the experiment while the full extent of the low transmission values (observed at slower switching speeds) is not attained at 2 and 1 second switching times. Further analysis of this type of switching data would allow for the determination of the time required to attain 90, 95, or 100% of the full switching contrast for that polymer, though this analysis will not be described in this document[105]. Finally, it should be noted that not all ECP films are stable to excessively high switching speeds (e.g. sub-quarter second switching), and care should be taken in the examination of these switching times.

2.4 Colorimetry

Characterization of the electrochemical and optical responses of conjugated polymers on redox cycling are vital points of the description of a material. For the application of polymers designed around their electrochromic properties though, a means of precisely describing the color of a system is greatly valuable. Common language, and even the scientific literature are filled with relative and general terms used to describe color: a ball is red, a wall is painted cherry red, the sky looks burnt red, the ground was reddish-brown, etc. Still, short of a unique name for every color it's possible to perceive, for comparative or research purposes, language is grossly inefficient in accurately describing color. Efforts have been made to fill this need to accurately describe color through quantitative means, beginning in earnest at the end of the 19th century with the Munsell color system, which sought to define groups of colors of a certain similarity[106-107]. The most important aspect of the early Munsell system though was its basis on the human perception of color, rather than the specific groupings described. While the Munsell system is rarely used outside of specialized areas today, the grounding of the Munsell system in the physical phenomena of human color vision became the basis for most modern systems of color quantification, most notable the International Commission on Illumination (Commission Internationale De L'Eclairage) or CIE systems. In the

following section, the theory behind both the human perception of color and the means of quantifying that perception will be discussed.

2.4.1. Color Theory and the CIE Color Systems

One property of ECPs stands in notable contrast to systems that commonly come to mind when displays are considered: electrochromic polymers are non-emissive materials. The colors observed in the neutral states of many electrochromic polymers are not produced through the emission of photons at specific wavelengths, but rather through the reflection (or transmission) of incident light, with portions of the spectrum coinciding to the absorptive properties of the ECP in question diminished or removed. This property is particularly important in the consideration of mixing colors to produce a third color state.

The majority of modern display technologies make use of emissive materials, which mix color stimuli in an additive fashion (where the primaries sum to produce white light), allowing the familiar red-green-blue (RGB) color system to produce full color displays. In contrast, non-emissive materials mix color stimuli in a subtractive fashion (where the primaries sum to remove all light, producing black), leading to the cyan-magenta-yellow (CMY) color system, and these two contrasting color wheels are shown in Figure 2.4.1.1.

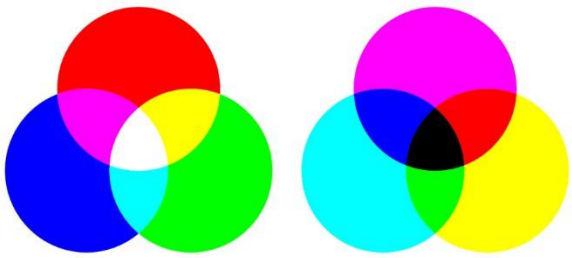

Figure 2.4.1.1. Red-Green-Blue (RGB) and Cyan-Magenta-Yellow (CMY) color wheels, representing additive and subtractive color mixing, respectively.

With a long-term desire for full color display applications for electrochromic polymers, and as a consequence of this correlation between non-emissive materials and a subtractive color mixing system, color mixing in electrochromic polymers is largely dependent on materials displaying neutral-state colors representative of the cyan-magenta-yellow primaries while attaining largely colorless, transmissive oxidized (or bleached) states. Numerous examples of ECPs might be found in the literature which exhibit two distinct color states on either side of its electrochromic switch, for instance from yellow to red, or blue to red, etc. However, these materials are largely unsuitable for the production of full-color displays, due to their incompatibility with the CMY color mixing system. The mixing of polymers exhibiting the desired CMY-to-transmissive switching behavior, and assessments of the accuracy of predicting the color properties of that mixing can be found in Chapters 4 and 5. Before mixing can be discussed in an accurate fashion though, color stimuli must first be quantified in some fashion.

The task of establishing a system for the quantification of color has been undertaken, and further extensively developed, by the International Commission on Illumination (Commission Internationale De L'Eclairage, or CIE)[108]. However, to refer to the guidelines established by the CIE as a quantification of color could be misleading. A more accurate description would be the quantification of the human perception of color. The human perception of a color stimulus begins first in the eye, which is comprised of both "rod" and "cone" light sensitive cell structures. Where rod cells detect merely the intensity and presence of light, cone cells are differentiated into long, medium, and short cones cells, each variety having unique sensitivities to the various wavelengths that form the visible spectrum. Long cones (L-cones) are more responsive to longer wavelength, low energy stimulation, while short cones (S-cones) are more sensitive to short wavelength, high energy stimulation and the sensitivity of middle length cones (M-cones) falls somewhere between. These relative sensitives are illustrated in Figure 2.4.1.2. As mentioned, human perception of color begins in the stimulation of these cells

by light, and this stimulation is transmitted along the optic nerves to the brain, where the sensation of color perception is formed.

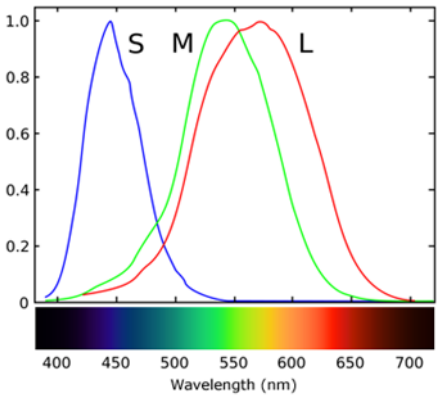

Figure 2.4.1.2. Relative sensitives of short, medium and long light sensitive cone cells comprising the human eye, and the basis of human color vision. Adapted from Ohta *et al*[109].

In order to quantify color perception in the human eye, the spectral sensitivities of the three cone cell types were rendered to numerical descriptions, referred to as color matching functions, and given the names $\bar{x}(\lambda)$, $\bar{y}(\lambda)$, and $\bar{z}(\lambda)$, reflecting the sensitives of L-, M- and S-cones respectively. Taken together, these functions describing the spectral response of the human eye are referred to as the CIE standard observer, shown in Figure 2.4.1.3.

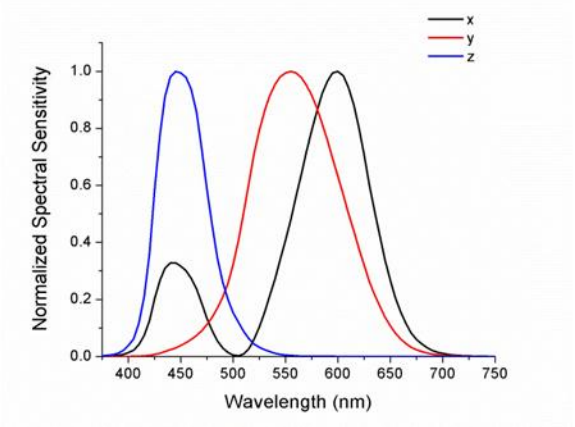

Figure 2.4.1.3. Functions of Standard Observer Functions, describing the activity of the human eye during normal color vision. Adapted from Ohta *et al*[109].

The interplay, or more rudimentarily the overlap, between these three color matching functions with a luminous stimulus having a specific spectral power distribution I(λ) is used to quantify the CIE tristimulus values X, Y, and Z. The equations describing this quantification, assuming a definition of the "visible spectral region" as spanning 380 to 780 nm, are shown below as Equation 2.4.1.1.

$$X = K\int_{380}^{780} I(\lambda)\bar{x}(\lambda)d\lambda \quad Y = K\int_{380}^{780} I(\lambda)\bar{y}(\lambda)d\lambda$$

$$Z = K\int_{380}^{780} I(\lambda)\bar{z}(\lambda)d\lambda \quad K = \frac{100}{\int_{380}^{780} I(\lambda)\bar{y}(\lambda)d\lambda}$$

Equation 2.4.1.1. Relationships between observer functions and the spectral power distribution of a stimulus, producing the tristimulus values X, Y, and Z.

These equations can further be adapted to better suit conditions where light is reflected off of or transmitted through an absorptive material. For the purposes of consistency, the CIE has also described a number of "standard illuminants" for the function of I(λ) (e.g. D50, D65, Illuminant D, etc.) as it is fairly clear that the calculated tristimulus values describing a color are dependent on the power distribution of the illuminant considered. Finally, the K factor calculated as shown in Equation 2.4.1.1. is a normalization constant, ensuring that the values of X, Y, and Z calculated all fall within a certain set of bounds described for the illuminant used.

The tristimulus values X, Y, and Z, while integral to the quantification of a color stimulus, do not themselves describe any particular color. Instead, the relative values of the tristimulus values describe a series of color coordinates that might be plotted into what is more commonly viewed as a "color space". These values describing the relative contributions of the tristimulus values are given the names x, y, and z, and their calculation is shown below in Equation 2.4.1.2.

$$x = \frac{X}{X+Y+Z} \qquad y = \frac{Y}{X+Y+Z} \qquad z = \frac{Z}{X+Y+Z}$$

Equation 2.4.1.2. Calculation of the CIE color descriptors x, y, and z from the Tristimulus values X, Y, and Z.

The color space described by the terms x, y, and z is named the CIE 1931 color space, or the CIE xyY color space and is the characteristic "horseshoe" described by this color system is shown in Figure 2.4.1.4. Within the color space described by the terms x, y, and z are all possible color sensations commonly available to the human eye. The CIE xyz color space offers many unique advantages, such as simple illustration of the product of mixing color stimuli, but it is not without its faults. The work of MacAdam[110] showed that the distance on the chromaticity diagram did not correspond to the degree of difference between two sets of color coordinates. Further work on this notion resulted in the development of the concept of a MacAdam ellipse, which are collections of xyz chromaticity coordinates which describe color stimuli that are visually indistinguishable from one another to the human eye. Later color systems described by the CIE sought to describe a color space with perceptual uniformity, or a color space where the difference between two colors corresponds to their distance from one another within the color space.

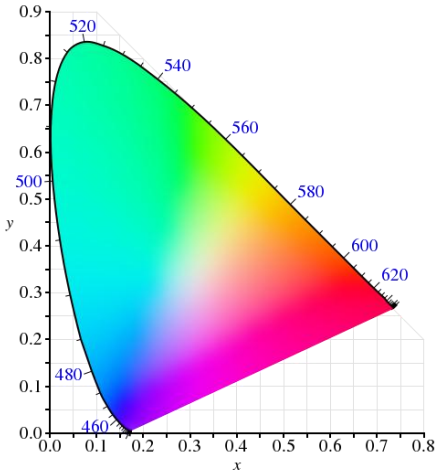

Figure 2.4.1.4. The CIE 1931 color space, described by each possible value for the terms x and y[111].

One result of these efforts is the CIE L*a*b* color space which is frequently used to describe the quantification of color in electrochromic polymers, and will be used throughout the remainder of this document for this purpose. The L*a*b* color space is generated from the tristimulus values X,Y, and Z described above. The equations pertaining to the description of the L*a*b* coordinates are shown in Equation 2.4.1.3., and a visual representation of the L*a*b* color space is shown in Figure 2.4.1.5.

$$L^* = 116\left(\frac{Y}{Y_n}\right)^{\frac{1}{3}} - 16 \qquad a^* = 500\left[\left(\frac{X}{X_n}\right)^{\frac{1}{3}} - \left(\frac{Y}{Y_n}\right)^{\frac{1}{3}}\right] \qquad b^* = 200\left[\left(\frac{Y}{Y_n}\right)^{\frac{1}{3}} - \left(\frac{Z}{Z_n}\right)^{\frac{1}{3}}\right]$$

Equation 2.4.1.3. Equations describing the calculation of the CIE L*a*b* coordinates from the CIE XYZ tristimulus values.

In this color space the value of L* ranges from 0 to 100, and describes the balance between the white-black component of a given color stimulus, 0 representing a black stimulus, and 100 corresponding to a white stimulus. The a* coordinate describes the green-red balance, with negative a* values representing more green, and positive a* values corresponding to reds. Similarly, the b* coordinate describes the blue-yellow balance of a color stimulus, with negative b* values reflecting blue stimuli and positive

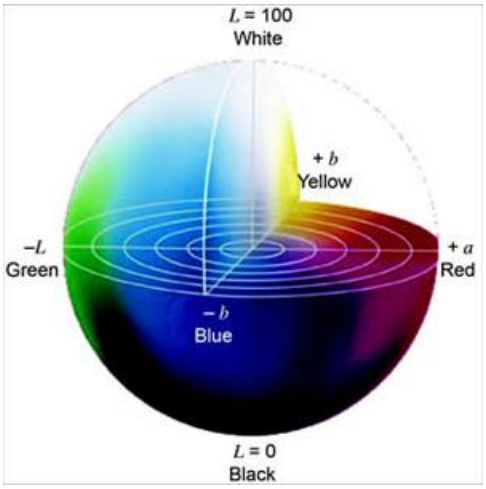

Figure 2.4.1.5. An artist's representation of the CIE L*a*b* color space[111].

b* values indicating a more yellow stimulus. The unique combinations of a* and b* coordinates are used to describe unique and visually distinguishable colors (commonly

referred to as hue), while the increasing values (away from the origin) of these coordinates describe the increasing saturation or intensity of those colors (also referred to as chroma).

2.4.2. Quantification of Color via Instrument and Calculations

When pertaining to the quantification of color in electrochromic polymers, a spectroelectrochemical series as described above will provide the data required for the calculation of color coordinates illustrating the switching behavior[112]. Each spectrum gathered within the series is treated in the fashions described above to yield L*, a*, and b* coordinates, and the series of these L*a*b* coordinates is plotted to describe the chromatic changes undertaken by the ECP under examination throughout its switching behavior. Today, this treatment will most frequently be handled by software designed for that purpose, namely the Star-Tek colorimetry software installed alongside the control programs for the Cary 5000 UV-Vis-NIR spectrometer. As a rule, the settings used to perform these calculations are as follows; a simulated D50 standard illuminant was used, a 2 degree observer function was selected, and values were calculated directly to L*a*b* coordinates rather than say xyY coordinates or tristimulus values. This software package performs no calculations in the calculation of colorimetry data that cannot be performed with a sufficiently sophisticated Excel spreadsheet, as shown by Mortimer *et al*, but it can directly read the .csv files generated by the Scan function of the Cary, which is useful[112]. Additionally, this software can be made to read spectral data produced by other spectrometer control programs, provided sufficient work is put into formatting the data to replicate the style of data produced by the Cary software.

By way of example of the results of this process, a*b* plots and the L* vs voltage (V) trend generated from the spectroelectrochemical series shown in Figure 2.3.1.1 are shown in Figure 2.4.2.1. In this example, of a sample of ECP-Magenta to be specific, relatively high values of both a* and –b* start indicate a fairly colorful neutral state, with

a roughly equal contribution from red and blue stimuli, indicating the purple-magenta neutral state of that polymer. Additionally, at low potentials where this magenta state is dominant, we can see a lower value for L* being recorded, as some portion of the visible spectrum is being attenuated. As the applied potential is increased (as in Figure 2.3.1.1), the values for the a* and b* coordinates decrease towards the origin, until a virtually colorless state is attained at the fully bleached state, and similarly, the L* value is raised as the applied potential increases, as the absorption in the visible is attenuated.

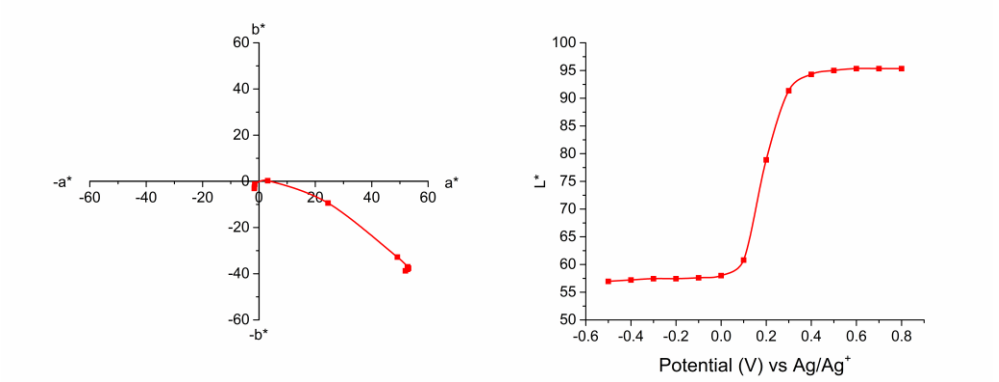

Figure 2.4.2.1. Representative plots of the a* vs b* coordinates and of the L* vs Applied Potential (V).

2.5 Photography

An additional note should be made concerning the photography of electrochromic polymers. As mentioned in the quantification of color stimuli, the spectral power distribution of an illuminant or transmitted light can have a profound impact on the perception of the color of a material. This consideration is vitally important for the photography of ECPs, and care is taken to photograph materials in settings using an illuminant that closely reproduces the spectral power distribution of the standard illuminant used to calculate tristimulus values. In the work presented herein, and in the literature describing electrochromic polymers at large, a D50 light source (whether physically replicated or digitally simulated) is a common choice. The light booths of the Reynolds labs are constructed to simulate this light source. Additionally, as various wavelengths of light might be reflected or transmitted to various degrees depending on an

angle of incidence, care is taken to ensure that an illumination/viewing angle of 0/0 degrees is used for both quantification and photography. Additionally, photography should be performed both prior to and after the electrochromic break-in cycle.

2.6 Photostability of Electrochromic Polymers

The study of the photostability of electrochromic polymers, which in this document is undertaken through the long-term exposure of ECP films to a solar simulator lamp, represents an additional departure from the suite of methods commonly employed in synthesis and characterization. Rather than an emphasis on the immediate characterization of a cast material, samples are placed into a certain environment, and efforts must be taken to ensure that that environment is not perturbed throughout the exposure to the light source being used. The following sections will detail the steps taken to prepare and encapsulate the samples under investigation from the outside environment, the operation of the light source used to assess the photostability of these materials, and finally detail pertaining to the characterization of the samples used in this study after long-term exposure.

2.6.1. Sample Preparation and Encapsulation

As mentioned, a significant focus in the study of ECP photostability is given towards the encapsulation of samples within a specific atmosphere, and the long-term ability of the encapsulation method used to isolate samples from ambient atmospheric conditions. However, prior to encapsulation, films must be cast onto a substrate suitable for later characterization. In the study presented in Chapter 6, thin films of two polymers, the poly(ProDOT) homopolymer (ECP-Magenta) and an N-alkylated poly(ProDOP) (MCCP) were used. The casting of films of these two polymers followed the methodology outlined in section 2.1.1, with each sample being dissolved in toluene to a concentration of 5 mg/mL, and spray cast using nitrogen at a pressure of 20 psi, until an

absorbance of 1.0 ± 0.1 AU was reached as measured using the Cary 5000 UV-Vis-NIR. An ITO-glass substrate (8-12 Ω/sq) was used for casting, again, as described in section 2.1.1. Due to a need to minimize encapsulant material usage multiple films, each measuring roughly 7 x 50 mm, were cast onto substrates measuring 25 x 75 x 0.7 mm through the use of a shadow mask placed over the substrate. After irradiation, samples were cut to size (7 x 75 mm) through the use of a diamond-tipped etching tool (SPI Supplies, 90° tip angle).

Following the casting of films, samples were separated into two groups for encapsulation. The first group would be sealed on the benchtop with no steps taken to exclude atmospheric oxygen or moisture from the sample, ensuring ambient atmospheric conditions within the sample throughout the course of exposure. A second group was moved into a glove box with an argon atmosphere for encapsulation, preventing the interaction of oxygen or water with the polymer samples throughout the course of irradiation. Additionally, a third group of samples was encapsulated within the argon atmosphere of a glove box, however these samples incorporated a 0.5 M $TBAPF_6$/PMMA/PC electrolyte, prepared as described in section 2.1.2.

The encapsulant used throughout this study is composed of a polyisobutylene (PIB) tape provided by ADCO Products, Inc. (HelioSeal™ PVS 101), supplied by Prof. Samuel Graham of the Georgia Institute of Technology. This rubber was filled with desiccant materials to lower water transmission rates, and was further modified with silane coupling agents to promote bonding with glass surfaces[113]. In order to form a seal around the cast samples, thin ribbons of this tape (1-2 mm wide) were manually cut from the larger tape and placed around the edges of the substrates onto which polymer films had been cast. After placing the PIB ribbons on the film substrates, a microscope slide cut to match the size of the ITO-glass slide was placed on top, creating an impermeable top barrier. For samples incorporating the electrolyte mixture, the solution was pipetted into the reservoir created by the surrounding edge sealant prior to the addition of the top glass

slide. To ensure bonding to both glass slides, the samples were heated on a hot plate to a temperature of roughly 110 °C, and compressed for five minutes. After allowing the samples to cool, the atmospheric environment inside of the samples was protected by an edge sealant that has been shown to have very low oxygen and water transmission rates.

2.6.2. Atlas XLS+ Testing Chamber and its Operation

After the encapsulation of polymer samples, films were irradiated in an Atlas SunTest XLS+ benchtop testing system. This system features a single xenon arc lamp as its light source, and a glass window between this lamp and the sample testing bed was used to filter the light to approximate the spectral power distribution of natural sunlight. Further, the energy output of the Xe lamp may be tuned, to a certain degree, and the energy output of this lamp was adjusted to measure 1000 W/m^2, through the use of a calibrated silicon photovoltaic reference cell (Oriel I-V Test Station, Model 91150V, Newport Corporation). This was done in an effort to replicate the solar output expected from the AM 1.5 light source frequently employed in the study of photovoltaics, as defined by the American Society for Testing and Materials (ASTM)[114]. Once the output of the lamp has been set, the operation of this testing chamber is extremely simple. Through the use of a touch-screen interface on the front of the chamber, programs may be created for the irradiation of samples, with cut-offs based either on irradiation time, wattage output, or total experiment time may be selected. In the data presented in Chapter 6, the variable used to examine photostability in ECPs was the total irradiation time endured by samples, and programs were created for this purpose with irradiation times ranging from 24 hours out to 1 month of total irradiation time (or 744 hours, 31 days). In order to compare the irradiation time within the sample chamber to a "real world" parallel, many manufacturers may supply a spreadsheet capable of making a rough estimation upon (occasionally persistent) request. These conversions are largely predicated on the wattage setting used throughout irradiation, whether or not sample

heating was utilized, and the temperature of that heating, in combination with the duration of sample testing. The real world reference used to make these conversions are frequently dosimetry values for some prolonged period of time, in a specific geographic region. One commonly employed reference is referred to as a "Florida sun test". In practical terms, test samples are placed at some location in southern Florida, and exposed to the relatively harsh conditions of that environment months or years at a time. Using dosimetry values recorded during long-term testing sessions (years at a time), a rough equivalency can be drawn between the dosage with which a testing sample is irradiated in a testing chamber with that to which it may have received during one of these "Florida tests". It should be again stressed that these conversion values are in no way concrete values, having their basis as such variable factors such as the weather in southern Florida, but they might be used to offer a very rough guideline for actual usage conditions. In the case of the wattage used in these experiments, the dosage delivered to samples corresponds to a conservative estimate of 6-12 months in outdoor Florida testing conditions. Further, a subset of samples from each grouping were used as "standards" for the effects of the irradiation. These samples were fabricated and encapsulated in a fashion identical to those that underwent irradiation in the Suntest XLS+ system, however these samples were instead stored in darkness. These standard samples were stored for time periods identical to those used for irradiation. Following exposure or storage for the requisite time point, samples were gently heated on a hot plate (70 °C) and the top microscope slide cover and any remaining PIB sealant was removed from the ITO-glass substrates.

2.6.3. Sample Characterization: Spectroelectrochemistry and XPS

Following sample irradiation, sample characterization was directed towards assessing the electrochromic performance retained by samples, as well as an examination of what if any chemical transformations had taken place during the course of exposure to

the high-intensity light source. The first focus of characterization, the assessment of electrochromic performance, was carried out through the use of cyclic voltammetry and spectroelectrochemistry. The methodologies utilized for both of these techniques match those described in sections 2.2.1 and 2.3.1. A 0.5 M $TBAPF_6$/PC electrolyte system was used for both techniques, which were run concurrently for each sample. During cyclic voltammetry, a three electrode cell was constructed within a cuvette as described in section 2.2.1, and 5-10 cycles at a scan rate of 75 mV/s were used to break each sample in prior to spectral analysis. During spectroelectrochemistry, data was recorded in a window of 350-1600 nm.

In addition to the spectroelectrochemical characterization, x-ray photoelectron spectroscopy, or XPS, was used to probe composition of the surface of photostability samples. The instrument used to perform XPS studies on the samples prepared was a Thermo Scientific K-α X-ray photoelectron spectrometer. In short, this system, and most modern, commercially built XPS apparatuses function in the following fashion. An aluminum source is bombarded with high-energy electrons from a heated filament, inducing that source to emit primarily x-rays of an energy corresponding to the relaxation of an electron from the "L" shell or the 2p orbitals to the "K" shell, or 1s orbital of that aluminum source. The emitted x-ray light is non-monochromatic, and monochromation is normally produced by diffracting this beam off of a quartz disk, followed by re-focusing of the x-ray beam. This monochromated x-ray light, the energy of which is sufficient to liberate and eject core electrons, is directed onto the surface of the sample under examination. The ejected electrons are passed through an electron kinetic energy analyzer, which in this instance (and quite frequently) is a hemispherical kinetic energy analyzer (HKEA). By sweeping the pass energy of the HKEA, the full range of electrons ejected by the incident x-rays may be detected with a band pass dictated by the specifications of the HKEA, and a signal in electron counts is detected by some electron capture device following the energy analyzer. The binding energies of the detected

electrons is calculated, in a simple sense, via assuming a conservation of energy from the incident x-rays. As the x-ray photons have a well-defined energy upon monochromation (~1486 eV), the binding energy of an ejected electron corresponds to the energy of the x-ray photon that liberated it, less the kinetic energy retained by the electron on ejection. As electron binding energies are often characteristic to specific elements, and further specific to the chemical environment surrounding the atom from which it was liberated, XPS data is most often presented as the electron counts detected against an axis of binding energies in electron-volts (eV), as shown in Figure 2.6.3.1. Spectra are often presented either as including data from the entire breadth of binding energies examined, referred to as a survey spectrum, or as narrower, element and orbital specific scans.

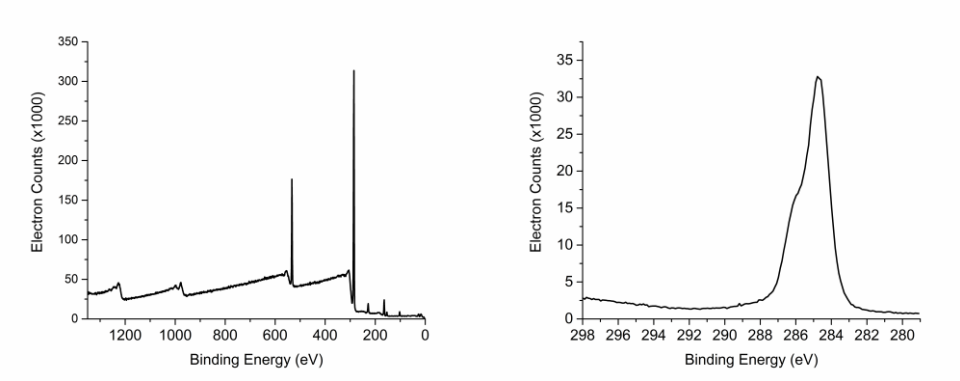

Figure 2.6.3.1. Representative survey (left) and element specific (right) spectra x-ray photoelectron spectrographs. The element specific spectrum corresponds to the binding energy of carbon 1s electrons.

Naturally, additional considerations must be taken when using this technique, the least of which is the necessity of an ultra-high vacuum (UHV) environment within the entire sampling chamber to allow for a sufficient flux of x-rays to the sample target, and an environment in which ejected electrons might have a mean free path sufficient to reach the detector assembly unperturbed. Due to the need for a UHV environment in particular, XPS samples are typically solid surfaces. Additionally, due to the requirement that ejected electrons have a mean free path long enough to reach the detector, electrons ejected from material any deeper than roughly 8-12 nm in a sample are rarely if ever

detected, as collision with sample material closer to the surface is nearly a certainty. This last aspect makes XPS a particularly surface-sensitive technique, and though depth profiling with reactive ion etching is a possibility, this technique was not employed in the work described in Chapter 6.

Both the ProDOT and ProDOP polymer samples mentioned above were analyzed via XPS, and element specific spectra were gathered for the C1s and O1s orbitals for all samples, and the S2p and N1s orbitals for the thiophene and pyrrole based materials, respectively. Repeated scans were signal averaged to produce the acquired data, and the number of scans collected for the C1s, O1s, S2p and N1s orbitals were 4, 4, 16, and 12, respectively. Prior to each scan, the analysis chamber of the XPS system was permitted to reach a pressure no greater than 10^{-8} torr. An elliptical spot size of 400 μm (long axis) was used to irradiate the surface of samples. Further, due to the semiconductor nature of the conjugated polymer films examined, a low energy electron "flood gun" was used to minimize sample charging throughout examination, and maintain sample neutrality.

CHAPTER 3

SUPERCAPACITORS UTILIZING HIGH SURFACE AREA CARBON SUBSTRATES MODIFIED WITH REDOX-ACTIVE POLYMERS

In this chapter, we will be examining the application of redox-active, conjugated polymers for charge storage applications. The faradaic processes tied to the redox reactions can be viewed as analogous to the static double layer capacitance encountered in common capacitors, however the energy and power densities frequently encountered in the application of pseudocapacitive polymers show the potential to bridge the gap between batteries and capacitors. Materials and devices with the potential to bridge this gap, discussed in Chapter 1, are often referred to as supercapacitors. Specifically, the following chapter describes the utilization of a recently developed aqueous solution processable PEDOT analog, and its application to "high surface area" carbon nanotube (CNT) electrodes. The fabrication of the composite polymer-CNT electrodes, as well as their utilization in a supercapacitive device will be described, followed by an examination of the charge storage properties of the resultant devices.

3.1. Pseudocapacitive and High Surface Area Electrode Materials

As discussed in Chapter 1 pseudocapacitive materials such as conjugated polymers or redox-active transition metal oxides are, when properly utilized, often observed to demonstrate energy and power densities characteristic of the "supercapacitor" region of the Ragone plot[69]. However, pseudocapacitive materials are not the only class of materials able to attain these values. Supercapacitors predicated on carbon electrode materials, such as activated carbon powders, graphene and its oxides, as well as carbon nanotubes have become a major focus in the development of

supercapacitive materials[20, 75-77, 115-119]. As the mechanism of charge storage in many of these carbon-based electrode materials centers around the formation of a double layer, as in a traditional capacitor, the particularly high surface areas frequently observed in many carbon materials is the route through which supercapacitive behavior is reached. These high surface areas also makes them an attractive candidate for the creation of composite electrodes, as the charge stored by pseudocapacitive materials is also a function of surface area. Further, while the thermal and electrical properties of many carbon based electrode materials are excellent, the mechanical and flexibility properties of one material in particular drew attention. This material, a non-woven CNT textile or fabric produced via a continuous vapor deposition process, is an excellent candidate for pseudocapacitive material functionalization and indeed reports of such efforts can be found in the literature[99, 120-121]. Of particular note is a report of the functionalization of this non-woven CNT textile with PANI via electrodeposition, producing physically robust, flexible electrodes, photographs and SEM images of which are shown Figure 3.1.1.1. The images shown serve to demonstrate the mechanical flexibility of the CNT substrate both (a) pre- and (b) post-PANI deposition, and illustrates various PANI morphologies obtained when electrodeposition is performed at various current densities, ranging from 2 to 16 mA/cm^2, showing the retention of an open, porous morphology. The demonstration of this material's utility in the fabrication of composite carbon-based electrodes brought the material to our attention, and samples of this CNT textile were generously provided by the research group of Dr. Gleb Yushin of the Georgia Institute of Technology.

As with the double layer capacitance of carbon electrodes, the charge stored by pseudocapacitive materials is a function of surface area. Further, the contribution to the total capacitance in a device from pseudocapacitive materials may be much higher than double layer capacitance, by as much as 100 fold[122]. It therefore becomes desirable to merge these two classes of supercapacitive materials so to speak, utilizing carbon substrates as high surface area scaffolds onto which pseudocapacitive materials might be

deposited. The fabrication and study of carbon-pseudocapacitor composites has been an active field of research, making use of a broad variety of both carbon and pseudocapacitive materials[99, 123-130].

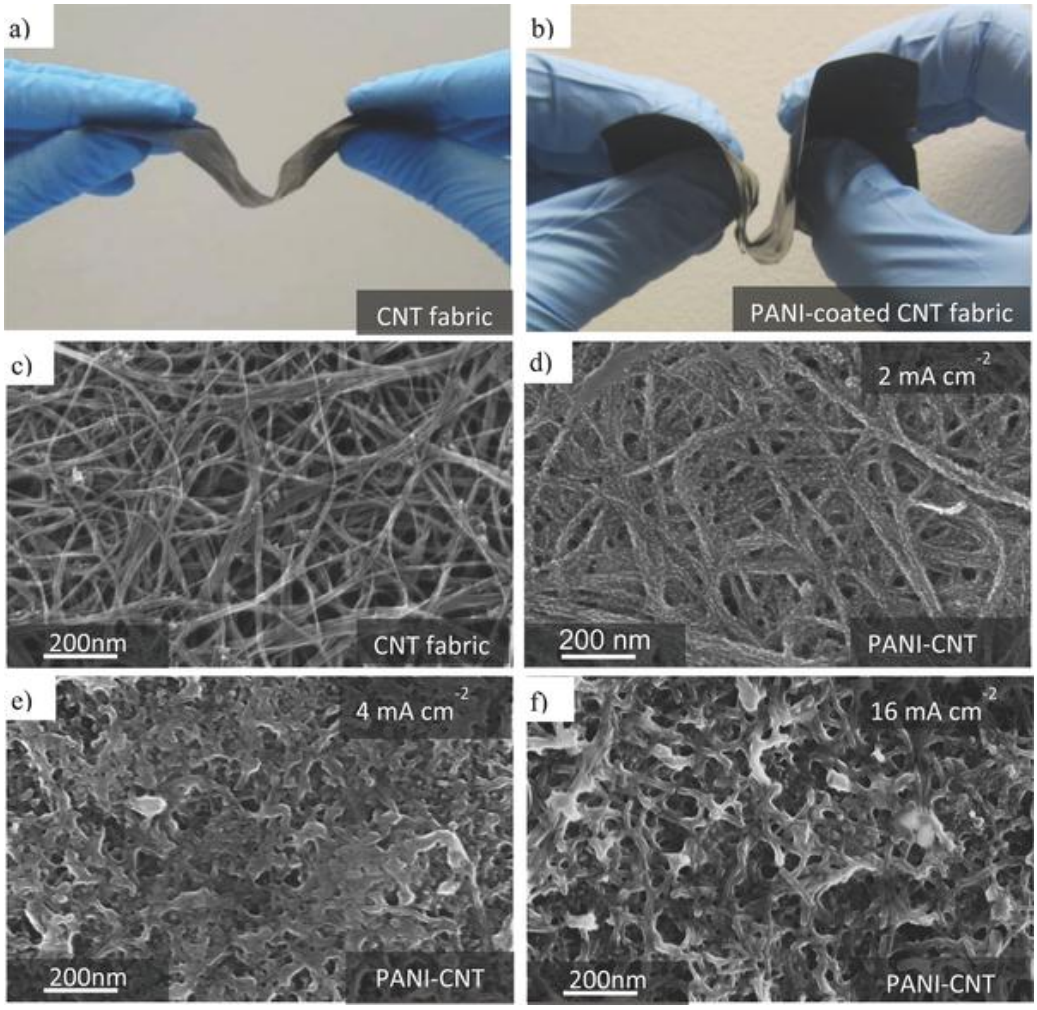

Figure 3.1.1.1. Photographs and SEM images of PANI-coated non-woven CNT textile. Reproduced with permission from Benson *et al*[99]. Copyright 2013, Wiley-VCH.

Focusing particularly on the application of conjugated polymers, polyaniline (PANI), polypyrrole (PPy) and poly(3,4-ethylenedioxythiophene) (PEDOT) have been utilized in the production of these composite electrodes[86-96]. As discussed in Chapter 1, many of these reports utilize electrochemical polymerization as the means through which carbon electrode substrates are modified with pseudocapacitive polymers, a process which is fairly difficult to bring to a large, high-throughput scale[90, 99-100]. In specific

relevance to the work detailed in this chapter while the redox characteristics of PEDOT, such as a low onset of oxidation, broad electroactive window, and stability to repeated cycling, are desirable, due to its lack of appended solubilizing groups PEDOT itself (and its propylene bridged analogs) are all but insoluble and are commonly electrodeposited[131-133]. Recently, synthetic efforts directed towards the creation of soluble PEDOT analogs, chiefly through copolymerization of ProDOT and EDOT monomer units (the prior being modified with solubilizing groups) has produced a soluble, solution-processable polymer with remarkably similar redox properties to pure PEDOT. The repeat unit structure of this polymer is composed of one ProDOT unit flanked by EDOT units, and therefore referred to as solvent resistant ProDOT-$EDOT_2$ (shortened to SR-ProDOT-$EDOT_2$) throughout this document, is shown in Figure 3.1.1.2.

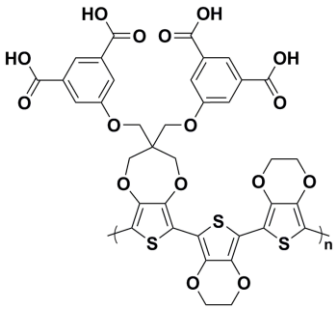

Figure 3.1.1.2. Repeat unit structure of SR-ProDOT-$EDOT_2$.

The synthesis and characterization of this material will be detailed elsewhere, however its utilization as an organic and aqueous solution processable, pseudocapacitive PEDOT analog is described in the following sections. Further, a specific nomenclature has been develop to refer to this material based on its solubilizing functionalities, which will be discussed further in section 3.2.1.

3.2 Solution Processing of Pseudocapacitive Material

As previously mentioned, the overwhelming majority of research into the application of pseudocapacitive, conjugated polymers for charge storage applications have utilized electropolymerization as the means through which electrode surfaces are

modified. While the production of solution processable conjugated polymers was reported years ago, via the addition of alkyl chains in the case of organic solubility and functionalization with carboxylate groups in the case of aqueous solubility, the materials produced through these means displayed redox properties with greatly reduced potential for applications in charge storage, owing to their narrow electroactive windows[32, 134]. Recently, efforts to create materials which possess both the redox properties desirable for charge storage application and solution processability have produced the polymer shown in Figure 3.1.1.2., opening new avenues for composite electrode supercapacitors fabrication. Naturally, the application of solution processing to supercapacitor fabrication presents a new suite of challenges, and preliminary attempts in this direction are described in the following section.

3.2.1. Polymer Drop Casting

As described in Chapter 2, the solution processing technique chosen for the production of composite CNT-polymer electrodes was drop casting. With the goal of creating a homogenous coating of pseudocapacitive material throughout as much of the porous carbon textile as possible, this technique was chosen in favor of other solution casting techniques such as spray casting, due to the longer drying times associated with drop casting. While amenable to the casting of films onto non-porous surfaces, the drying times of aerosolized droplets of polymer solutions (frequently seconds in the case of organic solvents or aqueous solutions cast onto a heated substrate) are likely too short to allow for any form of penetration into the porous network of CNT fibers that comprise the CNT textile substrate. Additional detail pertaining to the drop casting carried out to produce the composite CNT-polymer electrodes examined in this chapter may be found in Chapter 2, however a description of the modification of the solubility of ProDOT-$EDOT_2$ used to achieve the final electrode structures is warranted, and a scheme of this process is shown in Figure 3.2.1.1. As synthesized, ProDOT-$EDOT_2$ features branched 2-

ethylhexyloxy solubilizing groups, frequently utilized to impart solubility in organic solvents such as toluene or chloroform[32]. To render this structure soluble in an aqueous environment, the 2-ethylhexyloxy moieties are saponified via reflux in the presence of potassium hydroxide, producing the polycarboxylate salt referred to as water soluble ProDOT-EDOT$_2$ (WS-ProDOT-EDOT$_2$)[134].

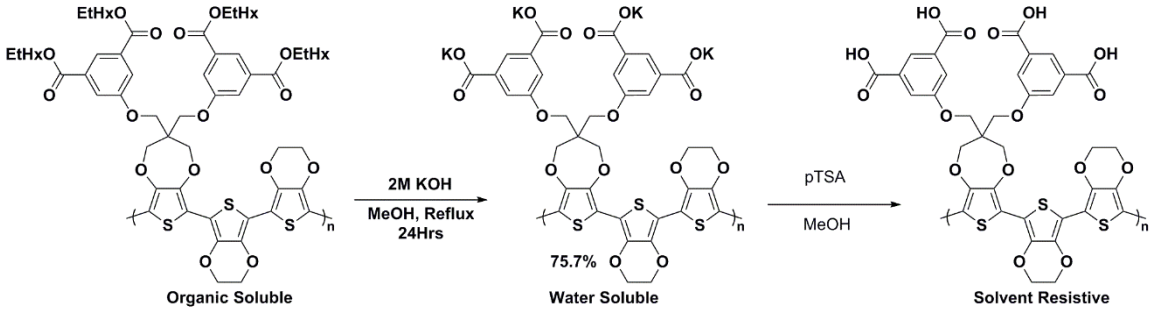

Figure 3.2.1.1. Defunctionalization of an organic processable ProDOT-EDOT$_2$ structure to a water processable salt, followed by protonation to a solvent resistant acid.

Solutions of this polycarboxylate salt were prepared, as described in Chapter 2, and were drop cast onto the surface of samples of the non-woven CNT textile substrate, described above. After allowing sufficient time for solvent evaporation, polymer films were observed to solidify on the surface of the CNT textile samples, and ostensibly, within the interior of these substrates as well. It is well worth noting that a number of caveats are deserving of recognition in this process. First, while polymer films were observed to solidify following drop casting onto the CNT substrates, in all likelihood, some casting solvent remains in the cast films. The description of these films as "dry" only serves as a relative description, and does not attempt to describe the cast films as devoid of solvent. Second, in the absence of the physical observation of penetration of cast polymer into the interior of the CNT substrate, polymer films can only be assumed to be in contact with any of the interior surface area of the CNT substrate. The application of electron microscopy techniques, such as scanning electron microscopy (SEM), to a cross section of the composite electrodes offers to clarify this point, which will hopefully be addressed in the near future. As mentioned, drop cast solutions were allowed to dry,

and the resulting CNT-polymer composites were subsequently immersed in a solution of para-toluenesulfonic acid (pTSA) in methanol to pronate the carboxylate salts, rendering the cast ProDOT-$EDOT_2$ films largely insoluble.

In order to gauge the capacitive contribution of cast ProDOT-$EDOT_2$, the modification of the CNT substrates was carried on a percent weight (wt%) basis. In this scheme, the mass of ProDOT-$EDOT_2$ added to each CNT substrate was set to be some percent of the average weight of the CNT textiles, i.e. if a CNT textile was seen to have a mass of 2.0 mg, a 50 wt% modification of this substrate with ProDOT-$EDOT_2$ would see 1.0 mg of polymer cast onto the substrate, and the resulting composite would have a nominal weight of 3.0 mg. In this fashion, composites electrodes were fabricated at weight percent modifications of 20, 40, 60, 80, 100, and 150 wt%. The mass of ProDOT-$EDOT_2$ cast onto the CNT textiles was controlled via variation of the volume of drop cast polymer solution, as the solution was produced at a known concentration of 5 mg/mL.

3.3 Supercapacitors Utilizing HSAE-Redox Polymer Composites

Following fabrication of the composite non-woven CNT textile-ProDOT-$EDOT_2$ electrodes, characterization of capacitive performance was carried out in a symmetrical device setting. The following sections describe the fabrication of supercapacitor devices utilizing the composite electrodes described above, as well as the characterization of the capacitive properties of composites as a function of weight percent ProDOT-$EDOT_2$ added.

3.3.1. Device Preparation

Following the casting of ProDOT-EDOT2 onto the non-woven CNT textile substrate to produce the composite CNT-polymer electrodes, pairs of these electrodes were used to produce supercapacitor devices, and a more detailed description of this process may be found in Chapter 2. In this process, pairs of composite electrodes

(featuring the same wt% polymer modification) were wet with a previously prepared aqueous electrolyte solution. Due to the mechanical flexibility of the CNT substrates (and the resulting composites), a metallic flag made from stainless steel shim stock was used as a more rigid current collector. The stainless steel flags used were expected to contribute very little capacitance to the completed device structure and to evidence this cyclic voltammograms, collected from devices fabricated with stainless steel alone vs unmodified CNT textile placed in contact with the stainless steel shim stock, are shown in Figure 3.3.1.1., showing the minimal charge contribution of the stainless steel electrode.

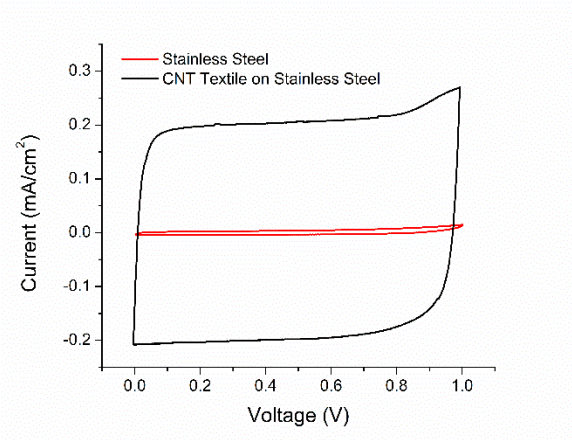

Figure 3.3.1.1. Cyclic voltammograms of capacitive devices utilizing stainless steel electrodes vs electrodes of CNT textile on stainless steel backing.

The composite electrodes, following wetting with the aqueous electrolyte, were placed on the surface of the stainless steel flags. It should also be noted that prior to device fabrication, a bias which is expected to oxidize the cast ProDOT-$EDOT_2$ was applied to one electrode, and that this "pre-doping" is essential for optimal device performance, as has been documented elsewhere[132]. Pairs of electrodes (CNT-polymer composite on a stainless steel shim backing) were separated using cellulose filter paper soaked in the aforementioned electrolyte solution, and glass slides were used as an outer housing for the "device", which was held together via the compression supplied by a pair of binder

clips. Connections were made to either electrode via the stainless steel flags, the ends of which extended out of the glass slide housing.

3.3.2. Device Characterization

Initial characterization of devices utilizing the composite CNT:ProDOT-$EDOT_2$ electrodes consisted primarily of cyclic voltammetry, carried out as described in Chapter 2. Cyclic voltammograms were recorded at various scan rates (20, 50, 100, and 200 mV/s) in a one volt range (0 to 1 V, a range determined by the stable cycling range for the aqueous electrolyte mixture) for devices comprised of composite electrodes featuring each wt% ProDOT-$EDOT_2$ modification previously mentioned, from 0 wt% (unmodified CNT textile) to 150 wt%. Cyclic voltammograms recorded at 20 mV/s representative of devices produced using composite electrodes of each wt% modification produced are shown in Figure 3.3.2.1., illustrating the roughly linear trend in peak current values recorded and increasing ProDOT-$EDOT_2$ content.

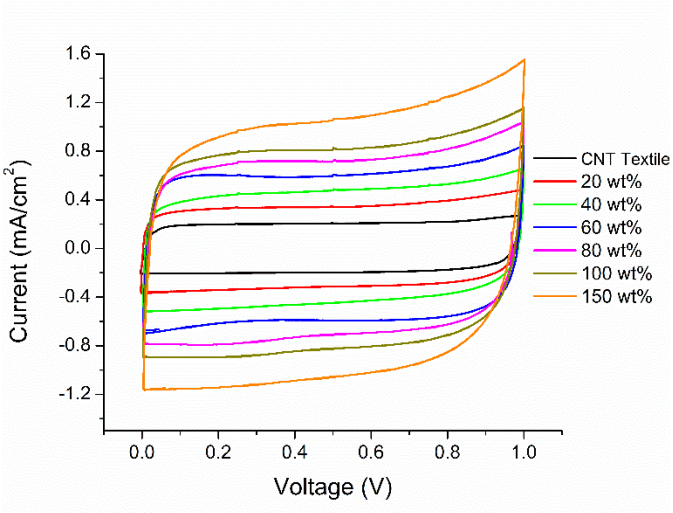

Figure 3.3.2.1. Cyclic voltammograms of prototype supercapacitor devices, composed of unmodified non-woven CNT textile and various weight percent additions of the ProDOT-$EDOT_2$ pseudocapacitive polymer, recorded at a scan rate of 20 mV/s.

Worth noting here is the range of scan rates applied in the course of cyclic voltammetry, which were 20, 50, 100, and 200 mV/s. A challenge frequently encountered in the use of

high surface area electrode materials, particularly those predicated on double layer capacitance, is the that there is often a trade between ever higher surface areas (and consequently energy densities) and the speed at which charge may be added or removed from electrode materials. As a consequence of this, scan rates commonly employed in characterizing high surface area materials (optimized for energy density) are low, on the order of single to tens of millivolts per second, with values ranging from 2 to 20 mV/s frequently cited[92, 135]. In regard to a one volt operating window, these scan rates correlate to anywhere from 200 second to 50 second charge/discharge times, directly impacting the metric of power density (kW/kg). Naturally, the vast range of opportunities for the employment of supercapacitive devices means that and equally vast range of power and energy density requirements will need to be met. However the redox properties of ProDOT-$EDOT_2$, which is observed to switch very rapidly, allows for higher scan rates and therefore higher power densities to reasonably, i.e. without an excessive loss in capacitive performance, be examined.

As previously mentioned, a roughly linear trend is seen in the correspondence between peak current values observed during the recording of CV experiments and the wt% ProDOT-$EDOT_2$ modification. This roughly linear trend is further evidenced when the average values for capacitance, calculated on the basis of both areal and mass capacitance (mF/cm^2 and F/g, respectively), is plotted vs the percent substrate mass polymer addition, as is done in Figure 3.3.2.2., for capacitances calculated at a scan rate of 20 mV/s. It should be duly noted that the mass values used to calculate the data shown in Figure 3.3.2.2. represent the mass of the composite electrodes alone (the sum of the CNT and ProDOT-$EDOT_2$), and that the masses of the electrolyte, filter paper separator, stainless steel electrode, or glass slide housing were not taken into account. Further, this is also the case wherein energy and power density values are discussed later.

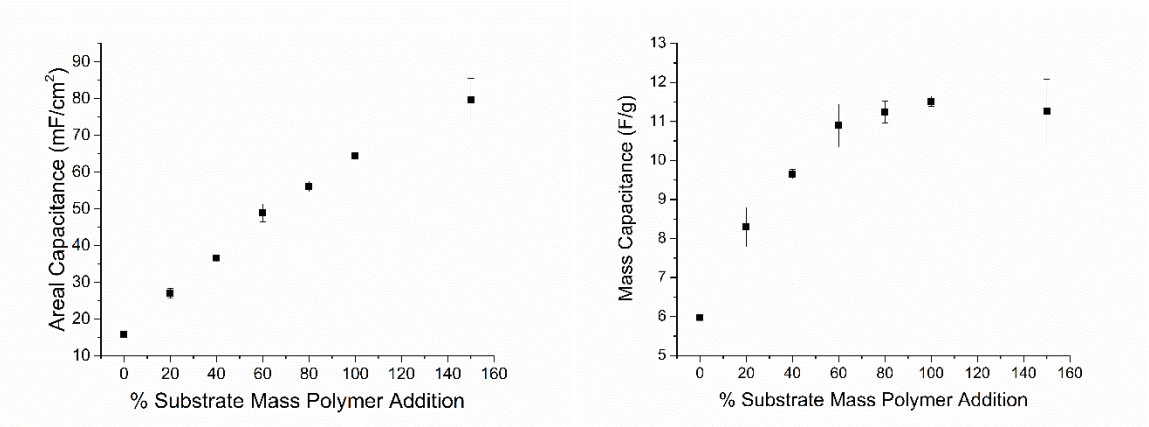

Figure 3.3.2.2. Trend in areal and mass capacitance values vs weight percent addition of ProDOT-EDOT$_2$, calculated at a scan rate of 20 mV/s.

The trend in areal capacitance is observe to increase throughout the wt% modification range examined. This particular trend is not unexpected, as the geometric area of the CNT substrates was fixed at 1.56 cm^2 while additional pseudocapacitive material was added throughout the trend. More telling however is the trend observed in the mass capacitance values. At lower wt% values, a linear growth is observed, ranging from 0 wt% to roughly 60 wt%, and representing nearly a doubling in the mass capacitance values recorded (6 vs 11 F/g). However following this range, beginning at 80 wt% added ProDOT-EDOT$_2$, values calculated for mass capacitance are observed to plateau as expected, with a minimal change in mass capacitance observed between 80 and 100 wt%, and a slight loss recorded at 150 wt%. This observation served to further qualify the trend observed in Figure 3.2.2.1., by determining the optimal wt% ProDOT-EDOT$_2$ modification. Given its position as the highest observed mass capacitance prior to the first observed loss, samples with 100 wt% cast ProDOT-EDOT$_2$ were determined to be the "optimal" electrode composition. Cyclic voltammograms representative of devices fabricated using this electrode composition are shown at various scan rates in Figure 3.2.2.3.

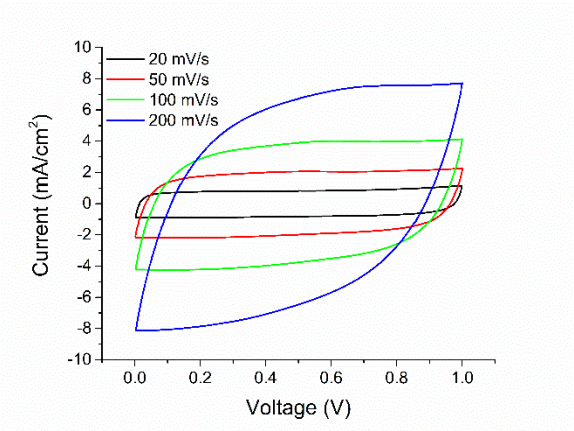

Figure 3.3.2.3. Cyclic voltammograms of non-woven CNT textile/ProDOT-EDOT2 composites with 100 wt% ProDOT-$EDOT_2$ content at various scan rates.

As previously mentioned, the exceptional redox properties of ProDOT-$EDOT_2$ (to be detailed elsewhere at a later date), allow for the examination of capacitive characteristics at much higher scan rates than are commonly employed, and the CV traces shown in Figure 3.3.2.3. illustrate desirable characteristics for charge storage applications, such as a nearly rectilinear I-V relationship at scan rates as high as 100 mV/s, while a nominal loss in this aspect of performance is noted at 200 mV/s. Recently, a method to qualify this desired capacitor behavior has been suggested in the literature as borrowing from a common method of photovoltaic characterization, in the form of calculator of the CV "fill factor"[132]. In short, the ideal performance of a capacitive device would be an entirely rectilinear I-V relationship, and the calculation of a fill factor value attempts to quantify the deviation from this ideal behavior. The higher the degree of "fill" in this ideal behavior observed in a CV trace recorded for a device, the more ideal its capacitive behavior. This concept is illustrated in Figure 3.3.2.4., showing the cyclic voltammogram of a device fabricated with 100 wt% composite electrodes. Further, fill factor values were calculated for this "optimum" electrode composition at various scan rates, and these values are also shown in Figure 3.3.2.4.

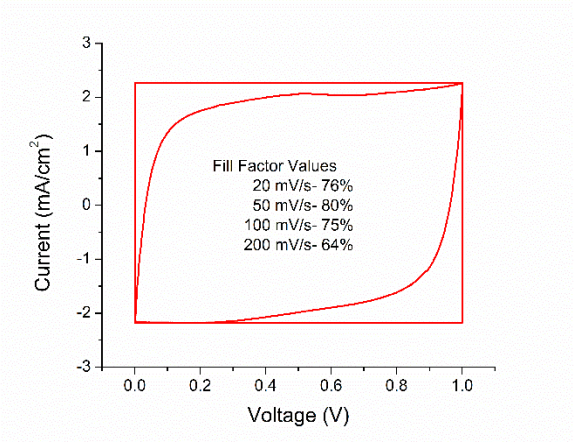

Figure 3.3.2.4. Representative cyclic voltammogram recorded at 50 mV/s, illustrating the concept of calculating fill factor in a charge storage application.

The loss in capacitive performance at higher scan rates shown in Figure 3.3.2.3. and Figure 3.3.2.4. is, to varying degrees based on electrode composition, nearly a universal feature of the CNT:ProDOT-EDOT$_2$ electrodes described in this work, and indeed in nearly all reports of composite pseudocapacitive electrode materials. To further demonstrate the trends in capacitance values at higher scan rates, average values for areal and mass capacitance are shown as a function of scan rate in Figure 3.3.2.5.

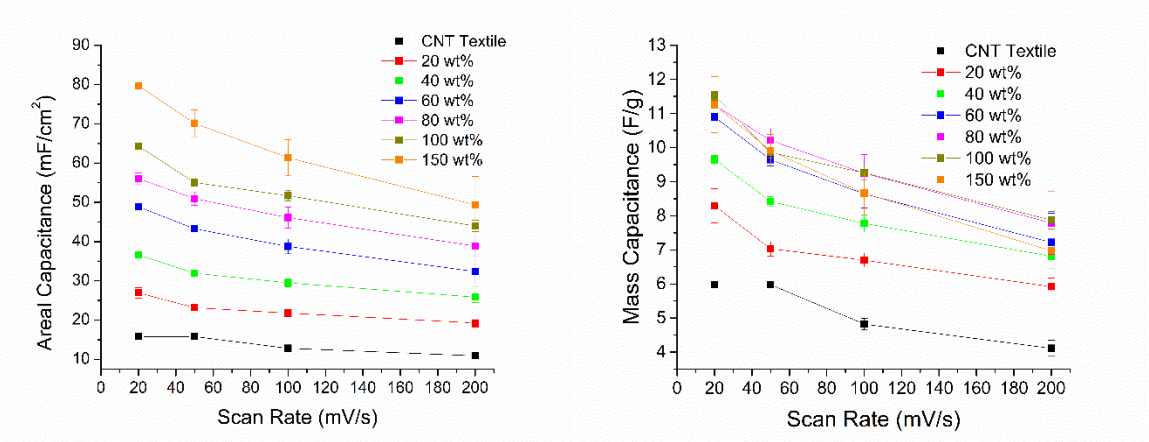

Figure 3.3.2.5. Scan rate dependence of areal and mass capacitance for various non-woven CNT textile/ProDOT-EDOT$_2$ composite devices.

As mentioned, an inverse relationship between scan rate and capacitive figures of merit is seen for each electrode composition. However, the trends observed in Figure 3.3.2.5. extend beyond the quantification of areal and mass capacitance values. The trend in the

energy density (given units of W*h/kg), shown in Figure 3.3.2.6., is observed to follow closely with the trends seen in the values of mass capacitance vs percent polymer addition and capacitance vs scan rate. At a constant scan rate, values are seen to climb as a function of percent substrate mass polymer addition, plateauing at 80 to 100 wt% cast ProDOT-$EDOT_2$, and descending to a very minor degree at 150% polymer addition. Further, each of these values is seen to decrease with increasing scan rate. The trend recorded in power density (in units of kW/kg) however, follows a slightly different albeit expected pair of trends. As with the previously calculated capacitive figures of merit, the value of power density is seen to increase with increasing ProDOT-$EDOT_2$ content in the composite electrodes, again plateauing at values of 80 to 100 wt%, and decreasing to some nominal degree at a composition of 150 wt% ProDOT-$EDOT_2$. However, the trend in power density as a function of scan rate follows an inverse relationship with regard to scan rate, in contrast to all other figures of merit used to qualify device performance. Given the definition of power as the transfer of energy as a function of time, this relationship with scan rate is hardly unexpected.

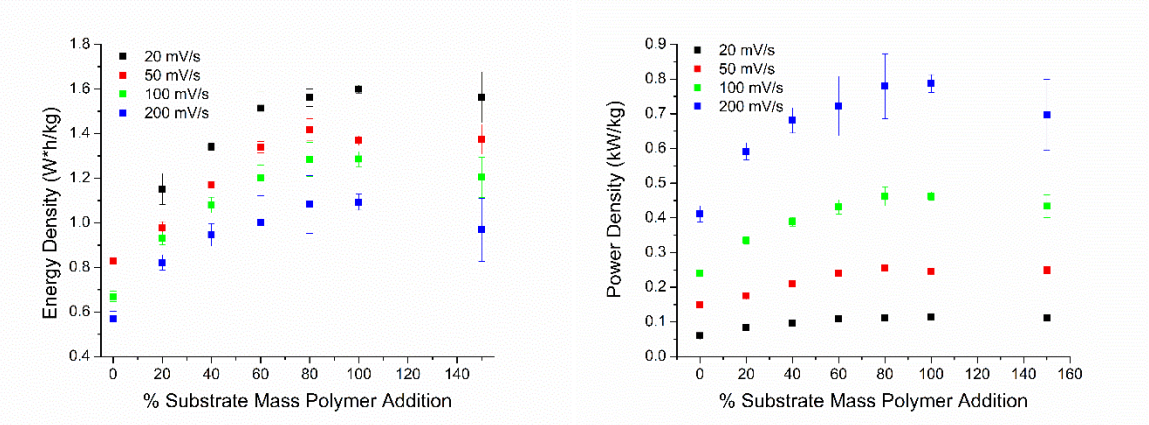

Figure 3.3.2.6. Trends for the values of energy density and power density in supercapacitor devices utilizing CNT/ProDOT-$EDOT_2$ composite electrodes of various percent weight polymer modifications, at various scan rates.

The last figure of merit employed to qualify the performance of supercapacitive devices fabricated using composite CNT:ProDOT-$EDOT_2$ electrodes is stability with

recorded to repeated cycling. Using the optimized electrode composition (100 wt% cast ProDOT-$EDOT_2$), a device was cycled repeatedly at 50 mV/s. Cycling was ended after 5000 cycles had been recorded, and the areal capacitance was calculated from data collected every 1000 cycles. These cyclic voltammograms are shown in Figure 3.3.2.6., along with the trend observed in areal capacitance over the course of cycling.

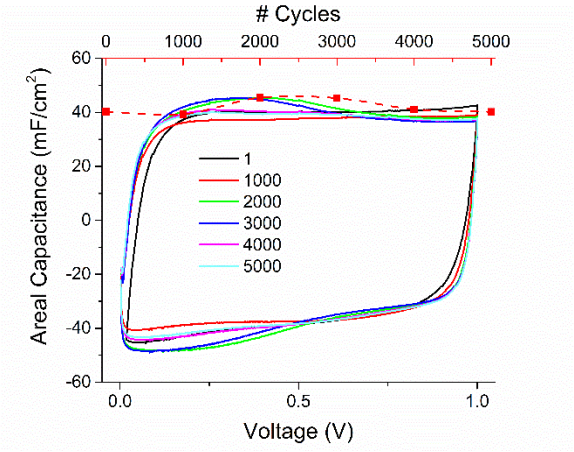

Figure 3.3.2.6. Cyclic voltammograms and areal capacitance values illustrating the stability of a non-woven CNT textile:ProDOT-$EDOT_2$ composite device.

While referring to 5000 cycles as "long term" cycling stability might be spurious, it is worth observing that no loss in capacitive performance is observed over the course of cycling. While variations are in the value of areal capacitance are reported throughout the course of cycling, the difference between the initial and final values is nearly negligible, illustrating that the composite CNT-polymer electrodes described in this chapter are, at least with regard to the length of 5000 cycles, stable to repeated cycling. Further, in the work published on the PANI-CNT composite electrodes developed within the Yushin group, cycling stability out to 30,000 cycles was demonstrated.

The devices described in this chapter serve to illustrate the potential application of pseudocapacitive polymers in charge storage applications, via the modification of high surface area electrode substrates. Following modification, the capacitive performance of non-woven CNT textile electrodes (excellent electrode materials in and of themselves) was seen to roughly double in the case of mass capacitance, energy density, and power

density when cycled at 20 mV/s. Further, at a scan rate of 20 mV/s, values for areal capacitance were observed to roughly quintuple at the optimal electrode composition, and suitable values for CV fill factor were observed for scan rates <200 mV/s. Finally, stability to repeated cycling at a scan rate of 50 mV/s was demonstrated, a result in line with reports of polymer supercapacitors showing stability to multiple hundreds of thousands of cycles.

Additionally, as mentioned the most frequently cited method for the deposition of pseudocapacitive polymers is electropolymerization of monomer unit onto a substrate electrode. Solution processing of polymer pseudocapacitive material demonstrated here finds potential utility in the high through-put fabrication of supercapacitive electrodes, and further potential for large area substrate modification. As this work represents particularly preliminary methodologies and results, there is a great deal of room for improvement in all aspects of the work, from the casting of polymer solutions, to characterization and optimization of the resulting CNT-polymer composites, and finally in device architecture and construction.

CHAPTER 4

ELECTROCHROMIC DEVCIES FOR COLOR MIXING AND HYBRID DEVICES

In Chapter 3, the reductive-oxidative cycling of conjugated polymers was exploited to produce devices capable of storing charge in a pseudo-capacitive fashion. In this chapter, we will be detailing another facet of redox cycling in certain conjugated polymers, namely the evocation or elimination of color in the materials being cycled, or electrochromism. Specifically, we will be focusing on ECDs. Within this chapter, electrochromic devices will be used to study the production of mixed color stimuli by layering ECP films spatially in a "dual active" ECD. This work on dual active ECDs, described in Sections 4.1 through 4.2., is largely adapted from the published article listed as reference 59, "Mapping the Broad CMY Subtractive Primary Color Gamut Using a Dual Active Electrochromic Device"[59]. Further, in Section 4.3. of this chapter an alternative device structure is described, which features photovoltaic materials integrated into the ECD structure, producing a self-powering "photoelectrochromic" device. This section is adapted from the published article listed as reference 136, "A Vertically Integrated Solar-powered Electrochromic Window for Energy Efficient Buildings"[136].

4.1. Color Mixing in Electrochromic Polymers

As was described in Chapter 1, considerable effort has gone into the development of the family of ECPs which span the visible spectrum. The following section will briefly describe a few previous efforts to circumvent this effort in the creation of new electrochromic color states through the route of color mixing, or the usage or multiple electrochromic layers with differing optical properties to produce a mixed or summed color stimulus.

4.1.1. Device Models: Electrochromic Pseudo-devices

Prior efforts in the application of color mixing to conjugated polymers using electrochromic devices have been reported in the literature, though many of these initial studies focused on the design of a device to produce a particular (often achromatic) color state[46, 58, 137-138]. In many of these efforts, the extreme color states, i.e. the fully reduced and fully oxidized states of both ECPs used, was the primary focus, however the work reported by Unur *et al*[138] represented an early effort to systematically map the color states produced upon the progressive bleaching of each of the active ECP layers. Due to the need to individually address each active material layer, a cell arrangement referred to as a "dual polymer electrochromic device" was constructed featuring a pair of "working" electrodes sharing a common counter and reference electrode, and controlled via bipotentiostat. This cell arrangement is shown in Figure 4.1.1.1.

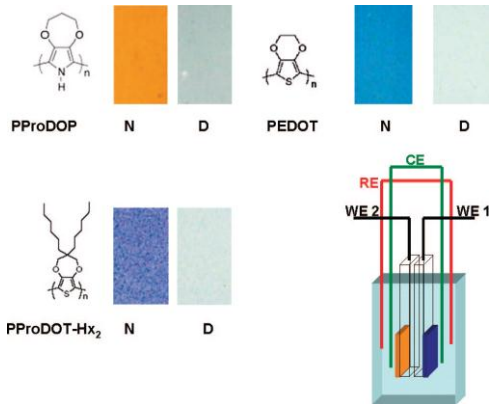

Figure 4.1.1.1. Chemical structures of ECPs examined utilizing the "dual polymer electrochromic device" and a schematic representation of the pseudo-device. Reprinted with permission from Unur *et al*[138]. Copyright 2008, American Chemical Society.

Due to its reliance on counter and reference electrodes, this arrangement was later referred to as a "pseudo-device" architecture, however the design proved useful in the study of color states produced in the progressive and step-wise oxidation of each of the "active" polymer layers. The charts of color states accessible through this cell configuration, shown in Figure 4.1.1.2. served as the inspiration for the presentation of data used in the study of color states accessible through the CMY color mixing scheme

discussed in this chapter, and the cell configuration used to attain this data was modified for a true "ECD" arrangement and renamed a "dual-active ECD", further discussed Chapter 4.2.

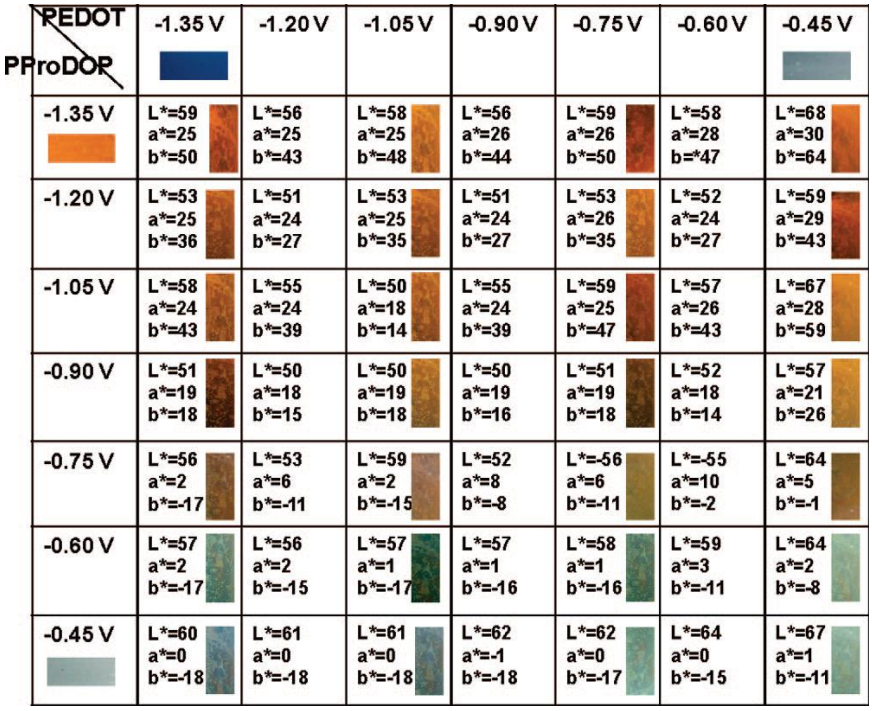

Figure 4.1.1.2. L*a*b* color coordinates and photographs of intermediate color states observed upon the progressive oxidation of polypropylenedioxypyrrole and PEDOT films. Reprinted with permission from Unur *et al*[138]. Copyright 2008, American Chemical Society.

4.1.2. Utility and Applicability of Color Mixing Strategies

The effort of producing a new ECP frequently takes the course of synthetic development of a novel polymer structure, followed by characterization of the material properties of that polymer, which in turn informs our understanding of the structure-property relationships in ECPs. However, considerable time and labor is required for this process. Further, while these synthetic efforts have been fruitful in coarse color control, variations to a polymer backbone are less likely to allow for the fine control necessary to access the variations and shades of color needed in display type applications. Through the use of thin films of cyan, magenta, and yellow ECPs, subtractive color mixing allows the hue of an electrochromic device (ECD) to be selected and tailored to an application

significantly increasing access to various subtle shades. At the level of material application, particularly when their optoelectronic properties become the focus of a researcher's interest, electrochromic polymers could potentially be thought of as pigments, or a set of materials that alter the color of reflected or transmitted light due to the selective absorption of portions of the visible wavelengths of light. Following on this pigment train of thought, in printing and dyeing, multiple pigments are frequently mixed together to produce a color stimulus that is a product of its constituent pigments. As such, a similar approach might be applied to ECPs. This approach could reasonably be examined via two avenues; first, films might be layered or spatially separated such that light from a source is modified by each ECP layer separately prior to reaching an observer and alternatively, ECPs with differing color properties might be more intimately mixed through co-processing, producing a single film with color properties representing the sum of its constituent ECPs. An examination of the first route, wherein films are separated spatially, is described in the following section, while the latter co-processing approach will be discussed in Chapter 5.

4.2. Dual Active Electrochromic Devices for Color Mixing

Among the family of ECPs described in Chapter 1, section 1.1.3. "History of ECP Development – Completing the Color Palette", are three polymers of particular note, namely the ECPs that exhibit a magenta-, cyan-, or yellow-to-transmissive transition, often referred to as ECP-M, ECP-C, and ECP-Y, due to their amenability to color mixing via the subtractive CMY color model (see Figure 2.4.1.1.). The structures of these materials may be found in Figure 1.1.3.2., but are reprinted in Figure 4.2.1.1. below. In order to spatially separate the ECP films under examination, such that they are individually addressable and selectively bleached, an ECD analogous to the 3 electrode pseudo-device shown in Figure 4.1.1.1. was produced. The structure of this device is shown in Figure 4.2.1.1., and owing to the dual, separately addressable active ECP layers,

this architecture is referred to as a "Dual Active" ECD. The following sections serve to describe its fabrication, as well as the colorimetric properties observed upon its characterization.

4.2.1. Device Structure and Fabrication

To construct the dual active ECDs, ECP films were first spray cast onto ITO-glass substrates to the appropriate optical density. Films were cast until an optical density of 0.8 absorbance units at λ_{max}, or 0.4 in the case of MCCP, as monitored on a Varian Cary 5000 UV-vis-NIR spectrophotometer, was reached. Each film was sprayed over an area measuring 1.2 x 1.7 cm, through the use of a shadow mask. Two borders were created using strips of VHB foam acrylic tape; the first border is placed around the ECP films cast onto the center of the substrate, and then a second border is placed around the outer edges of the substrates, shown in Figure 4.2.1.1.c (gray gasket). The LiBTI gel electrolyte mixture (described in Chapter 2) was transferred into the reservoir created by the tape, and the counter electrode slide placed on top. The process of creating borders of VHB tape around the edges of both the cast ECP and ITO-glass substrate, followed by the addition and encapsulation of gel electrolyte is repeated on the reverse of the double-sided ITO-glass slide used as the counter electrode layer to add the second ECD portion and to create the completed device. Contact was made to the devices using ½ inch EMI shielding copper tape.

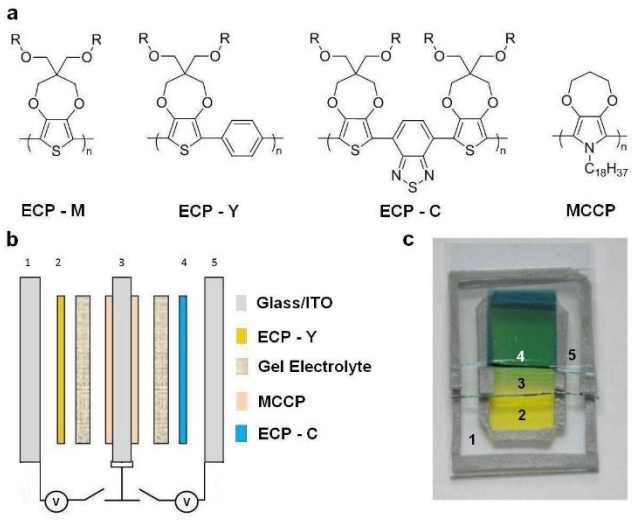

Figure 4.2.1.1. (a) Structures of ECPs-M, -Y, -C, and the DOP-based MCCP (R=2-ethylhexyl). (b) Exploded view and (c) photograph of a "dual active" ECD, including voltage control scheme. Reproduced with permission from Bulloch *et al*[59]. Copyright 2014 American Chemical Society.

Cyclic voltammetry was used to establish stable switching voltages for each ECP-MCCP pairing. Cyclic voltammograms for individual, i.e. not dual active, ECDs utilizing ECP-M, ECP-C, and ECP-Y as the working electrode materials and MCCP as the counter electrode material are shown in Figure 4.2.1.2, alongside photographs of these devices in their voltage extremes, i.e. fully colored and fully bleached states. The windows established were -0.6 to 1.4 V, -0.4 to 1.4 V, and -0.2 to 1.6 V for magenta, cyan, and yellow ECDs, respectively. Owing to the construction of the dual active device allowing each working electrode to be controlled independently, the voltage windows established with these ECDs are translatable to the dual active architecture.

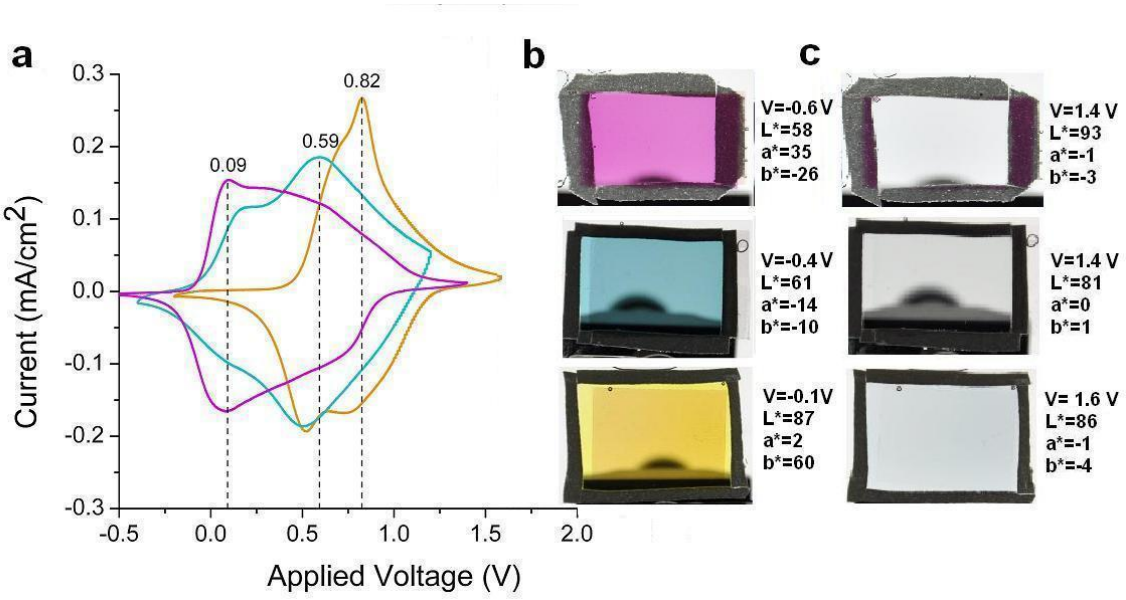

Figure 4.2.1.2. (a) Cyclic voltammetry and photographs of the (b) colored and (c) bleached states of ECDs utilizing ECPs-M, -C, and –Y as the "active" or colored ECP. Reproduced with permission from Bulloch *et al*[59]. Copyright 2014, American Chemical Society.

4.2.2. Comparison to Stacked Devices and Saturation

Initial color mixing experiments were performed using a simple "stacked" device architecture which lacked the central double sided counter electrode (layer 3 in the device cutaway shown in Figure 4.2.1.1.), and were instead comprised of two independent ECDs, of the type shown in Figure 4.2.1.2., placed back to back. To gain a better view of how color mixing is achieved in both dual active and stacked devices, each side might be envisioned as a tunable filter. The two ECP films in series will absorb a portion of the light from the illuminant before reaching an observer, producing a mixed color stimulus. Tuning these ECP filters is accomplished by independently controlling the voltage applied to each device, decreasing light absorption in the visual region as each ECP is oxidized. Unlike a simple filter, the construction of both dual active and stacked devices include a number of optical interfaces (e.g. air to glass, glass to ITO, etc.), which also play a role in the spectral profile of light reaching an observer[139]. The influence of these interfaces in the stacked device structure on color properties is illustrated in Figure

4.2.2.1., which compares the color states accessible in a cyan + yellow (green) stacked device (a) with the corresponding dual active structure (b). The color gamut produced in each architecture was probed by gradually increasing the voltages applied across each film, and recording a photograph and the colorimetric data of the mixed color stimuli as a function of these two applied voltages. The differences in the two device architectures are visually apparent via the photographs, with the stacked device shown in the upper half of Figure 4.2.2.1. exhibiting muted, or less saturated, color states. The L*a*b* coordinates associated with each color state can then be used to quantitatively demonstrate the larger degree of color saturation seen in the dual active structure via the equation where color saturation (S_{ab}) is the ratio of chromatic color (C^*_{ab}) to the total color sensation[140-141].

$$S_{ab} = \frac{C^*_{ab}}{\sqrt{{C^*_{ab}}^2 + L^{*2}}} * 100\% = \frac{\sqrt{a^{*2} + b^{*2}}}{\sqrt{{C^*_{ab}}^2 + L^{*2}}} * 100\%$$

Equation 4.2.2.1. Equation for the calculation of color saturation.

As shown in Table 4.2.2.1., using this measure to compare the saturation of the color states at the four color extreme corners of Figure 4.2.2.1. (green, cyan, yellow, and transmissive color states), higher degrees of saturation are observed in the green and cyan states of the dual active device relative to the stacked device.

a

Cyan / Yellow	-0.4	-0.2	0.0	0.2	0.4	0.6	0.8	1.0
0.0	L*=58 a*=-12 b*=31	L*=58 a*=-12 b*=31	L*=59 a*=-10 b*=32	L*=60 a*=-4 b*=34	L*=64 a*=2 b*=38	L*=69 a*=6 b*=43	L*=72 a*=5 b*=44	L*=75 a*=2 b*=46
0.4	L*=58 a*=-11 b*=29	L*=58 a*=-11 b*=29	L*=58 a*=-10 b*=30	L*=60 a*=-4 b*=32	L*=64 a*=2 b*=36	L*=69 a*=5 b*=41	L*=72 a*=5 b*=42	L*=75 a*=2 b*=43
0.6	L*=55 a*=-9 b*=17	L*=55 a*=-9 b*=17	L*=55 a*=-8 b*=17	L*=57 a*=-2 b*=19	L*=61 a*=3 b*=23	L*=66 a*=6 b*=27	L*=69 a*=6 b*=28	L*=71 a*=3 b*=30
0.7	L*=53 a*=-8 b*=5	L*=53 a*=-8 b*=3	L*=53 a*=-7 b*=3	L*=55 a*=-2 b*=5	L*=59 a*=3 b*=7	L*=63 a*=6 b*=10	L*=66 a*=5 b*=11	L*=69 a*=2 b*=12
0.8	L*=52 a*=-6 b*=-14	L*=52 a*=-6 b*=-14	L*=53 a*=-5 b*=-14	L*=54 a*=-1 b*=-13	L*=58 a*=4 b*=-11	L*=63 a*=6 b*=-9	L*=65 a*=6 b*=-9	L*=68 a*=3 b*=-8
1.2	L*=59 a*=-10 b*=-17	L*=59 a*=-10 b*=-17	L*=59 a*=-9 b*=-17	L*=61 a*=-4 b*=-16	L*=65 a*=0 b*=-13	L*=69 a*=3 b*=-11	L*=72 a*=2 b*=-11	L*=75 a*=-1 b*=-10

b

Cyan / Yellow	-0.4	-0.2	0.0	0.2	0.4	0.6	0.8	1.0
0.0	L*=64 a*=-26 b*=32	L*=63 a*=-22 b*=29	L*=63 a*=-19 b*=27	L*=69 a*=-16 b*=32	L*=73 a*=-8 b*=37	L*=76 a*=-4 b*=41	L*=79 a*=-4 b*=43	L*=82 a*=-6 b*=45
0.4	L*=62 a*=-25 b*=28	L*=63 a*=-21 b*=27	L*=63 a*=-19 b*=26	L*=70 a*=-12 b*=28	L*=73 a*=-6 b*=33	L*=76 a*=-3 b*=38	L*=79 a*=-3 b*=40	L*=81 a*=-4 b*=42
0.6	L*=59 a*=-22 b*=16	L*=63 a*=-21 b*=27	L*=60 a*=-17 b*=14	L*=62 a*=-11 b*= 15	L*=63 a*=-5 b*=17	L*=74 a*=0 b*=21	L*=76 a*=3 b*=24	L*=80 a*=-1 b*=27
0.7	L*=62 a*= -17 b*=-7	L*=62 a*= -15 b*=-8	L*=63 a*= -11 b*=-6	L*=64 a*= -7 b*=-4	L*=66 a*= -3 b*=-2	L*=69 a*= -1 b*=1	L*=71 a*= -1 b*=2	L*=73 a*= -3 b*=3
0.8	L*=56 a*=-18 b*=-11	L*=56 a*=-16 b*=-12	L*=57 a*=-14 b*=-12	L*=59 a*=-8 b*= -11	L*=65 a*=-3 b*=-7	L*=71 a*=1 b*=-4	L*=73 a*=3 b*=-2	L*=77 a*=0 b*=3
1.2	L*=58 a*=-18 b*=-17	L*=59 a*=-16 b*=-16	L*=60 a*=-14 b*=-15	L*=62 a*=-9 b*=-13	L*=66 a*=-4 b*=-9	L*=70 a*=3 b*=-7	L*=76 a*=2 b*=-4	L*=79 a*=-2 b*=-1

Figure 4.2.2.1. Comparison of the color states in stacked (a) and dual active (b) cyan + yellow ECDs. Photographs are shown alongside the L*a*b* coordinates corresponding to the accessed color, and the applied voltages at which that color is accessed. Reproduced with permission from Bulloch *et al*[59]. Copyright 2014, American Chemical Society.

Table 4.2.2.1. Comparison of saturation values calculated for dual active and stacked devices shown in Figure 4.2.2.1.

Color state	S_{ab} (Dual Active)	S_{ab} (Stacked)
Green	54	49
Cyan	39	31
Yellow	48	52
Transmissive	2	13

Further, the color saturation of the transmissive state in the dual active device is seen to be lower than that of the stacked device, indicating that a more color neutral and

transmissive bleach state is produced using the dual active device. Interestingly, a higher degree of yellow saturation is observed in the stacked, rather than the dual active device, though the difference is slight. Following this demonstration of a generally higher saturation of color in the dual active device structures, devices designed to mix ECP-M and ECP-C stimuli were constructed, as well as devices for ECP-M and ECP-Y mixtures. Photographs of the color states observed, as well as the L*a*b* coordinates corresponding to those color states and the voltages at which they were observed are shown in Figure 4.2.2.2.

a

Magenta / Cyan	-0.6	-0.4	-0.2	0.0	0.2	0.4	0.6	0.8
-0.2	L*=39 a*=14 b*=-29	L*=40 a*=13 b*=-28	L*=46 a*=7 b*=-18	L*=54 a*=-3 b*=-11	L*=56 a*=-5 b*=-11	L*=57 a*=-6 b*=-12	L*=58 a*=-6 b*=-15	L*=59 a*=-7 b*=-16
0.0	L*=41 a*=17 b*=-27	L*=42 a*=17 b*=-27	L*=47 a*=12 b*=-19	L*=54 a*=4 b*=-10	L*=57 a*=-1 b*=-9	L*=58 a*=-1 b*=-11	L*=59 a*=-3 b*=14	L*=60 a*=-4 b*=-15
0.2	L*=42 a*=23 b*=-26	L*=42 a*=23 b*=-25	L*=45 a*=22 b*=-22	L*=54 a*=13 b*=-8	L*=59 a*=7 b*=-5	L*=60 a*=5 b*=-7	L*=62 a*=3 b*=-10	L*=63 a*=2 b*=-12
0.4	L*=46 a*=29 b*=-20	L*=46 a*=29 b*=-20	L*=48 a*=28 b*=-17	L*=58 a*=19 b*=-2	L*=62 a*=13 b*=2	L*=64 a*=11 b*=0	L*=66 a*=9 b*=-3	L*=67 a*=9 b*=-5
0.6	L*=48 a*=32 b*=-17	L*=48 a*=32 b*=-17	L*=49 a*=31 b*=-16	L*=59 a*=23 b*=0	L*=65 a*=16 b*=5	L*=67 a*=13 b*=3	L*=69 a*=11 b*=0	L*=70 a*=11 b*=-2
0.8	L*=49 a*=32 b*=-18	L*=49 a*=32 b*=-18	L*=50 a*=31 b*=-17	L*=60 a*=25 b*=-2	L*=66 a*=17 b*=4	L*=68 a*=14 b*=2	L*=70 a*=12 b*=-1	L*=71 a*=12 b*=-3

b

Magenta / Yellow	-0.6	-0.4	-0.2	0.0	0.2	0.4	0.6	0.8
0.2	L*=57 a*=22 b*=27	L*=59 a*=26 b*=26	L*=66 a*=21 b*=33	L*=72 a*=13 b*=40	L*=75 a*=10 b*=43	L*=78 a*=8 b*=41	L*=78 a*=8 b*=39	L*=81 a*=4 b*=36
0.4	L*=56 a*=23 b*=24	L*=59 a*=26 b*=26	L*=66 a*=21 b*=34	L*=72 a*=13 b*=40	L*=75 a*=10 b*=43	L*=78 a*=8 b*=41	L*=78 a*=8 b*=40	L*=81 a*=4 b*=36
0.6	L*=53 a*=22 b*=8	L*=58 a*=25 b*=21	L*=63 a*=20 b*=17	L*=69 a*=12 b*=26	L*=74 a*=10 b*=39	L*=76 a*=7 b*=33	L*=77 a*=8 b*=37	L*=79 a*=4 b*=26
0.7	L*=51 a*=21 b*=-8	L*=56 a*=23 b*=7	L*=61 a*=19 b*=7	L*=67 a*=11 b*=11	L*=71 a*=8 b*=26	L*=73 a*=7 b*=15	L*=75 a*=6 b*=25	L*=76 a*=4 b*=11
0.8	L*=51 a*=25 b*=-16	L*=54 a*=23 b*=-13	L*=61 a*=18 b*=-3	L*=67 a*=10 b*=5	L*=69 a*=7 b*=4	L*=72 a*=6 b*=8	L*=73 a*=5 b*=4	L*=76 a*=3 b*=4
1.0	L*=54 a*=28 b*=-18	L*=56 a*=26 b*=-19	L*=63 a*=20 b*=-10	L*=69 a*=11 b*=-3	L*=71 a*=9 b*=-2	L*=75 a*=5 b*=-1	L*=75 a*=5 b*=-5	L*=78 a*=1 b*=-7
1.2	L*=57 a*=27 b*=-20	L*=58 a*=27 b*=-18	L*=65 a*=19 b*=-9	L*=71 a*=10 b*=-2	L*=74 a*=8 b*=-1	L*=77 a*=4 b*=0	L*=77 a*=4 b*=-5	L*=79 a*=1 b*=-6

Figure 4.2.2.2. Examination of the gamut of color states in dual active (a) magenta + cyan and (b) magenta + yellow devices. Reproduced with permission from Bulloch *et al*[59]. Copyright 2014, American Chemical Society.

The results shown in Figures 4.2.2.2. further emphasizes the tunable nature of the color states exhibited by the ECPs used in the device construction, with each color state readily accessed via the application of a specific pair of voltages across each portion of the device. In addition to the comparison of saturation values between devices, comparison of the L*a*b* coordinates of the colors produced in the ECDs with color standards commonly perceived as saturated colors, such as those of the Munsell color checker system, can be used to gauge the performance of color production[142]. While other color standards exist, such as the Pantone system, the Munsell color system is based on the human perception of color, whereas most other systems are intended for use in textile dyeing or printing settings. The ability to match colors can be quantified through the value of ΔE_{ab}, the color difference or the "distance" between two points in a color space. In the CIELAB color space, this value is calculated via the equation shown as Equation 4.2.2.2.

$$\Delta E^*_{ab} = \sqrt{(L^*_2 - L^*_1)^2 + (a^*_2 - a^*_1)^2 + (b^*_2 - b^*_1)^2}$$

Equation 4.2.2.2. Equation for the calculation of the color difference between two sets of chromaticity coordinates in the CIE L*a*b* color system.

When comparing the green states of the dual active and stacked devices in Figure 4.2.2.1. with Munsell green (which has L*a*b* coordinates of 55, 38, 31), the value of ΔE_{ab} is determined to be 50 in the stacked device, but only 15 in the dual active device. This smaller color difference in the dual active device indicates it to better match a hue commonly accepted as "green" to the casual observer. The ability of the dual active device to produce more saturated shades that better match color standards extends to the cyan (ΔE_{ab}=16 in dual active and ΔE_{ab}=23 in stacked vs Munsell Cyan) state as well, though both devices are nearly equal in their ability to match the Munsell standard yellow (ΔE_{ab}=36 in dual active, ΔE_{ab}=35 in stacked). These measures of performance, higher values of color saturation, as well as the ability to produce less muddled shades that more

accurately match color standards indicate that the dual active device architecture is a preferable model to use in ECD color mixing studies.

4.2.3. The Full Dual Active ECD Gamut

We have discussed and seen it demonstrated that green and its primary colors are well represented with a dual active device, but a full color display needs more than just variations of green. If colors ranging from oranges to yellows and purples to blues are to be generated, the color mixing of other primary pairs is necessary. For this reason dual active devices with cyan-magenta (top) and magenta-yellow (bottom) combinations were constructed and characterized as illustrated by the photographic and colorimetric results shown in Figure 4.2.2.2. While this device does produce blue tones, the coordinates of the fully neutral state of this device (cyan -0.2 V, magenta -0.4 V) are closer to a purple than a blue with a ΔE_{ab} of 14 vs Munsell purple as compared to the ΔEab of 23 vs Munsell blue. This shift in the secondary color, moving from blue to purple, is likely due to the difference in saturation of the films used. The color saturation (S_{ab}) in an ECP cyan device shown in Figure 4.2.1.2. is 27, as compared to the magenta device also shown in Figure 4.2.1.2. for which S_{ab}=60. A similar disparity in the saturation of the constituent ECP films of the magenta-yellow device in Figure 4.2.2.2. lends to the orange hue of the fully neutral color state. This difference in saturation could be overcome by, in the case of the cyan-magenta device, increasing the thickness of the deposited cyan film, and thereby increasing the chromaticity and saturation of that component. However the optical density of the films employed in devices were set equal to one an-other for the purposes of this investigation[143]. What is evident from Figures 4.2.2.1. and 4.2.2.2. is the ability to "dial in" a color state by applying a set of particular voltages across the two halves of a dual active ECD.

Taken together, the breadth of the color states accessed using these dual active devices form a color gamut, particular for these ECP materials at a specific optical

density. This gamut, shown plotted in the a*b* color space in Figure 5, is to our knowledge the first of its kind to be produced using subtractive color mixing in electrochromic polymers, where the color points shown correspond to the color points from Figures 3 and 4.

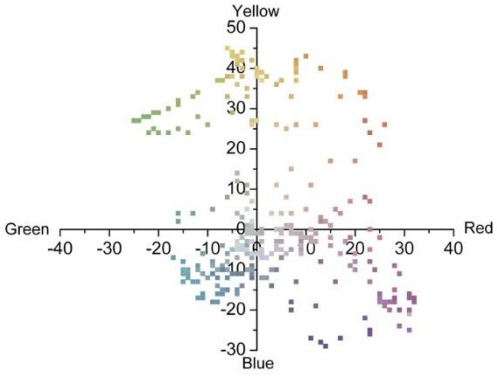

Figure 4.2.3.1. Plot of a*b* values of all color points recorded with dual active devices. Reproduced with permission from Bulloch *et al*[59]. Copyright 2014, American Chemical Society.

This gamut, plotted as if all points were of equal L* value, shows a broad range of accessible color states. The coloration of points shown in Figure 4.2.3.1. are not photographs of devices, as is the case in Figures 4.2.2.1. and 4.2.2.2., but rather a color mapping performed during data work up, by converting the L*a*b* coordinates for each point to RGB values. It should be noted that the space between the plotted points, or the color resolution of the displayed gamut, is a function of the voltages applied to the dual active device. These measurements were made utilizing 200 mV steps through-out stable switching ranges. By utilizing smaller voltage steps, additional color states not shown can be accessed. The only exception to this voltage stepping regime is made in the case of ECP-Y films, which include an oddly spaced point at 0.7 V, which was included due to the large degree of change that occurs at this voltage in order to illustrate a more smooth transition. If a finer control of the applied voltages can serve to “fill in” the accessible color states of the gamut, the features of greatest interest then become the color states

with the greatest chromaticity, or the points that make up the outer bounds of the gamut. These boundaries, shown below in Figure 4.2.3.2., reflect the limits of color production in these materials, at the specific optical density examined.

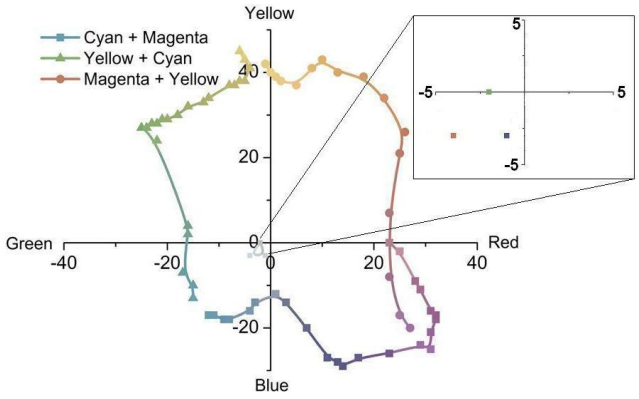

Figure 4.2.3.2.. Exterior and interior bounds of the color gamut generated through subtractive mixing of ECPs –C, –M, and –Y. Reproduced with permission from Bulloch *et al*[59]. Copyright 2014, American Chemical Society.

A number of points are brought up by the examination of boundaries of the accessed color gamut. First, the borders displayed include a tail in the lower right quadrant, shown to be from the magenta + yellow device. The reason for the inclusion of this tail is to demonstrate variability between devices. Given the variability inherent in lab-built devices, these bounds can be expected to fluctuate to a certain ex-tent with the assembly of each device, and with a sufficient number of devices this variability would likely average out. Second, while there is variation from device to device, each dual active device can achieve a very transmissive state. This is provided in the inset to Figure 4.2.3.2., which shows the coordinates for each of the dual active devices with the ECPs in their fully oxidized states. Third, while points are plotted in accordance with their a*b* values, a third dimension (L*) is not represented, save by the coloring of plotted points. Were the L* dimension taken into account in plotting the mapped gamut would appear as an ovoid shape in the L*a*b* color space, with an apex towards the yellow and a nadir in the purple-blue region, rather than a distorted circle. Consideration of this third L* dimension brings up another point of interest. While precise control over the a*b* color

state has been demonstrated utilizing this type of dual active ECD, variation in L* occurs as a consequence of the bleaching and evocation of color in the ECPs used. No direct control over the lightness or darkness of the color states produced using a dual active device is present.. To address the absence of control over the white-black balance in this type of device, a fourth "ECP-Black" component could also be incorporated into a hypothetical pixel, varying in shades of black[38]. This practice is common in printing, where the subtractive color mixing system employed here is almost exclusively referred to as "CMY-K", with K short for "Key", a press printing term for black. Direct control over the L* value would allow for further expansion of this three dimensional color gamut, permitting access to color states otherwise precluded by the bleaching of the cyan, magenta and yellow ECPs. With the incorporation of this fourth element to control luminosity of mixed colors, the concern once again becomes the ability of the ECPs to produce a wide gamut of saturated color states. If instead the bounds laid out by the saturation of the primaries are of concern, then one source of limitation is plain to see in Figure 4.2.3.2., namely the lack of saturation in the cyan primary. In summary, it has been demonstrated here that ECPs are suitable for the generation of a wide gamut of colors through secondary mixing when layered as two distinct films, exhibiting both vibrantly colored and highly transmissive states in equal measure. In addition, color states may be selectively tuned as intermediate partially bleached color states, readily accessed by the judicious application of voltages. The large number of distinct color states accessible through this partial oxidation of ECP materials, in either individual films or when coupled as two or more tunable filters, result in a wide color gamut encompassing a considerable variety of color permutations within its bounds

4.3 Hybrid Photoelectrochromic Devices

The following section departs from the ECDs intended for the study of color mixing discussed above, and branches to address another challenge of electrochromics

application: powering a device. The work described in this section is largely adapted from the published article listed as reference 136, "A Vertically Integrated Solar-powered Electrochromic Window for Energy Efficient Buildings", and describes the fabrication and characterization of a fully solution processed, tandem photovoltaic-electrochromic device assembly.

4.3.1. Device Overview and Deposition of OPV Device

Each of the electrochromic devices discussed so far in this dissertation have required an external source to provide the bias and current needed for the reduction or oxidation of their ECP components. Several groups have made efforts to fabricate devices with power generating structures either integrated into a device architecture or into an integrated assembly, creating what might be termed self-powering, or photoelectrochromic, devices[144-148]. Often, the photovoltaic component of these devices are merely incorporated into the periphery of a device, however even when incorporated into the layered stack of the PV component must be highly transparent, often leading to the use of sputter deposited materials or some external power source to facilitate one half of the electrochromic switch. As an alternative to these methods, an organic photovoltaic (OPV) device was solution processed onto a transparent electrode, with the top-most layer deposited consisting of a thin, nearly transparent, and conductive PEDOT:PSS coating. Onto this PEDOT:PSS layer, ECP films were cast as described in Chapter 2, making use of ECP-M as the active material and MCCP as the counter polymer. Various schema related to the fabrication and operation of this device, such as an illustration of each of the layers composing the device, the scheme for ECD encapsulation, as well as the switching scheme are shown below in Figure 4.3.1.1. For the sake of completeness and to avoid ambiguity, we'll make a brief discussion of the casting of the OPV device layers, which was performed by Dr. Yinhua Zhou. These fabrication steps are more completely discussed in Chapter 2, Section 2.1.5.For a more complete description of the

deposition, operation of, and synthetic and design strategies used in the fabrication of the OPV device shown in Figure 4.3.1.1. and in this section, the reader is directed to published article from which this section is adapted[136], as well as further publications describing the OPV materials employed[149-151].

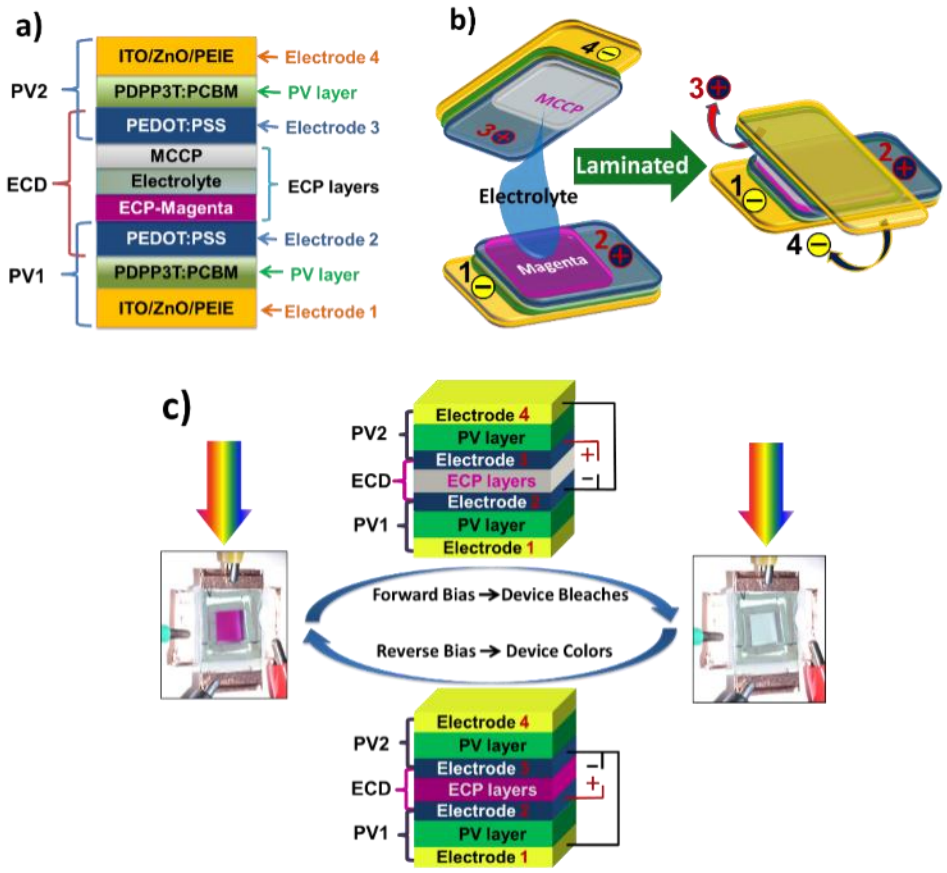

Figure 4.3.1.1. Photoelectrochromic schema illustrating (a) full device layering (b) ECD encapsulation scheme, and (c) switching arrangements. Reproduced with permission from Dyer *et al*[136]. Copyright 2014, Wiley-VCH.

The selection of materials for the OPV portion of the photoelectrochromic device hinges on the use of one material in particular, poly(diketopyrrolopyrrole-terthiophene) or PDPP3T, the structure of which is shown in Figure 4.3.1.2.

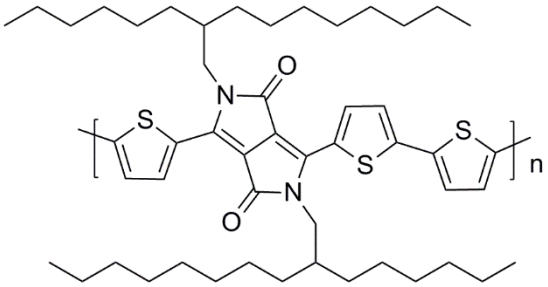

Figure 4.3.1.2. Structure of poly(diketopyrrolopyrrole-terthiophene) (PDPP3T)

Due to PDPP3T's nature as a conjugated polymer with a relatively low band gap, the majority of its absorbance lies in the near infrared, rendering it nearly transparent in the visible region. This property more than anything else renders PDPP3T particularly well suited towards application in visibly transparent OPV applications[149].

Prior to processing, ITO substrates were rinsed via ultrasonic bath, and following this, a ZnO solution was cast onto the surface by spin coating. Following this, polyethylenimine ethoxylate (PEIE) was cast via spin coating, and samples were transferred into a glovebox with a nitrogen atmosphere. Inside the glovebox, the photoactive layer, consisting of PDPP3T:phenyl-C61-butyric acid methyl ester (PCBM) was deposited via spin casting. Subsequent to the casting of the photoactive layers, a film of PEDOT:PSS was cast as the final layer of the OPV device. Again, for characterization results of the OPV layers utilized in this work, the reader is directed to the original publication.

4.3.2. Casting of Electrochromic Polymers

To cast the ECD portions of the photoelectrochromic device, solutions of ECP-Magenta (ECP-M) and the DOP-based Minimally Color Changing Polymer (MCCP) were prepared in toluene. Solutions were filtered, and cast via airbrush as described in Chapter 2. Thin films of each ECP were cast onto the outer PEDOT:PSS surface of the OPVs described in the previous section, and acrylic tape were used to produce device boundaries, again, as described in Chapter 2. A gel electrolyte composed was pipetted

into the device area, and sealed as other ECDs described. Finally, contact to the device was facilitated via strips of copper tape.

4.3.3. Characterization of Photoelectrochromic Device

The completed photoelectrochromic device is operated via a series of external connections, from the appropriate PV electrodes to the EC electrodes. This scheme is illustrated in Figure 4.3.1.1. This scheme works off the selective reduction of one of the two ECP layers, meaning when the device is in its colored state, a reducing bias is applied to the ECP-M coated electrode, causing the oxidation of the opposing MCCP layer. Conversely, the bleached state of the device is accessed by applying a reducing bias to the MCCP-coated electrode and causing the oxidation of the ECP-M layer on the opposing electrode.

Spectroscopically, the majority of the visible absorbance observed in this device structure is due to the cast ECP-M layer in the device. The OPV device layers themselves are reasonably transmissive, with one cell maintaining a transmittance of 76% at 550 nm (the wavelength of greatest sensitivity in the human eye), while a pair of cells maintains a transmittance of 58% together. The spectra of the uncoated OPV cells is shown in Figure 4.3.3.1. Further, spectra taken of the completed photoelectrochromic device, with the ECD portion in its fully bleached and fully colored states is also shown in Figure 4.3.3.1., illustrating a break in the various absorbance motifs represented throughout its spectra. Within the visible (below roughly 680 nm), the absorbance profile is dominated by the ECD portion, namely ECP-M in its colored and bleached states. Above this threshold and entering the NIR (between 680 and 1100 nm), the spectral profile is dominated by the absorbance of the doped PEDOT:PSS layers. Further into the NIR (>1100 nm), absorbance is likely dominated by the bipolaron absorbance created in the ECD layers, and this profile changes little at either extreme electrochromic switching, as one ECP component (either ECP-M or MCCP) is ensured to be oxidized at any given time.

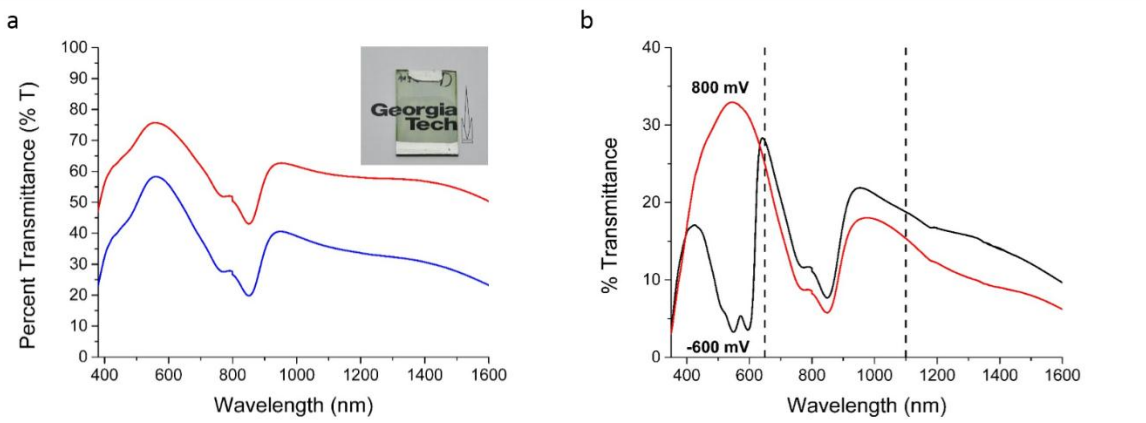

Figure 4.3.3.1. Spectra (a) both a single (red) and a pair of (blue) OPV devices utilizing PDPP3T, and (b) spectroelectrochemistry of a photoelectrochromic device in its extreme color states. Reproduced with permission from Dyer *et al*[136]. Copyright 2014, Wiley-VCH.

The spectroelectrochemical data shown in Figure 4.3.3.1., for the purposes of comparison with more traditional ECD structures, was gathered under potentiostatic control. Further, the use of a potentiostat to record this data provides a baseline for comparison of the performance of the ECD under the self-powering conditions utilizing the OPV layers by applying voltages similar to those recorded during the testing of the OPV devices. As an acceptable degree of transmittance is observed in the completed photoelectrochromic device structure, gauging the electrochromic performance under the self-powering conditions was warranted. Given that the voltages produced by the OPV layers was observed to be high enough to cause oxidation or reduction of the selected ECP, the largest limiting factor to electrochromic performance under this regime was believed to be the rate at which the OPV layers could generate charge sufficient to complete the reduction or contra-oxidation. To gauge this performance, a device was connected via the scheme shown in Figure 4.3.1.1., however the addition of a single pole-single throw (SPST) switch between the connected electrodes allowed for the interruption of the bias application and subsequent flow of current. Under illumination of a solar simulator (Oriel, output intensity of AM 1.5, or 1000 W/m^2), the connection scheme shown in Figure 4.3.1.1. was maintained via the SPST switches for a fixed amount of time, in order

to gauge the degree of switching attained. This process was repeated in both the forward (bleaching) and reverse (coloring) connection scheme, and the results of this test are shown in Figure 4.3.3.2.

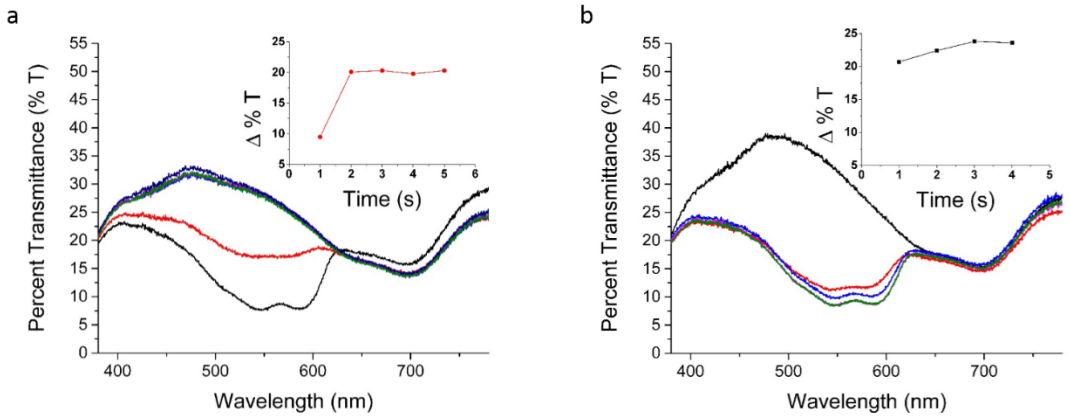

Figure 4.3.3.2. Switching of a photoelectrochromic device during the (a) bleaching and (b) coloring processes against time. Reproduced with permission from Dyer *et al*[136]. Copyright 2014, Wiley-VCH.

In the spectra shown in Figure 4.3.3.2., the spectrum of the initial state (either (a) fully colored or (b) fully bleached) is shown in black, and spectra for subsequent time points are shown as colored traces (red = 1 second, blue = 2 second, etc). Seen in the inset to the spectra for the bleaching process in Figure 4.3.3.2., the contrast attained under this connection scheme plateaus rapidly, with an almost negligible increase in observed contrast beyond a 2 second connection. Further, the reverse or coloring process is observed to be equally fast or faster, with the majority of the observed contrast being attained in under one second, though there is an appreciable increase in the observed contrast out to three seconds, where the value seems to plateau. Additionally, the photoelectrochromic devices produced displayed a trait often observed in ECPs, namely electrochromic memory, or a bistability of oxidation states. Due to the oxidative stability of the neutral state of the polymer, the color of an ECP film is not expected to spontaneously oxidize to the bleached state. Conversely, the stability of the bipolaronic oxidized state is sufficiently high that the bias used to attain that state can be

disconnected entirely from an ECD system, and the colorless state will persist for some time, often for a length of 10-20 minutes in bench top fabricated devices, independent of the external bias. This behavior was observed in the photoelectrochromic devices by recording reflectance spectra of devices throughout the application of the bias provided by the OPV layers, and further recording data following disconnection of that external bias. This behavior is illustrated in Figure 4.3.3.3., which reports the percent reflectance at 550 nm, throughout the application of a device bleaching potential and into an open circuit state, with this transition denoted by dashed lines colored to the respective bleaching bias application time. In Figure 4.3.3.3., the reflectance values recorded prior to the open circuit state (to the left of the dashed line) illustrate the change in reflectance brought about in the photoelectrochromic device through the application of a bleaching bias for the lengths of time denoted in that Figure's legend. At the point of disconnection from that external bias (the dashed line), in almost all cases the reflectance increase observed (brought about by the bleaching of the ECD portions).

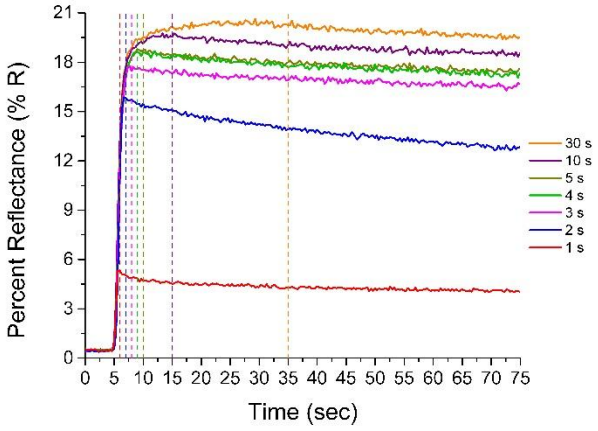

Figure 4.3.3.3. Observation of electrochromic memory in photoelectrochromic devices. Reproduced with permission from Dyer *et al*[136]. Copyright 2014, Wiley-VCH.

The memory effect is apparent in the low rate of "drift" to a lower degree of reflectance following the removal of an external bias (dashed lines). Interestingly, the electrochromic memory appears to be largely independent of the degree of bleaching attained with the

rate of downward drift (recolorization), following the application of a bleaching bias for 1 second, is rather low after an initial nominal drop immediately following removal of the external bias. The rate of recolorization after the application of a bleaching bias at longer application time points is similarly low, though the rate of drift observed after a 2 second application is rather large when compared to other time points observed. It should be noted that each measurement recorded to observe this memory effect was limited to a time frame of 75 seconds, due to sampling limitations in the software used to control the spectroradiometer employed to gather this data. Due to this limit, the "memory" period recorded after a bleaching bias was applied to the device for 1 second (following an initial 5 second rest period) is 69 seconds of "memory", while the memory period following a 30 second application of the bleaching bias was only 40 seconds, again, following an initial 5 second rest.

The results observed show this device architecture as a promising proof-of-concept for self-powering electrochromic windows. Further, the use of methods such as solution processing in the fabrication of the devices can be made amenable to large-scale and high throughput processes. However while a promising proof-of-concept, much additional work is required before this process might be adapted on an industrial scale as some of the techniques used, such as spin coating, are likely incompatible with a large-scale setting. Finally, while device optimization is likely to improve both photovoltaic and electrochromic performance, the techniques used might also be adapted for use on a flexible, transparent and conductive substrate.

CHAPTER 5

SOLUTION CO-PROCESSING FOR COLOR MIXING APPLICATIONS

In chapter 4, the use of novel electrochromic device types served to examine, to a limited extent, the color mixing properties of several series of electrochromic polymers spatially separated into a "dual active" structure[59]. The neutral state color properties of the polymers used in the dual active devices allowed for color mixing along the well-established cyan-magenta-yellow subtractive color mixing scheme, and in this chapter we will be taking that color mixing scheme one step further. Rather than spatially separate pairs of ECPs to achieve the production of a secondary color state, materials have been co-processed from the same solution, to create a single, visually homogenous ECP film[60].

An additional goal will be to shed light on a possible means of predicting the color properties of these co-processed films, and further, to quantify of the accuracy of that means. Mixtures of ECPs intended to produce vividly hued films will be examined, and this work, described in Sections 5.1 through 5.3, is largely adapted from the published article listed as reference 60, "An Electrochromic Painter's Palette: Color Mixing via Solution Co-processing". Following the production of vivid, multicolored films, the co-processing method will be extended to the production of achromatic mixed ECP films and a comparison of these blended films to the synthetically produced ECP-Black will be made.

5.1 Subtractive Color Mixing via Solution Co-processing

The solution processability of the electrochromic polymers produced in the Reynolds' labs over the previous decades opens a number of avenues to address

challenges in inventive ways[27-28, 33, 152]. This section will describe how the solution processability of ECPs can be used for the purposes of tailoring the color properties of cast films. In order to properly discuss the control of color properties through control over ECP mixture compositions though, a description of the theory behind this fashion of subtractive color mixing is in order.

5.1.1. Theory of Subtractive Color Mixing

Non-emissive technologies, such as liquid crystal, electrophoretic, and electrochromic displays produce a visual stimulus in a subtractive fashion, i.e. through interactions with transmitted or reflected, rather than emitted, light. This light can be produced from ambient sources, or be the result of a back lighting display element, but regardless of the source of the attenuated light, the mechanism of subtractive color generation is largely the same. The development of colored-to-clear ECPs discussed so far in this document employed synthetic design strategies, i.e. modulation of electronic absorption transitions through structure-property relationships, for broad color targeting in order to create polymers of a specific hue[27-28, 38]. However, subtleties of color perception and the intricacies of polymer structure and material color relationships mean that fine color control is, at best, difficult. Color mixing, or more specifically the mixing of pigments of differing optical properties to produce a new color state, serves as an alternative to synthetic routes of color control and is a well-established practice in the printing industry. Color mixing theory asserts that if two color stimuli are mixed, the resulting color stimulus will lie at some point along a line connecting the two mixed stimuli on a chromaticity diagram[153]. Practically, this observation has resulted in the CMY-K and RYB color mixing systems, commonly used as the models of subtractive color mixing.

Among the family of electrochromic polymers developed in the Reynolds' labs, three vibrantly colored to highly transmissive switching polymers, representative of the

cyan, magenta, and yellow subtractive mixing primaries are available for the study of color mixing in ECPs. The repeat unit structures of these polymers, along with photographs of thin films of each at both potentials producing fully colored and fully bleached states are shown in Figure 5.1.1.1. To demonstrate the color mixing that can be produced in solution, photographs of ECP solutions are shown at the bottom of that same figure, illustrating the vibrant colors of the CMY materials, as well as their ability to produce the highly saturated secondary green, red, and blue hues.

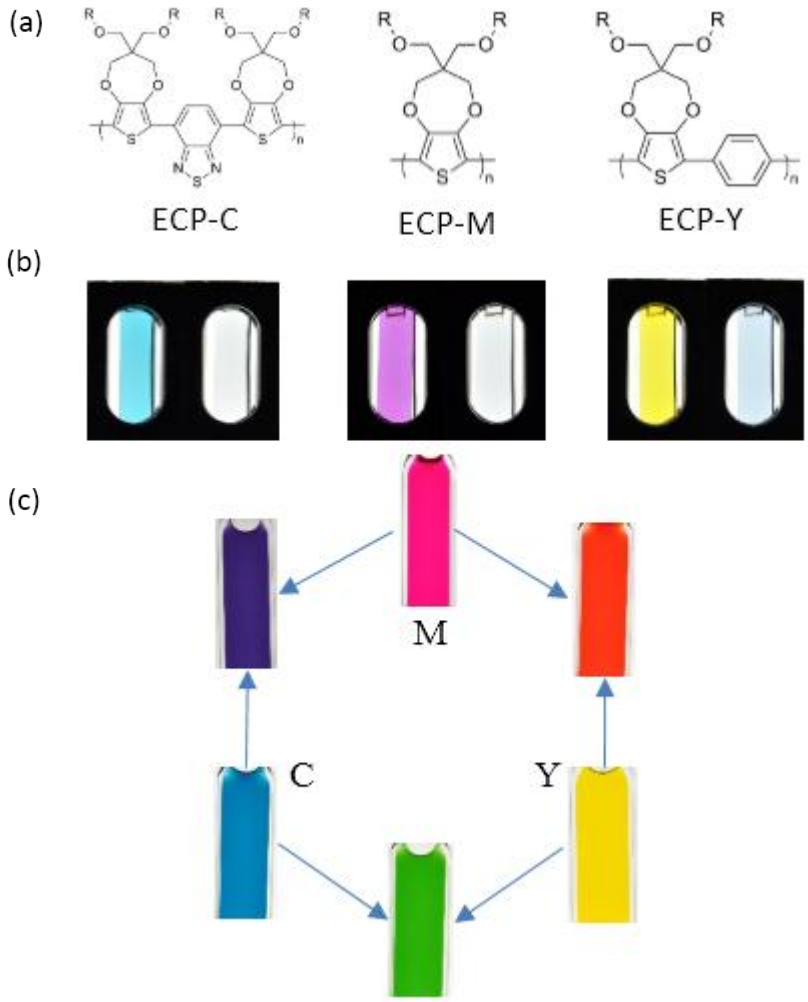

Figure 5.1.1.1. Structures and photography of CMY representative electrochromic polymers in solution and thin films. (a) The repeat unit structures of each of the three ECPs selected are shown above, where R= 2-ethylhexyl. (b) Photographs of colored and bleached polymer thin films are shown below their respective repeat unit structures. (c)

Solutions of ECPs-C,-M, and Y at concentrations of 2 mg/mL, and 1:1 w/w ratios of these solutions. Figure reproduced with permission from Bulloch *et al*[60]. Copyright 2015, American Chemical Society.

In order for color mixing to be performed in a precise fashion, the link between relative "strength" of the pigments used and the quantity of pigment physically present in a sample must be established. The elucidation of this link, in terms of extinction coefficients, is described in the following section.

5.1.2. Determination of ECP Mass Extinction Coefficients

As was discussed in Chapter 4, where the solution processing and examination of the color properties of ECPs is concerned, treating the materials as inks is at least on a technical level a reasonable approach to take. If one desired to mix two pigments into an ink such that each pigment contributed equally to the mixed color stimulus produced, you would need to know how "strongly" each pigment absorbed it's respective band of light, allowing you to adjust the relative masses of each pigment in the mixture to balance them out. Where most pigments are concerned, the quantification of absorptive strength takes the form of a molar absorptivity or extinction coefficient, and is given the symbol "ε". In materials where the chromophore units consist of molecules with a well-defined molecular or molar mass, this determination is relatively straight forward, utilizing spectroscopy of solutions of a known concentration and following largely on the assumptions made within the Beer-Lambert law. The determination of extinction coefficients becomes slightly more complex when the chromophore units are distributed along some number of repeat unit heterocycles (as is the case in electrochromic polymers), rather than neatly packaged within one discrete molecule. The determination of extinction coefficients becomes even further complicated when a fair portion of a material's mass is included in non-absorptive moieties, as is the case of the alkoxy solubilizing chains appended to the ECPs. Due to these considerations, experimental

determination of the "molecular weight" of the distributed chromophore within ECPs is particularly difficult.

Alternatively, the total mass of the polymer in solution can be substituted for the molecular weight normalization, i.e. substituting a g/mL term for a mol/L concentration term in the Beer-Lambert law, producing a mass extinction coefficient (ε_{mass})[33]. For the purposes of the experiments described in this chapter, the density of the polymer samples was assumed to be 1.0 g/cm^3, however the densities of ECPs-Cyan, -Magenta, and –Yellow were experimentally determined to be 1.06, 1.02, and 1.01 g/mL, via flotation measurement. In order to determine polymer mass extinction coefficients (ε_{mass}), dilute ECP solutions (50 μg/mL in chloroform) of ECPs-Cyan, -Magenta, and -Yellow were prepared and spectra of these solutions were recorded with a Varian Cary 5000 UV-Vis-NIR spectrophotometer. Values for ε_{mass} were calculated via the Beer-Lambert law, again, substituting a sample concentration in units of g/mL for the molar mass term for the analyte concentration term[33]. The extinction coefficients of ECPs-Cyan, -Magenta, and -Yellow are shown below in Figure 5.1.2.1. as a function of wavelength.

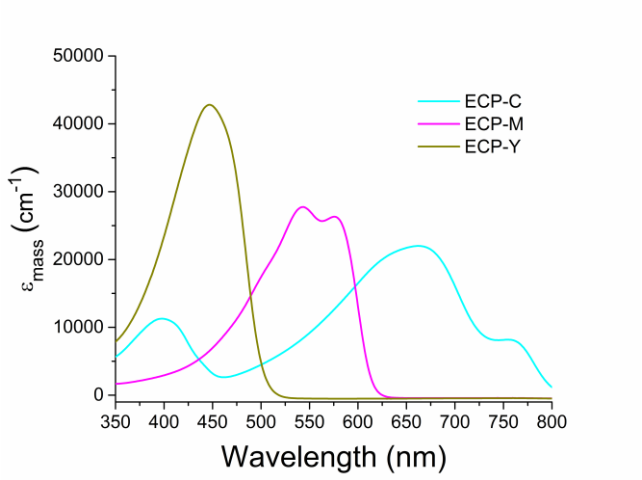

Figure 5.1.2.1. Mass extinction coefficients, in chloroform, as a function of wavelength illustrating the increasing relative absorptivity in the order of ECPs-C, -M, and –Y. The extinction coefficients shown were calculated by assuming a polymer density of 1 g/cm^3. Figure reproduced with permission from Bulloch *et al*[60]. Copyright 2015, American Chemical Society.

The value of the extinction coefficients for each of the CMY polymers at the wavelength of maximum absorption (λ_{max}) was used as the basis on which mixture compositions were determined. By way of example, the values of ε_{mass} at λ_{max} for ECPs Magenta and Cyan were determined to be 2.9×10^4 and 2.5×10^4 cm^{-1}, respectively. The ratio between the values of ε_{mass} for ECPs Magenta and Cyan is 0.87, and therefore to produce a mixture with equal contributions to the visual stimulus from the components, 0.87 parts of ECP-Magenta should be used to 1 part ECP-Cyan. It should be noted however that this method produces mixtures with equivalent contributions to a visual stimulus, however only at the λ_{max} for each polymer. Using this method, two component ECP mixtures of the CMY representative polymers were made at 1:1 ratios. Mixtures were again composed at a concentration of 50 μg/mL, and the spectra recorded for these solutions are shown below in Figure 5.1.2.2..

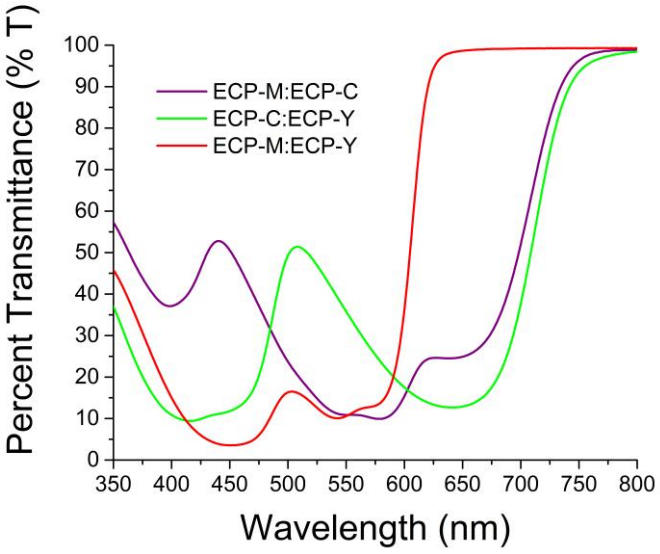

Figure 5.1.2.2. Spectroscopy of 1:1 ECP mixtures in chloroform solution. The relative masses of each component ECP in these mixtures was informed by the mass extinction coefficients observed. Figure reproduced with permission from Bulloch *et al*[60]. Copyright 2015, American Chemical Society.

It should be understood that this method is only accurate to a first approximation for the mixture of any given pair of ECPs, due to the number of factors not addressed by this method, such as the differences in chromophore mass or size between polymers, the non-

absorptive weight fraction of the respective polymer masses mentioned previously, and the non-linearity of the eye's color sensitivity. Further, overlap in the spectral profile of each component ECP, such as the overlap of the profiles of ECP-C and ECP-Y around 400 nm.

5.1.3. Calculation of Theoretical Mixed ECP Color Stimuli

The use of any experimental method calls for controls against which the veracity of data obtained might be gauged. Where the co-processing of ECP mixtures is concerned, the experimental method in question is using the calculated mass extinction coefficients to produce ECP mixtures with specific color properties. The control against which this method will be compared is the calculation of the color properties of theoretical mixtures of ECPs at identical mixing ratios to those used experimentally. As per the theory of color mixing described above, if the chromaticity coordinates of a mixed color stimulus (a^* and b^* in the CIELAB system) lie along a line connecting the two stimuli being mixed, then it follows that the mixed chromaticity coordinates should follow the trend expressed in Equation 5.1.3.1.:

$$a_3^* = \left((a_1^* * x) + (a_2^* * y)\right)$$

$$b_3^* = \left((b_1^* * x) + (b_2^* * y)\right)$$

Equation 5.1.3.1. Equations to calculate chromaticity coordinates of a mixed color stimulus in the CIE L*a*b* color space.

where a_1^* and a_2^* are the a^* coordinates of the materials being mixed, x and y are the fraction contributions of each component, and a_3^* is the a^* coordinate of the mixture produced. Similarly, b_3^* is the b^* coordinate of the mixture produced, calculated in an identical fashion. As ECPs-Cyan, -Magenta, and -Yellow are the pigments being mixed in this series, the a* and b* values of neat films of each polymer will produce the values of a_1^* and a_2^* or b_1^* and b_2^* used in these calculations.

By way of example, if a 3:1 mixture of two pigments were to be made, and pigments 1 and 2 had a^* values of 50 and 25, respectively, the calculation of the a^* value of the mixed stimulus (a_3^*) would be as follows:

$$a_3^* = (50 * 0.75) + (25 * 0.25)$$

Predicted color values for mixtures with compositions of 3:1, 1:1, and 1:3, weighted by the value of ε_{mass} at λ_{max} for all mixtures.

5.2. Solution Co-Processing of ECP Mixtures

Using the mass extinction coefficients to produce some degree of parity in the contribution from the ECP pigments being mixed, in coordination with the calculation of theoretically mixed color coordinates as a basis for comparison, the physical deposition of the ECP mixtures becomes the next step in the assessment of this mixing method. This section will discuss the details immediately pertaining to the deposition and spectroscopy of the unswitched or "as cast" mixed ECP films. For a more complete description of the method of spray casting polymer solutions, the reader is directed to the section dedicated to that topic in Chapter 2.

5.2.1. Casting of ECP Mixtures

ECP samples were prepared by mixing samples with compositions conforming to the ratios described for the calculation of theoretical color values, i.e. mixtures were made at ratios of 3:1, 1:1, and 1:3, for each ECP combination. Each mixture was dissolved in chloroform to a concentration of 2 mg of polymer per mL of solvent, and neat chloroform was used for each sample to ensure complete dissolution. Mixtures were allowed to stir over night, with no additional heating. Following mixing, no resistance in filtration was noted, suggesting total dissolution of the polymer samples into the chloroform solutions. Prior to casting, ITO-glass slides were rinsed using isopropanol, followed by acetone, and were wiped dry. Films were cast over an area roughly of 25 x

50 mm, using an Iwata-Eclipse airbrush with nitrogen at a pressure of 20 psi. Films were cast until an absorbance of 1.0 absorbance units was reached, regardless of the wavelength which reached that benchmark first.

5.2.2. Color Properties of As Cast Films

Prior to the electrochemical cycling of the cast ECP films, a comparison was made between the observed and calculated chromaticity coordinates for each mixture. As the chromaticity coordinates being assessed in this case pertain to dry or "as cast" films, the chromaticity coordinates for ECPs-Cyan, -Magenta, and -Yellow in this as cast state were used to calculated the theoretical color points under consideration. The theoretical points are shown alongside the experimentally observed points in Figure 5.1.3.1.

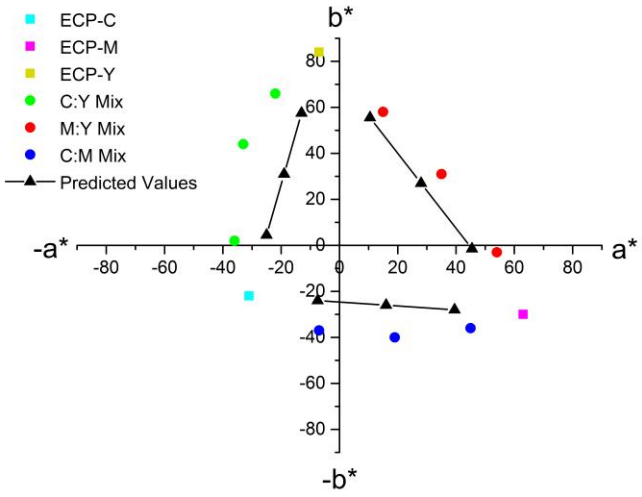

Figure 5.1.3.1. Predicted and observed a*b* chromaticity coordinates in as sprayed ECP films. a*b* values for neat CMY ECP films as well as varying ratios of each binary ECP mixture. Chromaticity values estimated from the chromaticity coordinates of the neat CMY ECPs are shown as black triangles. Figure reproduced with permission from Bulloch *et al*[60]. Copyright 2015, American Chemical Society.

By way of a qualitative assessment of the general trends observed, an underestimation of mixture chromaticity is a universal feature in the application of this model to "as cast" films, evidenced by all predicted color values lying closer to the origin than the

experimentally observed values. Further, values for the quantification of the color difference between the experimentally observed and theoretically predicted chromaticity values are fairly large (≥10 in any one chromaticity coordinate) in the ECP-C:ECP-Y (green) and ECP-C:ECP-M (blue) mixtures shown, but much closer agreement is seen in the ECP-M:ECP-Y (red) mixture. A description of the calculation this color difference term may be found in section 5.3.1.

A degree of outward "bowing" in the experimentally observed chromaticity values is also observed for each mixture examined. A number of factors might influence this bowing behavior, such as differences between the optical properties of the solution environments used to estimate mass extinction coefficients and those encountered in the thin film environment, or other differences discussed above, such as the use of extinction coefficient values corresponding to λ_{max} values alone. While a comparison of the theoretical and experimentally observed chromaticity coordinates in the as cast state is a good place to begin the assessment of this method, in order to properly assess the predictability of CMY color mixing using ECPs, they should to be regarded as the functional, electro-active materials they are, and they are handled as such in the following section.

5.3. Characterization of Mixed ECP Films

Prior to spectroelectrochemical characterization, films were switched via cyclic voltammetry, utilizing an EG&G PAR 273A potentiostat and a three electrode cell arrangement, as described in Chapter 2, section 2.2.1. An electrolyte consisting of 0.5 M $TBAPF_6$ in propylene carbonate was used, and films were potential cycled 2-3 times, after which point no further differences in spectral properties were observed on repeated cycling. Following this initial cycling, a potentiostatic regime was used to record spectra of each film in the fully neutralized and fully oxidized (colored and bleached, respectively) states. This section will discuss the features observed within this

spectroelectrochemical interrogation, as well as the color properties derived from the spectral data and a comparison to the theoretically calculated chromaticity coordinates for switched films.

5.3.1.Spectroelectrochemistry

In order to treat the cast ECP films as electroactive coatings, thin films corresponding to the solutions shown in Figures 5.1.2.1. and 5.1.2.2, i.e. neat solutions of ECPs-C, -M, -Y, and the 1:1 ε_{mass} : ε_{mass} mixtures, were spray cast onto ITO-coated glass slides in order to spectroscopically monitor the oxidation and re-neutralization of the films prepared, referred to as switching. The spectra recorded for these films are shown in Figure 5.3.1.1. As previously discussed, differences in optical properties are often observed when moving from solution to thin film environments. However, particular note should be made of the changes observed upon the initial oxidation-reduction cycling of some ECP films (referred to as the electrochemical break-in). For many polymers, these observed differences are minor, but in the case of ECP-M, a notable degree of peak sharpening is observed, along with an increase in the absorption maxima at λ_{max} for both observed peaks in that sample. This sharpening is readily apparent in Figure 5.3.1.1 (compare with the ECP-M trace shown in Figure 5.1.2.1 and 5.1.2.2.), the transmission spectra of the neutral (colored) and oxidized (bleached) states of films after their electrochemical break-in cycles.

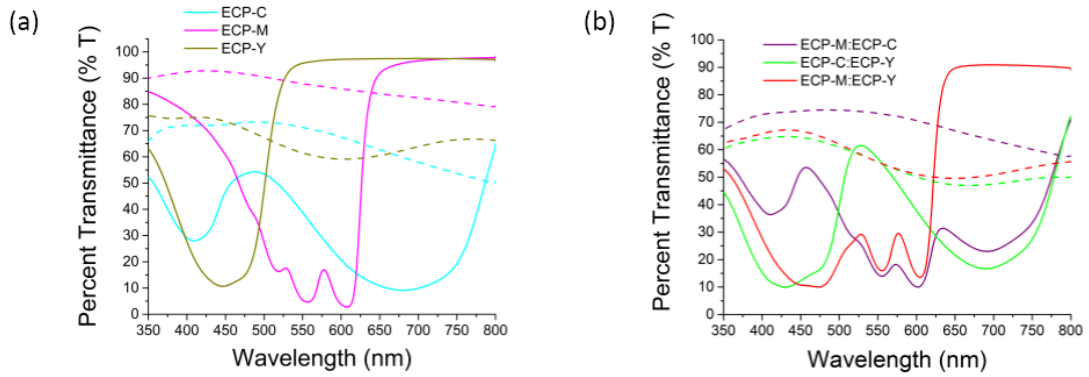

Figure 5.3.1.1. Spectra of the fully colored state and most transmissive states attained are shown for films of (a) neat ECPs-C, -M, and –Y, and (b) 1:1 ECP mixtures. These spectra serve to illustrate both the high contrast available in the neat ECP films, as well as the effect of lower contrast components on the transmissive state of a mixture. Figure reproduced with permission from Bulloch *et al*[60]. Copyright 2015, American Chemical Society.

This shift in optical properties becomes an important factor when attempting to quantify the color contributions from ECP-M to a given mixture. This effect can most easily be seen when comparing the ECP-M spectra shown in Figure 5.1.2.2. and 5.3.1.1.b, recorded prior to and after potential cycling, respectively. Films were originally sprayed until an optical density of 1.0±0.05 AU at λ_{max} was reached, but upon switching, an increase in the ECP-M absorption intensity is again observed, coinciding with the sharpening of the peaks observed in the absorption profile. This shift in optical properties upon electrochemical switching, and it's influence on the final color properties of the ECP mixtures will be revisited in the discussion of the prediction of an ECP mixture's color properties.

The spectra shown in Figure 5.3.1.1. also allows for the examination and comparison of the oxidized (bleached, transparent) states in both the neat and mixed ECP films. The electrochromic contrast, measured as the difference in transmittance at λ_{max} between the colored and bleached states of a given ECP at is highly dependent on the extent to which a material can bleach it's color upon oxidation. The CMY ECP materials employed in this study exhibit varying degrees of this ability, shown as the dashed traces in Figure 5.3.1.1., and from these it can be seen that ECP-Y retains the highest level of visible light absorption upon bleaching and ECP-M the lowest. This observation becomes especially important in the context of retained absorption in the bleached state of a mixture. Figure 5.3.1.1. illustrates that the bleached state of an ECP mixture is limited by the component with the least transmissive bleached state, leading the mixture lacking ECP-Y entirely to have the most transmissive bleached state, while the mixture containing both ECPs-Y and -C in equal proportion has the least transmissive

bleached state. This observation should be qualified with the understanding that even the "least transmissive" bleached state reported in this study still exhibits a comparatively high degree of transmission and color neutrality, but the limiting effect of one of the components in a mixture is an influential factor. It should be noted that the data presented in this chapter, both spectral and colorimetric, was collected under a steady-state regime, i.e. a steady current response signifying a stabilization in the extent of film oxidation induced was observed prior to spectra being recorded. Likely due to the disparity in the onset potentials for oxidation between the CMY polymers, varying degrees of oxidation are observed in each component in a given mixture, producing a number of intermediate color states rather than a smooth, binary colored-to-bleached transition as observed in the neat ECPs.

Spectroelectrochemical series were generated for each mixture composition, at each mixing ratio. A representative series of spectra are shown in Figure 5.3.1.2, specifically of a 1:1 ECP-C:ECP-M film, illustrating the sequential initial bleaching of the ECP-M component at roughly 0.3 V (peaks ~550 nm, green trace), followed by bleaching of the ECP-C component (~400 and 700 nm), as the potential applied across the film is increased step-wise from -0.3 V to 0.9 V.

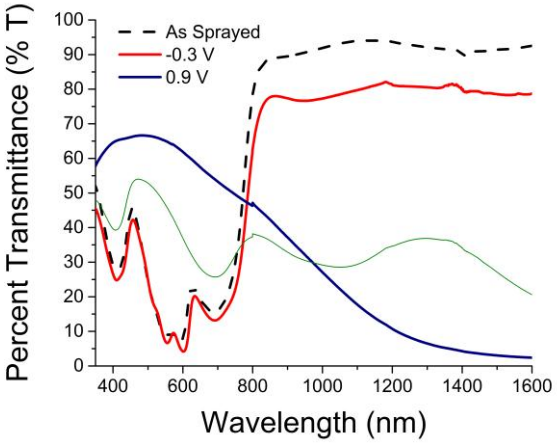

Figure 5.3.1.2 Representative spectroelectrochemical series of 1:1 ε_{mass} : ε_{mass} ECP-C:ECP-M mixture. Figure reproduced with permission from Bulloch *et al*[60]. Copyright 2015, American Chemical Society.

The application of this method to each cast film produced similar spectroelectrochemical series, often featuring the sequential bleaching of both ECP components as the potential applied to the film was raised incrementally. While the sequential bleaching effects observed are interesting, for the purposes of gauging the accuracy of color component prediction, the spectroelectrochemical data is much more valuable when rendered into L*a*b* chromaticity coordinates. Each of the spectra recorded were used to generate a set of chromaticity coordinates describing that spectra, via the method described in Chapter 2.4, through a software interface. The following section will feature a closer examination of the chromaticity coordinates observed, as well as a description of their proximity to the predicted values.

5.3.2. Colorimetry and Quantification of Divergence

After generating L*a*b* coordinates for both neat CMY films and those of the varying mixture compositions, values were plotted to illustrate how the chromaticities of the mixed ECP films varied with an increasing applied potential. The chromaticity values observed for each mixture of ECP-C and ECP-M produced, detailing both the a*b* chromaticity trends and the shift of the L* value throughout the electrochromic bleaching, are shown in Figure 5.3.2.1.

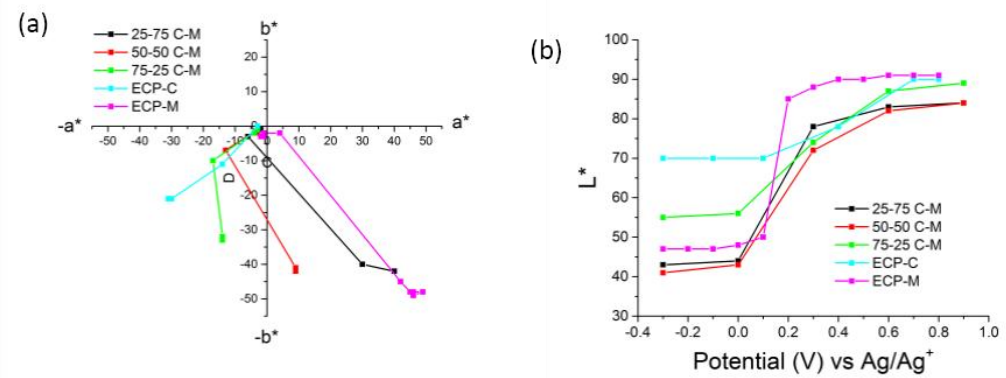

Figure 5.3.2.1. (a) Colorimetry of ECPs-C and –M, with the chromaticity (a* vs b*) of ECP-C:ECP-M mixtures, and (b), the luminance values (L*) against the applied potential for ECPs-C and –M, and the corresponding mixtures. Figure reproduced with permission from Bulloch *et al*[60]. Copyright 2015, American Chemical Society.

The trends in the observed values are characterized by the loss of chromaticity, first by the loss of the ECP-M contribution, producing a series of color states in the cyan range (-a*,-b*), followed by a loss of ECP-C color contribution as well, resulting in a final color neutral state, close to the origin. Associated with the loss of color contributions, there is an increase in the luminance, or L* value, brought about as the various ECP components are induced into highly transmissive bleached states.

The control of chromaticity and luminance in ECPs via the application of a potential as shown in Figures 5.3.1.2. and 5.3.2.1. is well documented, and the two states relevant to this study are those presented in Figure 5.3.1.1., namely the fully colored and fully bleached states[154]. The chromaticity coordinates for these states, for each of the ECP mixtures prepared as well as neat ECP films, are shown at left in Figure 5.3.2.2. Also shown in the plot shown in Figure 5.3.2.2. are the chromaticity values predicted via the method described above, based on a given mixture's composition. Finally, photographs of the mixed ECP films in both the vibrantly colored and highly transmissive bleached states are also shown at right in Figure 5.3.2.2., to illustrate the continuous and visually homogenous film properties obtained, as well as offering a means to better visualize the colors represented by the a* b* chromaticity coordinates plotted. Generally speaking, the chromaticity points in Figure 5.3.2.2. show a lesser degree of divergence from the values predicted than was observed in the "as cast" films, shown in Figure 5.1.3.1. The lowest degree of divergence is seen in the ECP-M:ECP-Y mixtures (red points) and the greatest divergence observed in the ECP-C:ECP-Y mixtures (green points), as was observed with the colorimetry of the "as cast" films. The divergences from the predicted values are quantified by the value of ΔE_{ab}^{*},or the color difference. This term, which calculates the Euclidian distance between two sets of chromaticity coordinates, is defined by the CIE 1976 conventions with the following equation:

$$\Delta E^*_{ab} = \sqrt{(\Delta L^*)^2 + (\Delta a^*)^2 + (\Delta b^*)^2}$$

Equation 5.3.2.1. Equation for the calculation of the color difference between two sets of chromaticity coordinates in the CIE L*a*b* color system.

A lower color difference (small ΔE) signifies a pair of colors that are closer to being identical, and a larger color difference (large ΔE) indicates a pair with a greater difference. The a*b* values recorded for the mixed ECP films are shown in Table 1, along with the values predicted using the L* a *b* coordinates of neat ECP films, and the value of ΔE_{ab}^* for these pairs. As mentioned, generally the highest degree of agreement between the predicted and observed values occurs in the ECP-M:ECP-Y mixtures, with values of ΔE_{ab}^* ranging from 12-14. To qualify these values a ΔE_{ab}^* value of less than ~2.3 signifies a pair of colors that are, commonly, perceptually indistinguishable. In essence, the difference between the pair of colors falls below a "just noticeable difference" (JND) threshold, and color pairs with ΔE_{ab}^* values in the range of ~10 will therefore be noticeably different from one another, though similar[155-156]. A poorer agreement between the predicted and observed color values is seen in the ECP-C:ECP-M mixtures, with values ranging from 15-19, though a fair degree of consistency is seen in the error in prediction for this mixture. Finally, a remarkable degree of inconsistency is noted in the ECP-C:ECP-Y mixtures, with the two lowest ΔE_{ab}^* values recorded (8 and 11), as well as the highest (25) seen in this family of mixtures.

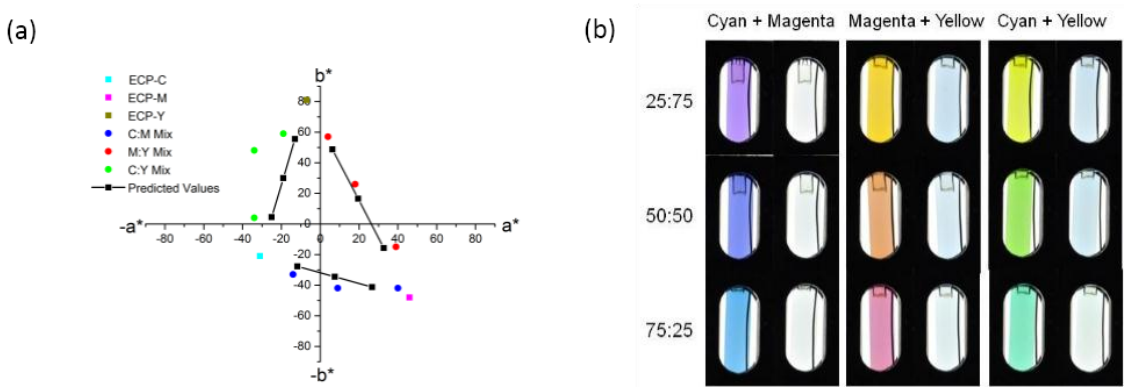

Figure 5.3.2.2. (a) Predicted and Observed a*b* Chromaticity Coordinates in Electrochemically Switched ECP Mixtures with Colored and Neutral State Photographs of Each Mixture. Chromaticity values of neat CMY ECPs and mixtures of varying composition, after electrochemical switching. Predicted values are again shown in black (squares). (b) Photographs of the mixtures in both the colored and bleached states are shown on the right. Figure reproduced with permission from Bulloch *et al*[60]. Copyright 2015, American Chemical Society.

By estimating the mass extinction coefficients of electrochromic polymers representative of the CMY color mixing models, the ability to estimate the colorimetric coordinates of a mixture of these ECPs has been demonstrated. This method, in its current form, makes a number of assumptions regarding variables that are likely to influence the accuracy of the predictive model described.

Table 5.3.2.1. Chromaticity (L*,a*,b*) values of each ECP mixture examined, experimentally observed and predicted from neat CMY-ECP color values. Quantification of agreement between the predicted and observed color values is shown as the value of ΔE_{ab}^{*}

Mixture Composition	Predicted			Observed			ΔE^{*}_{ab}
	L*	a*	b*	L*	a*	b*	-
75:25 C:M	41	-12	-28	55	-14	-33	15
50:50 C:M	58	7	-34	41	9	-42	19
25:75 C:M	53	27	-41	43	40	-42	16
75:25 M:Y	59	33	-16	47	39	-15	14
50:50 M:Y	71	19	16	61	18	26	14
25:75 M:Y	83	6	49	74	4	57	12
25:75 C:Y	89	-13	55	85	-19	59	8
50:50 C:Y	82	-19	30	73	-34	48	25
75:25 C:Y	76	-25	4	70	-34	4	11

The variable mass of solubilizing alkyl chains appended to the ECP backbones are not accounted for, and an estimation of polymer densities is made by fixing all density values at 1 g/cm^3, to name a few. Even with these assumptions having been made, a fair degree of accuracy in the prediction of a given ECP mixture's chromaticity coordinates is demonstrated, and by reducing the number of assumptions applied to the calculations it is likely that a much greater degree of accuracy may be demonstrated.

5.4. Optimizing Achromatic Mixtures for Contrast and Color

With a demonstration of the utility of solution co-processing in generating continuous and well switching mixed ECP films, efforts were directed towards producing achromatic ECP films. This strategy for color production and tuning offers an opportunity to recreate the broad and achromatic spectral profile of such materials as ECP-Black (the structure and spectra of which are discussed in Chapter 4.4.2.) through mixtures of electrochromic polymers. However, by substituting high contrast ECPs which do not feature D-A moieties (suspected to lead to a lower than desired optical contrast in ECP-Black) to cover wavelength regions that are otherwise absorbed by the complex repeat unit structure of ECP-Black, the electrochromic properties of the mixtures produced stand to see improvements in both optical contrast, owing to the minimization of the donor-acceptor content, and in color properties due to the ability to fine-tune the mixture compositions

5.4.1. Co-processing Mixtures for Achromatic Films

Following the traditional subtractive color mixing model centered around cyan, magenta, and yellow hues, a co-processed mixture of ECPs of those colors, referred to as Blend 1, was produced. Spectra and photographs of this CMY mixture are shown in Figure 5.4.1.1, and indeed produced notably achromatic films in the neutral state (a*=-3, b*=4). For the structures and spectra of ECPs-Cyan and -Magenta, the reader is referred

to Figure 5.1.1.1. above. It should be noted that the work regarding broadly absorbing, achromatic films makes use of an alternate polymer structure producing a vibrant yellow to highly transmissive switching pattern, referred to as ECP-Yellow-2 (referred throughout the remainder of Section 5.4 as simply ECP-Yellow), and the structure and spectra of this polymer can be found in Figure 5.4.1.2.[157] In order to produce a mixture with these color values, large contributions from both ECP-Cyan and ECP-Yellow were required, which has several drawbacks with regards to the fully oxidized state of the blend film. Upon oxidation, the donor-acceptor copolymer ECP-Cyan also exhibits a tailing into the visible region, similar to ECP-Blue[36]. While the incorporation of the donor-acceptor polymer ECP-Cyan is in contrast to the design logic of eliminating the use of donor-acceptor polymers, no all-donor material adequately captures light in the 650-750 nm region. Additionally, the increased donor content in ECP-Cyan allows for a more transmissive oxidized state as compared to ECP-Blue. Further, the incorporation of ECP-Yellow is also problematic due to this material being the highest gap material used in any of the mixtures. In order for this high-gap polymer to become fully transmissive, the neutral state absorption, which rests in the 400-500 nm range of the visible, must be shifted all the way to the near infrared. Such a large shift in spectral profile results in the polaronic and bipolaronic charge carrier absorptions being located closer to the visible region than would otherwise be desired and this proximity also leads to substantial tailing into the visible, leading ECP-Yellow to have one of the most substantial residual visible absorption profiles in the oxidized state of the ECPs used for mixing. As a result, the donor-acceptor character of ECP-Cyan and the high gap nature of ECP-Yellow, led the CMY mixture to have an integrated contrast across the visible of 42%, showing no improvement over ECP-Black, also at 42 %.

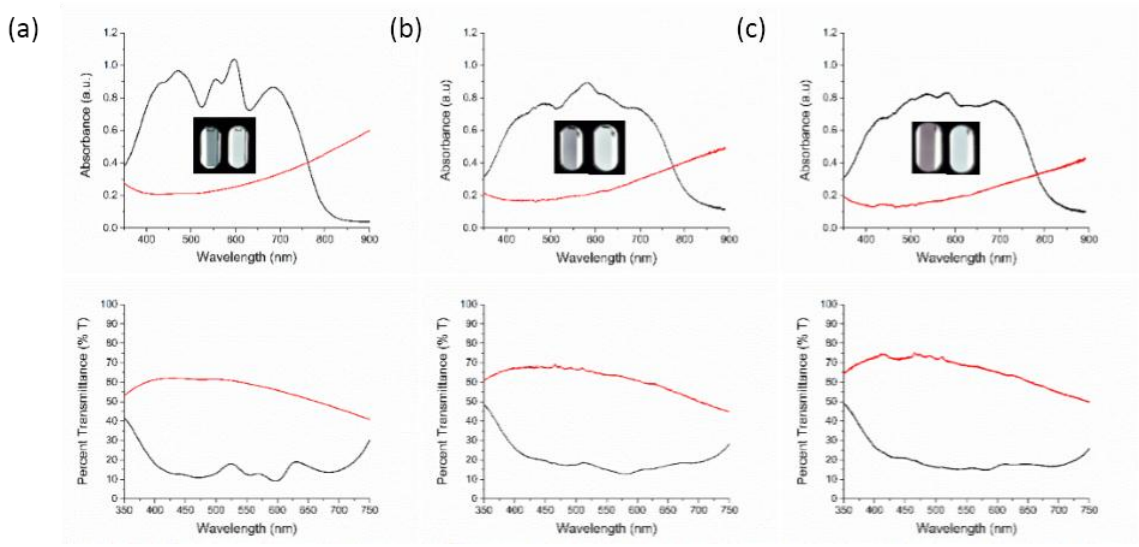

Figure 5.4.1.1. Spectra and photos of blends for black to transmissive electrochromic films: (a) Blend 1 - Cyan, Magenta, Yellow (b) Blend 2 - Cyan, Pink, Periwinkle, Yellow (c) Blend - Cyan, Pink, Periwinkle, Orange

Table 5.4.1.1. Comparison of contrast and CIELAB values for ECP-Black and ECP blends. Values in red are to highlighted to direct the reader to the blend exhibiting the lowest degree of chromaticity (Blend 2) and the highest contrast (Blend 3).

Blend	$\%T_{430-730}$		$\%\Delta T_{430-730}$	Reduced			Oxidized		
	Red	Ox	-	L*	a*	b*	L*	a*	b*
ECP-Black	19	61	42	47	3	-14	84	-5	-5
Blend 1	14	56	42	47	-3	4	81	-4	-3
Blend 2	17	61	44	46	0	-3	84	8	-4
Blend 3	17	65	48	36	6	-7	84	-4	-6

In order to improve on this formulation, the rather counter intuitive step was taken to replace the component with the highest contrast, ECP-Magenta. The replacement polymers, referred to as ECP-Pink and ECP-Periwinkle, are largely similar to ECP-Magenta, in that they are comprised of all donor repeat unit structures and exhibit a high contrast in the visible region. The structures and spectra of these two new components, along with those of the retained ECP-Cyan and –Yellow components are shown in Figure 5.4.1.2.

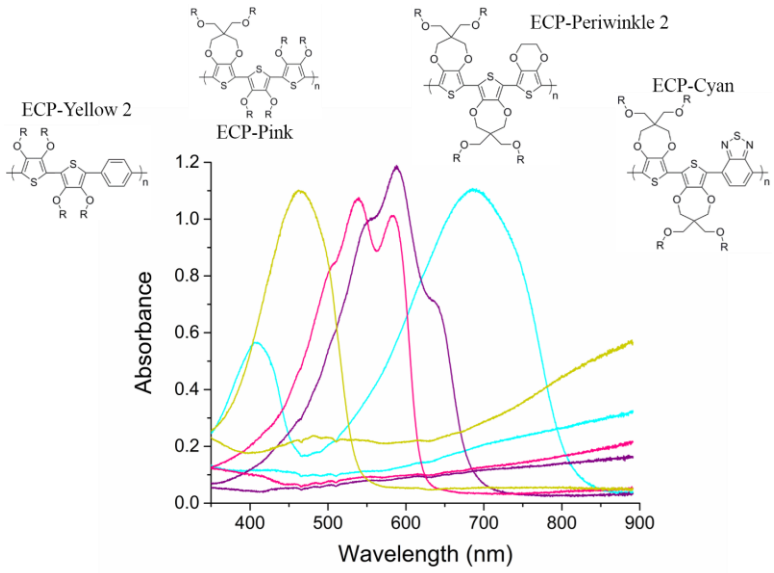

Figure 5.4.1.2. Structures of and neutral state spectra of components of Blend 2 (Cyan-Pink-Periwinkle-Yellow) four component blend; spray cast thin films on ITO-glass.

Further and most importantly, they possess similar band gaps to ECP-Magenta, ECP-Pink having a slightly higher gap and ECP-Periwinkle having a slightly lower gap. These substitutions were made to benefit mixtures in two ways. First, by adding a fourth component and spreading out the wavelength regions covered by those components, a more leveled and achromatic spectral profile could be produced via mixing, by fine-tuning the mixture composition to fill in gaps in the absorption profile observed in the CMY mixture. Second, by spreading out the absorption profiles of the ECPs covering the middle wavelengths (500-650 nm), the content of ECPs-Cyan and -Yellow required to produce an achromatic spectral profile could be reduced, and ideally the contrast of the subsequent mixture would be improved as a result. The spectral profile and photography of this mixture, referred to as Blend 2, is shown at center in Figure 5.4.1.1., and its colorimetric values are compared to both ECP-Black and the CMY mixture (Blend 1) in Table 5.4.1.1., showing that a mixture of very low chromaticity (a*=0, b*=-3) was produced. Further, a slight improvement in the contrast was indeed observed, with Blend 2 exhibiting an integrated contrast of 44%, compared to the 42% of both ECP-Black and the CMY mixture, Blend 1.

Given the improvements to the mixture properties seen with these methods of substitution, further formulations were sought. While an acceptable substitute for ECP-Cyan is not currently available, an alternative to ECP-Yellow is available as ECP-Orange, the structure and spectra of which are shown in comparison with ECP-Yellow in Figure 5.4.1.3.

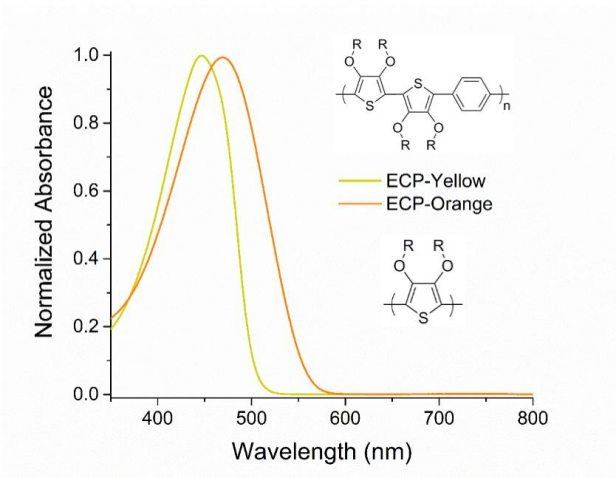

Figure 5.4.1.3. Comparison of the structures and normalized spectra of ECPs-Yellow and –Orange.

ECP-Orange is still a higher band gap material, though lower than ECP-Yellow, and this allows for the formation of polaronic and bipolaronic absorptions further into the near IR, leading to a lower residual visible absorption profile when compared to ECP-Yellow. Therefore, substituting ECP-Orange for ECP-Yellow produces a mixture that sacrifices the achromaticity of the resultant mixture to a slight degree, for the sake of producing a mixture with a notably improved contrast. This four component mixture, referred to as Blend 3, the spectra and photography of which is shown at right in Figure 5.4.1.1., does indeed possess a higher chromaticity when compared with Blends 1 and 2, with chromaticity values of a*=6, b*=-7 in the neutral state. It should be noted that these values still represent a largely achromatic color state, particularly when the luminance value of L* is considered, Blend 3 possessing an L* value of 36, much lower than any other blend. Further, the substitution of the lower contrast ECP-Yellow for the higher

contrast ECP-Orange did indeed produce the desired effect, with the integrated contrast of the mixture, at 48%, shows a considerable improvement over both ECP-Black and the alternative mixture formulations.

Within this chapter, we have explored the co-processing of polymer blends for the purposes of tailoring the color properties of a mixture. A demonstration of the application of traditional pigment color mixing principles was applied to conjugated polymers, though with many assumptions having been made in the process, and a few factors remaining unaccounted for. Despite the exploratory nature of the work described, a fair degree of agreement between the expected and observed chromaticity values is reported. This agreement suggests that the method shows promise in simplifying the route to practical applications for electrochromic polymers. Future efforts to address the methodological issues discussed in Sections 5.1-5.3, as well as continued synthetic efforts to produce novel materials with which to study color mixing properties, will also help to further that effort. Section 5.4 has highlighted the application of this color mixing method to a practical challenge, i.e. improving the spectral performance of a black-to-clear electrochromic film. Via this method, improvements in both the chromaticity and contrast of a mixture were reported. Further efforts to refine either the materials applied towards this practical challenge, or improvements in the mixture compositions discussed are likely to produce further improvements in electrochromic performance.

CHAPTER 6

PHOTOSTABILITY OF SELECT ELECTROCHROMIC POLYMERS

Prior chapters in this dissertation have largely discussed work geared towards the practical application of conjugated polymers, whether via the utility of electrochromic or charge storage properties. However, one aspect of the application of conjugated polymers has remained unaddressed in this dissertation and to an appreciable extent in the literature at large. Electrochromic films are, naturally, best utilized to modulate the intensity or spectral power density transmitted or reflected through them. The long-term effects of this ECP-light interaction regarding the continued performance of the ECP films, or the photostability of electrochromic polymers and conjugated polymers at large, remains a point of contention when discussing the practically of ECP applications. The work described in this chapter attempts to at least partially address the question of ECP photostability by exposing ECP films of varying composition, under varying atmospheric conditions, to the high intensity irradiation of a solar simulator and subsequently examining the electrochromic and chemical properties of the ECP films.

6.1 ECP Photostability : Design and Execution

While the interpretation of characterization data is essential as the work described in this chapter is frequently exploratory in nature, experimental design considerations are equally important to the conclusions drawn from that data, if not occasionally more so. The following sections discuss the selection of specific ECP samples for this study on photostability, as well as the steps taken to encapsulate and isolate ECP films and details pertaining to irradiation conditions employed.

6.1.1. ECP Sample Selection

The introductory chapter to this dissertation presented the reader with a large family of electrochromic polymers developed within the Reynolds labs, using various structural motifs to achieve different neutral state color properties. Further, materials based on both the DOT and DOP heterocycle unit were discussed, and regularly employed throughout the work detailed in the following chapters. When devising the experimental parameters of exploratory work on the photostability of electrochromic polymers, the initial question asked is "Which, if any, of these materials is best suited to serve as a general model for ECP photostability?". After deliberation, it was decided that two materials, ECP-Magenta and MCCP, offered to represented the broadest set of the ECPs described in Chapter 1, and the repeat unit structures of these materials are shown in Figure 6.1.1.1[32, 37].

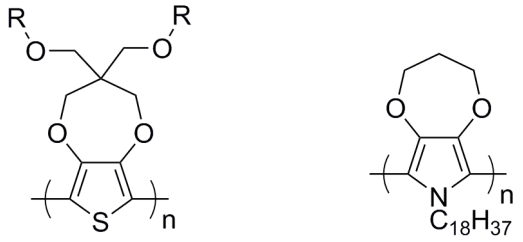

Figure 6.1.1.1. Structures of ECP-Magenta and MCCP

First, ECP-Magenta, or the poly(propylenedioxythiophene) homopolymer was selected to represent the dioxythiophene based polymers, as this structural unit is found in almost all of the DOT-based ECPs. Further, considering the exceptions of ECP-Red and ECP-Orange, which feature acyclic alkoxy groups appended to the 3 and 4 positions on the thiophene unit, the structures surrounding the center of conjugation (the thiophene core) are arguably similar enough to the ECP-Magenta repeat unit that similar phenomena would be encountered upon irradiation. The second material, MCCP, was chosen as representative of DOP-based repeat unit structures. While the family of ECPs discussed in Chapter 1 features only this example of a DOP-based polymer, MCCP is

employed almost universally in the window-type electrochromic devices discussed in this dissertation. Due to its degree of utility in window-type ECDs (the variety most likely to be employed in applications where a high degree of exposure to sunlight would be expected), the assessment of the photostability of MCCP was deemed worthwhile. The casting and encapsulation prior to exposure to an illuminant of these two ECPs is discussed in the following section.

6.1.2. Substrate Preparation and Film Casting

As the characterization of ECP samples following exposure to the source of illumination would entail cyclic voltammetry and spectroelectrochemical measurements to assess electrochromic viability, samples were cast onto a substrate of ITO-glass, in an identical fashion to the ECP casting practices discussed in Chapter 2. Prior to casting, ITO-glass substrates were rinsed with toluene, isopropanol, and finally acetone and allowed to dry. Films of ECP-Magenta were cast until an optical density at λ_{max} (556 nm) of 1.0 ± 0.15 AU (absorbance units) was reached. To reflect film thickness most often employed in the ECDs discussed in this dissertation, MCCP films were cast until an optical density at λ_{max} (315 nm) of 0.5 ± 0.1 AU was reached. To allow space for the addition of an encapsulating gasket, films were cast onto substrates measuring 25 x 35 mm, and films were cast to have an area similar to the spectrometer cuvette sized ITO-glass slides, with an area of ~ 7 x 25 mm through the use of a mask. Following the casting of ECP films, samples were transferred to a glove box with an argon atmosphere for storage prior to encapsulation.

It could reasonably be said that the highest hurdle to the examination of ECP photostability is the devising of an encapsulation scheme that is both practical and sufficiently robust to ensure the preservation of the atmospheric conditions under which ECP films are tested. With regard to the exclusion of both oxygen and water vapor, it is rather fortunate then that the development and study of barrier materials which prevent

the intrusion of water vapor and oxygen (herein referred to simply as “air”) is an active field of research, as the question of photo- and photo-oxidative stability does not pertain exclusively to conjugated ECPs. In a recent report from Kim *et al*, a polyisobutylene (PIB) edge sealant modified with desiccant materials and functionalized with silane coupling agents was used to encapsulate electrochromic devices[158]. A substantial improvement in device longevity was observed when compared to the use of a conventional epoxy sealant, under conditions of elevated temperature and humidity, though samples were not exposed to a high-intensity light source in that study. The barrier properties of this PIB sealant were demonstrated to be sufficiently robust that it could meet the challenge of maintaining the environmental conditions around encapsulated ECP films (atmospheric composition, absence of water vapor, etc.) during a prolonged period of irradiation, such that the long-term photo-stability of select electrochromic polymers might be assessed. Using the PIB sealant described by Kim *et al*, films of ECP-Magenta and MCCP were encapsulated in both air atmospheres (so as to promote photo-oxidation) and a dry argon atmosphere such that photo-oxidative degradation might be prevented, and this encapsulation scheme is shown in Figure 6.1.2.1.

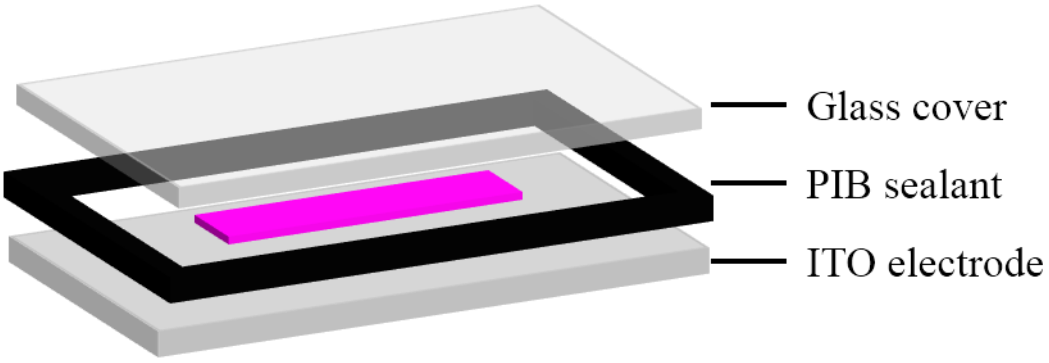

Figure 6.1.2.1. Schematic representation of encapsulation scheme used in photostability testing.

6.1.3. Irradiation of ECP Films

Following encapsulation, samples were transferred to the Atlas Suntest XLS+ testing station. Samples were placed on the floor of the testing chamber, with the uncoated glass cover slide closest to the lamp. Prior to testing, the output of the Xe arc lamp incorporated into the testing station was tuned to match the output of an AM 1.5 light source, and the details of this process can be found in Chapter 2.6[114]. As further described in Chapter 2, the spectral power density of this Xe lamp is filtered to approximate that of natural daylight, lending the irradiation conditions of the encapsulated ECP samples to be most closely matched to a thin film exposed to daylight, behind a thin (1.1. mm) pane of glass. All samples were irradiated under these conditions, with the length of the irradiation being the only factor differentiating samples within the same sample type. Irradiation times used throughout the study of ECP photostability were 24 hours, 48 hours, one week (168 hours), two weeks (336 hours), and one month (31 days, or 744 hours). Additional samples, referred to as "standards" were stored in darkness at a temperature of 25 °C for lengths of time identical to those used for sample irradiation. These standard samples were cast and encapsulated in a fashion identical to those samples which underwent irradiation. Following irradiation or storage, samples were gently heated on the bench top using a hot plate set at 70 °C for roughly five minutes to allow for removal of the glass cover slide, and any remaining sealant was removed from the ITO-glass substrate.

6.2 Characterization of ECP-Magenta Photostability

While films of both ECP-Magenta and MCCP were irradiated and characterized concurrently, we will begin our discussion first with the observations made in the case of ECP-Magenta.

6.2.1. Spectroelectrochemistry and Cyclic Voltammetry

Following irradiation, ECP-Magenta films were removed from the sample chamber of the Atlas SunTest system, and gently heated on a hot plate to allow for the removal of the glass cover slide as well as any sealant material remaining on the ITO surface. Following this preparation both ECP-Magenta films irradiated while under air and argon atmospheres, representing each irradiation time point designated, were switched (i.e. potential cycled) prior to the recording of spectroelectrochemical measurements. Additional spectra were recorded in this fashion for "standard" samples, which were identically encapsulated but were not exposed to the solar simulator, and rather stored in a darkened cabinet. Spectra were recorded at potentials at which the fully colored and fully bleached states are attained (-0.5 and 0.8 V vs Ag/Ag^{+}, respectively). After the recording of spectra for each sample, a ready basis for comparison of electrochromic performance is found in the measure of contrast, or the difference in percent transmittance (Δ%T) between the fully colored and fully bleached states. Given ECP-Magenta's dual peak absorption profile, the wavelength at which this contrast was measured was chosen to be 550 nm, in close correspondence to the higher energy peak in ECP-Magenta's characteristic spectrum ,and the wavelength to which the human eye is most sensitive.

Over the course of irradiation, a trend can be seen to emerge in the contrast values measured (and therefore the persistence of electrochromic and redox behavior) for each sample type, and this trend in contrast values at 550 nm against irradiation time is shown in Figure 6.2.1.1.

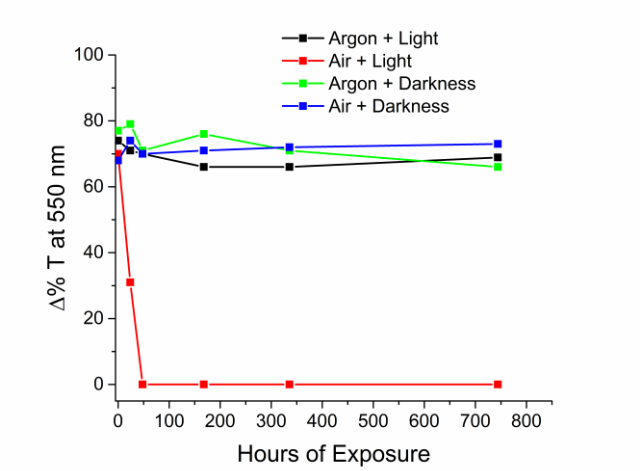

Figure 6.2.1.1. Electrochromic contrast recorded during the irradiation of ECP-Magenta films under varying environmental conditions.

Of immediate concern regarding the data shown in Figure 6.2.1.1. is the rapid decrease in contrast where films are irradiated in an air atmosphere, reaching a contrast of 0% within 48 hours. However, equally of note is the persistence of electrochromic contrast values where films of ECP-Magenta encapsulated with an argon atmosphere are concerned, with no significant decrease in the contrast values being observed after one month of irradiation. This result in particular serves to illustrate that, given proper handling conditions, DOT-based electrochromic polymers are potentially photo-stable for considerable lengths of time, even when exposed to a significant light source. Further, the trend seen in Figure 6.2.1.1. is largely in accord with previous reports regarding the stability of conjugated polymers; namely, that in addition to the presence of oxygen and/or water vapor, light is required for degradation processes to occur[159-163]. The contrast recorded for samples which were not exposed to the solar simulator, though samples were encapsulated in both argon and air atmospheres, is not seen shift over the course of their storage times.

Given the observation of this trend, a comparison of the spectra recorded at the final time point (744 hours, or one month) offers to further demonstrate the photo-stability of ECP-Magenta, given proper encapsulation. Shown in Figure 6.2.1.2. are two

sets of spectra corresponding to films encapsulated in air and argon environments and exposed to one month of continuous irradiation. Cyclic voltammograms, recorded during the initial potential cycling of the above films, are also shown in Figure 6.2.1.2. What is immediately apparent in the spectra recorded is the lack of both absorption within the visible region (red and black traces, largely overlaid) as well as the lack of redox activity in the samples irradiated in air.

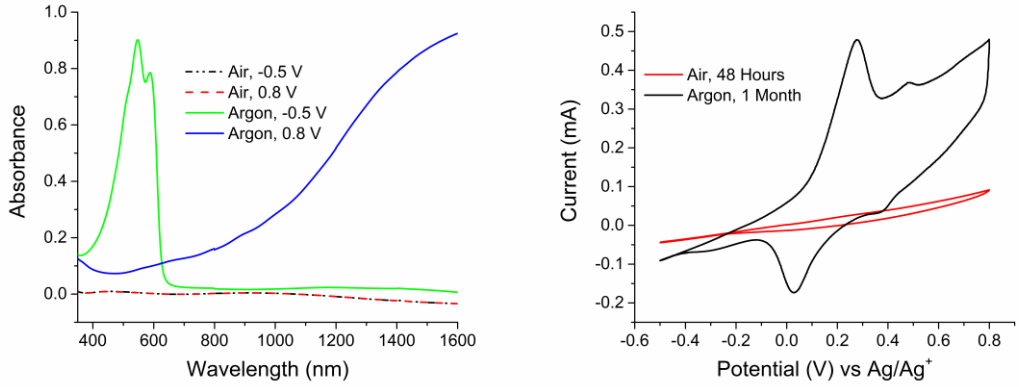

Figure 6.2.1.2. Spectroelectrochemistry and cyclic voltammetry of ECP-M samples irradiated in air and argon atmospheres.

The loss of the visible absorbance (a form of photo-bleaching) helps to qualify the loss of contrast seen in the air irradiated samples in Figure 6.2.1.1., illustrating that a value of 0% contrast is not a matter of simply non-existent electrochromic behavior, but rather more likely the result of some number of photo-oxidative processes, as previously suggested. Again though, notable is the perseverance of redox-activity in films irradiated under an inert, argon atmosphere, and the similar persistence of the characteristic redox activity of ECP-Magenta. Here, even after one month of continuous illumination with a solar simulator, no deleterious effects are noted for either the colored or bleached redox states, and the doublet peak structure of the colored state absorption as well as the highly transmissive bleach state spectrum are observed.

6.2.2. X-ray Photoelectron Spectroscopy (XPS)

While the comparisons of redox and electrochromic characteristics of encapsulated samples serves to illustrate that given proper care, DOT-based ECPs are likely photo-stable over significant lengths of time, little information is offered by these methods on the structure of the ECP structures following irradiation. For this purpose the surface of ECP films, encapsulated and exposed to a solar simulator as previously described, were probed via x-ray photoelectron spectroscopy (XPS). Spectra of the C(1s), O(1s) and S(2p) core level orbitals for films of ECP-Magenta were recorded, and the C(1s) and S(2p) spectra for films irradiated in air can be found in Figure 6.2.2.1. Similarly, films irradiated in an argon atmosphere are shown in Figure 6.2.2.2. As these spectra are often more useful for diagnostic purposes in identifying the products of degradation, we will address these first, and briefly discuss the O1s spectra, as well as the spectra recorded for the standard samples later on.

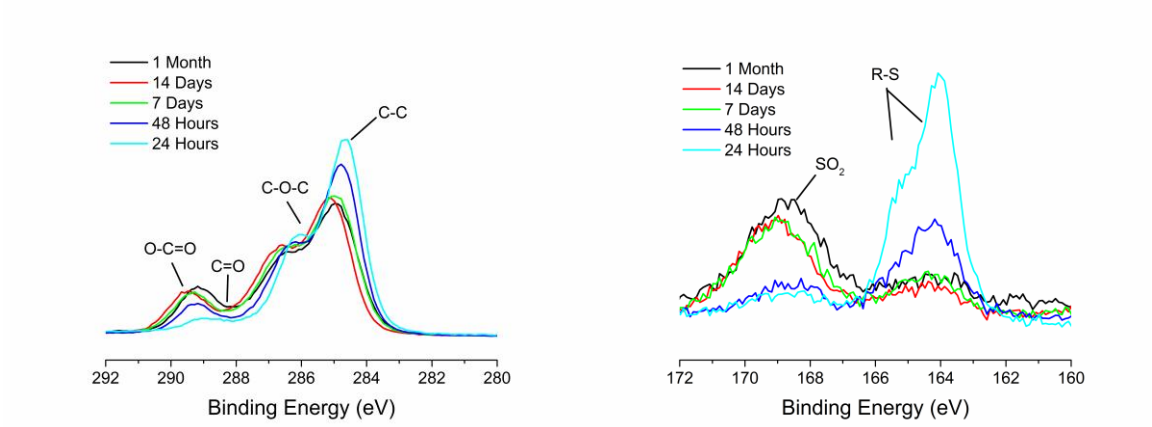

Figure 6.2.2.1. XPS spectra over time of the C1s and S2p orbitals in ECP-M irradiated under an air atmosphere.

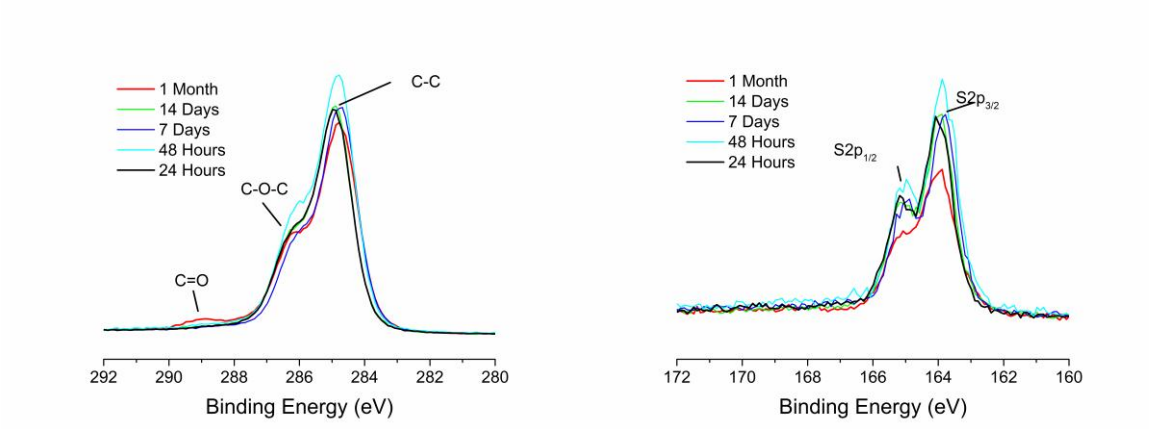

Figure 6.2.2.2. XPS spectra over time of the C1s and S2p orbitals in ECP-M irradiated under an argon atmosphere.

Identified in the XPS spectra shown in Figure 6.2.2.1., the C(1s) orbital of an ECP-Magenta film irradiated in an air atmosphere, are binding energy signals corresponding chemical environments expected in the ProDOT-based ECP-magenta, such as (C-C) at 284.8 eV and (C-O-C) at 286.6 eV[164]. In addition to these signals, peaks are identified at higher binding energies which suggest the addition of oxygen to the repeat unit structure upon photo-oxidation, such as (C=O) and (O-C=O) at 287.8 and 289.1 eV, respectively[164-167]. These C(1s) signals suggest the addition of oxygen to the repeat unit structure grow in over the course of the irradiation as the intensity of these peaks relative to the C-C peak at 284.8 eV peak grows, reaching a maximum at some point between 48 hours and 7 days of irradiation. Concurrently, the S(2p) spectra of the air-encapsulated samples initially show a doublet peak with high intensities at the binding energies for the S($2p_{1/2}$) and S($2p_{3/2}$) signals, at 164 and 165.2 eV[164, 167-168]. However as with the C1s spectrum, throughout the course of irradiation the relative intensities of these signals diminishes, to be largely replaced by a broad peak, likely a poorly resolved doublet, centered at 169 eV. This signal has been found to be indicative of the formation of sulfon (SO_2) moieties, further indicating the incorporation of oxygen into the polymer backbone structure[68, 164, 167].

However, this behavior is almost entirely absent in films encapsulated under an argon atmosphere. In the C(1s) spectra shown in Figure 6.2.2.2., while strong intensities are observed for the (C-C) and (C-O-C) signals throughout the irradiation time frame, only one additional signal appears rather anomalously at 289.1 eV, suggesting formation of (C=O) moieties, after a month of irradiation. Given the rapid time course of oxygen incorporation observed in the spectra shown in Figure 6.2.2.1., the emergence of this signal likely is a result of a developing fault in the encapsulant material, allowing for the introduction of atmospheric oxygen into the sample. As the PIB sealant was laid down in a rectangular pattern formed by stripes cut from the a ribbon, the corners where these strips are made to meet are the most likely locations for the development of faults in the encapsulation. Further, no growth of the binding energy signals indicative of the formation of the sulfon groups observed after irradiation in air is observed. These observations, both the perseverance of electrochromic contrast as well as the lack of growth of additional binding energy signals, serve to illustrate the photo-stability of ECP-Magenta, provided care is taken to preclude conditions which foster photo-oxidation specifically, and adequate barrier materials are used to ensure the persistence of those conditions.

Finally, as previously mentioned, while O (1s) spectra are often not as diagnostically useful, it is worth noting that in the spectra recorded for the ECP sample irradiated under and argon atmosphere, what is likely only one peak is observed, centered at 532.7 eV as seen in Figure 6.2.2.1.. Similarly, the O (1s) spectra recorded for films irradiated under and air environment has a maximum value at 532.7 eV, however the peak recorded is considerably broader towards the higher binding energy range, suggesting the formation of chemical environments around oxygen atoms in line with the formation of (C=O), (O-C=O), and (SO_2) signals.

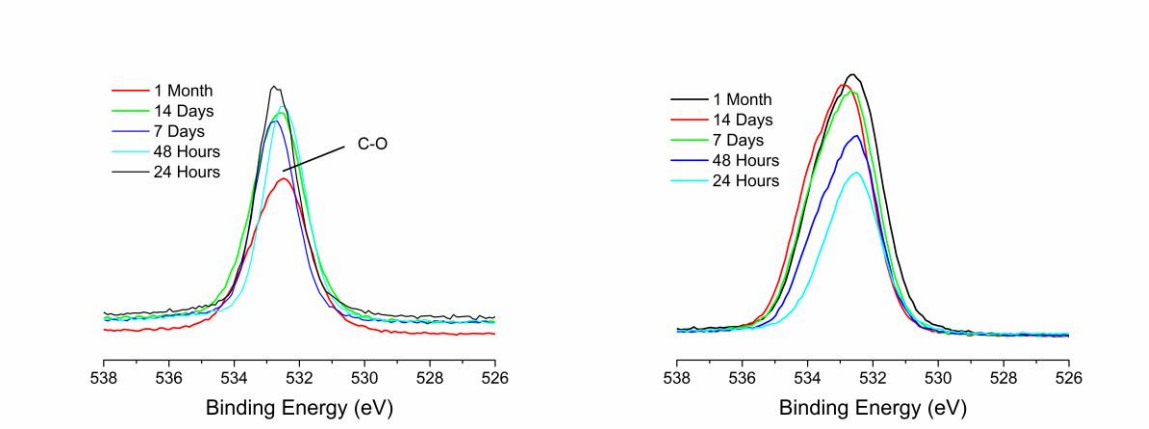

Figure 6.2.2.3. XPS spectra of the O1s orbital in ECP-M films irradiated in argon and air atmospheres.

As mentioned earlier, in order to qualify the spectra recorded for samples irradiated under air and argon atmospheres, ECP films were similarly encapsulated and stored in darkness for periods identical to those used for irradiation. Shown in Figure 6.2.2.4. are the C (1s) and S (2p) spectra recorded for these films at the longest time point used, 1 month. As can be seen from these spectra, no difference is noted between the binding energy signals between air and argon stored samples. For instance, in the C (1s) spectra, two signals in particular are observed, at 284.8 and 286.6 eV, corresponding to the (C-C) and (C-O-C) bonding scheme expected ab initio from the repeat unit structure. Similarly, a doublet peak is observed for both samples in the S (2p) signal, centered at binding energies expected for the $2p_{3/2}$ and $2p_{1/2}$ signals for the thiophenic sulfur.

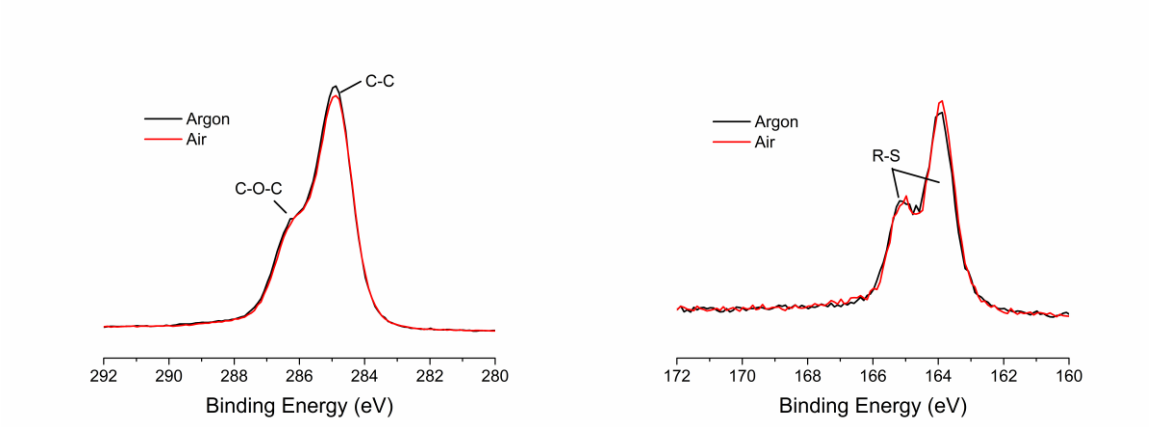

Figure 6.2.2.4. XPS spectra of C1s and S2p orbitals of ECP-M stored for one month in darkness, under both air and argon atmospheres.

6.3 Characterization of MCCP Photostability

In the previous section the characterization of ECP-Magenta samples following irradiation in various atmospheric conditions (or storage in darkened conditions) was discussed extensively. As mentioned, trials were run concurrently using both ECP-Magenta and MCCP films, and the following sections pertain to the analogous characterization of MCCP samples.

6.3.1. Spectroelectrochemistry and Cyclic Voltammetry

As previously mentioned, samples of the DOP-based MCCP were tested in an identical fashion to films of ECP-Magenta. In further similarity with ECP-Magenta, a trend emerged in the relationship between conditions of encapsulation during prolonged irradiation and the persistence of redox activity and subsequently electrochromic performance. This is demonstrated via the spectra recorded at either extreme of the potential window for MCCP (-0.5 to 0.7 V vs Ag/Ag+) following one month of continuous irradiation, as well as the CV traces, shown in Figure 6.3.1.1.

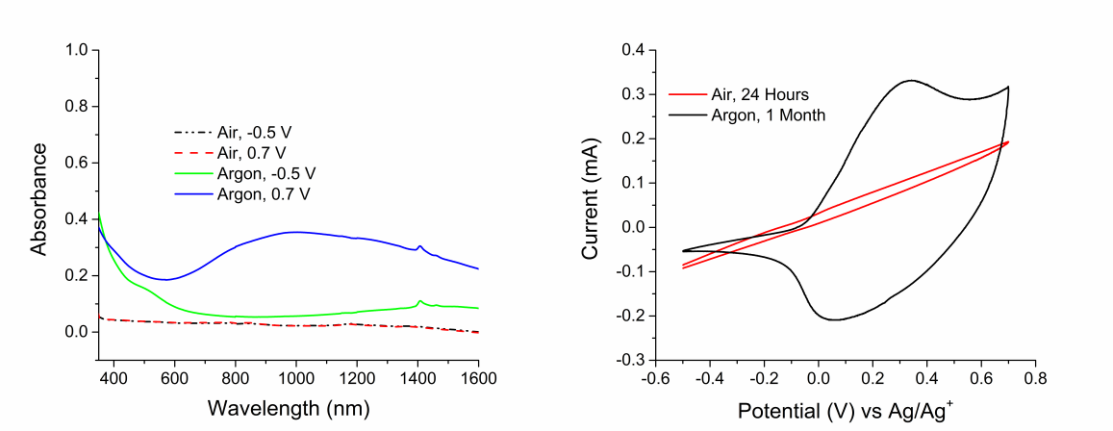

Figure 6.3.1.1. Spectroelectrochemistry and cyclic voltammograms of MCCP films irradiated for 24 hours (air) and 1 month (argon).

Those samples encapsulated in an air environment prior to irradiation with a solar simulator (red and black dashed traces) were seen to deteriorate relatively rapidly, with no redox or electrochromic behavior evident. Through the spectra shown are representative of films following one month of irradiation, similar behavior was observed after 24 to 48 hours of irradiation. Those samples sealed within an inert argon atmosphere however were observed to be stable throughout the time frame established for irradiations, and consequently the electrochromism and redox behavior characteristic of MCCP was observed.

6.3.2. X-ray Photoelectron Spectroscopy (XPS)

Following irradiation, the C (1s), N (1s) and O (1s) orbitals of films of MCCP were probed via XPS. Select spectra are shown in Figures 6.3.2.1. and 6.3.2.2., namely the C (1s) and N (1s) spectra for air encapsulated samples (Figure 6.3.2.1.) and the same spectra for the samples encapsulated within an argon atmosphere (Figure 6.3.2.2.). Further following the trend established in the case of ECP-Magenta, where films of MCCP were irradiated in the presence of an air atmosphere, new signals at binding energies associated with (C=O) and (O-C=O) units (287.8 and 289.1 eV) are seen to appear rapidly, in almost all cases in under 24 hours, a time point by which a loss in

electrochromic character is noted in MCCP as shown in Figure 6.3.1.1. In contrast to the growth of new peaks observed in the case of ECP-Magenta, and likely due to the different route to the addition of the solubilizing alkyl chain, these new peaks are much lower in relative intensity, when compared to the signals observed for the (C-C) and (C-O-C) chemical environments (284.8 and 286.6 eV). In the case of ECP-Magenta, the growth of higher binding energy peaks in the C (1s) spectra is seen to occur within roughly 48 hours, coinciding with the loss in contrast reported in Figure 6.2.1.1. This is a particularly important observation when considering that at the 48 hour time point in the S2p spectrum, while a shift in relative peak intensity is noted, the un-oxidized sulfer signal is still the dominant doublet peak, suggesting that the oxidation of the bridging ether moieties in ECP-Magenta occurs more readily, and is also closely tied to the loss of electrochromic and redox characteristics. This trend likely the case where MCCP is considered as well, with the relatively easy photo-oxidation of the bridging ether moieties occurring within 24 hours of irradiation in an air environment, severely curtailing the electrochromic properties of the polymer film. Further, in the N (1s) spectra obtained, while initially only a single peak is likely to be present, representative of the (-NR-) environment, the signal broadens at later time points, after at least two weeks of continuous irradiation. The growth of these new signals in the N (1s) spectrum however lags far past the loss of redox and electrochromic activity in MCCP samples.

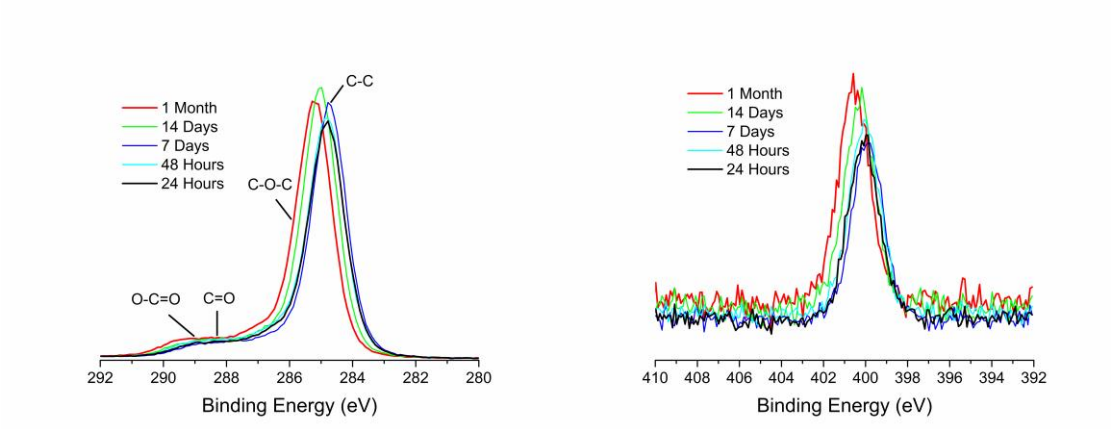

Figure 6.3.2.1. XPS spectra over time of the C1s and N1s orbitals in MCCP irradiated under an air atmosphere.

In those samples encapsulated under an argon atmosphere, little to no changes are reported during the course of irradiation. Present are the signals for the (C-C) and (C-O-C) chemical environments (284.8 and 286.6 eV), however the relative intensities of these to signals is not observed to shift over the course of sample irradiation. It should be noted however that, in some samples, a should appeared to form in samples irradiated for 14 days (green trace, Figure 6c), suggestive of the signals observed in the air encapsulated samples. For these reasons, and the absence of these signals in the samples irradiated for one month, this is likely the result of non-adequate sealing of sample films allowing trace amounts of air into the sample environment. Examination of the N (1s) spectrum in the argon atmosphere samples shows a signal fit with a single peak throughout the course of irradiation, centered at 399.6 eV, characteristic of the (-NR-) environment[165-166, 169-170].

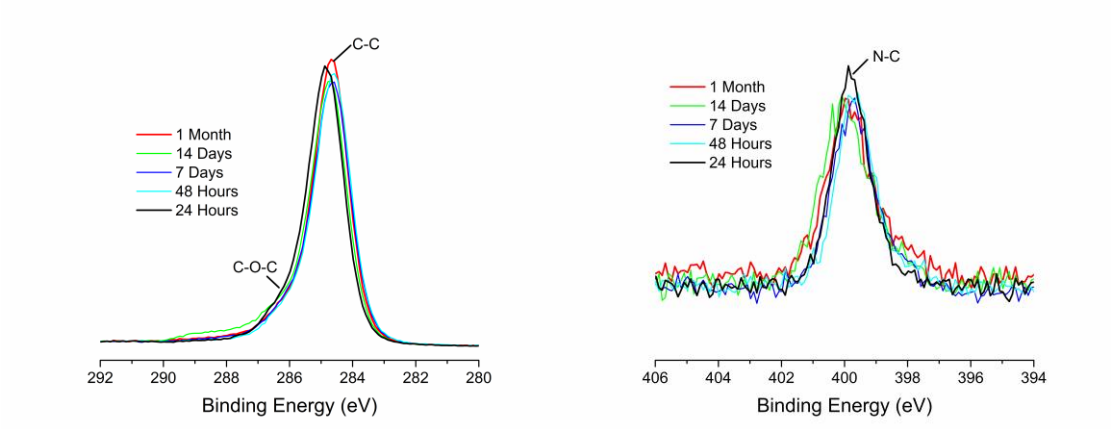

Figure 6.3.2.2. XPS spectra over time of the C1s and N1s orbitals in MCCP irradiated under and argon atmosphere.

Examination of the O (1s) spectra recorded, shown in Figure 6.3.2.3., follows almost implicitly the trend established by the ECP-Magenta samples detailed previously. In the air encapsulated samples, a large degree of peak broadening is observed throughout the course of irradiation, indicating the addition of new oxygen bonding motifs to the structure of MCCP. In contrast, the spectra recorded for the argon encapsulated samples do not demonstrate this peak broadening behavior.

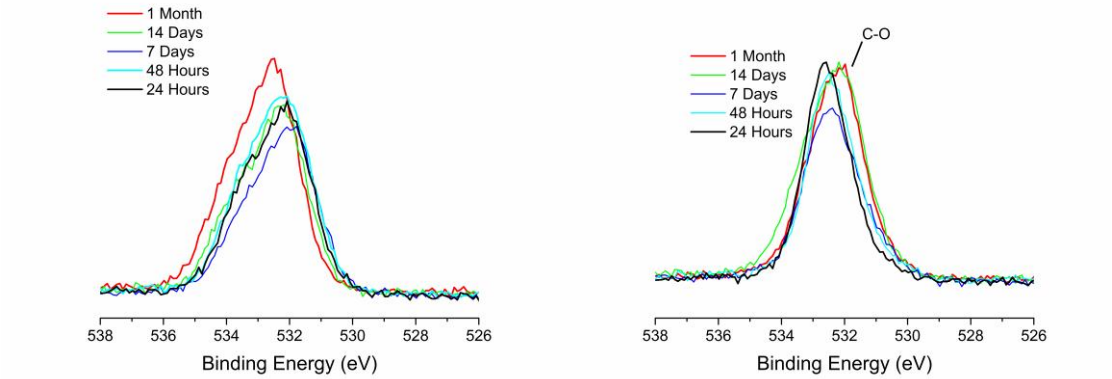

Figure 6.3.2.3. XPS spectra of the O1s orbital in films of MCCP irradiated under argon and air atmospheres.

6.4 Electrolyte-bearing Samples

The previous sections regarding the photostability of ECP materials have all dealt with, for the sake of experimental clarity, the simplest role an ECP film might take, i.e. as

a coating on a solid substrate. This arrangement is far removed however from the setting in which case practical usage might be found, such as in an electrochromic device, due to the absence of a supporting electrolyte or an opposing electrode surface. While the photostability of ECPs as no more than a material has been discussed in previous sections, photostability in slightly more complicated environments is well worth examining. To bring the ECP samples under examination one step closer to the ECD stage the addition of a gel electrolyte, commonly used in device prototyping, was carried out just prior to encapsulation. Further, as the instability of ECP samples in the presence of an air atmosphere has been established, electrolyte-ECP samples were only encapsulated under an argon atmosphere. Due to the more complicated chemical environment this would produce at the surface of the ECP films under study, following irradiation, films were not examined via XPS as before. However the observation of electrochromism via spectroelectrochemistry, or its absence, following irradiation when in physical contact with this electrolyte mixture, would suffice to demonstrate ECP stability given proper handling and encapsulation conditions.

6.4.1. Spectroelectrochemistry of Electrolyte-bearing samples

As with previous photo-stability samples, samples were examined following the various lengths of irradiation established, the longest of which was one continuous month of irradiation under a solar simulator. Spectra recorded following the final time point at one month, at bleaching and coloring potentials for both ECP-Magenta and MCCP, are shown in Figure 6.4.1.1. Illustrated in these spectra is the retention of electrochromic behavior following one month of irradiation, readily demonstrating two main points. First, films of each of these polymers, in the presence of this particular electrolyte formulation, are stable to prolonged irradiation.

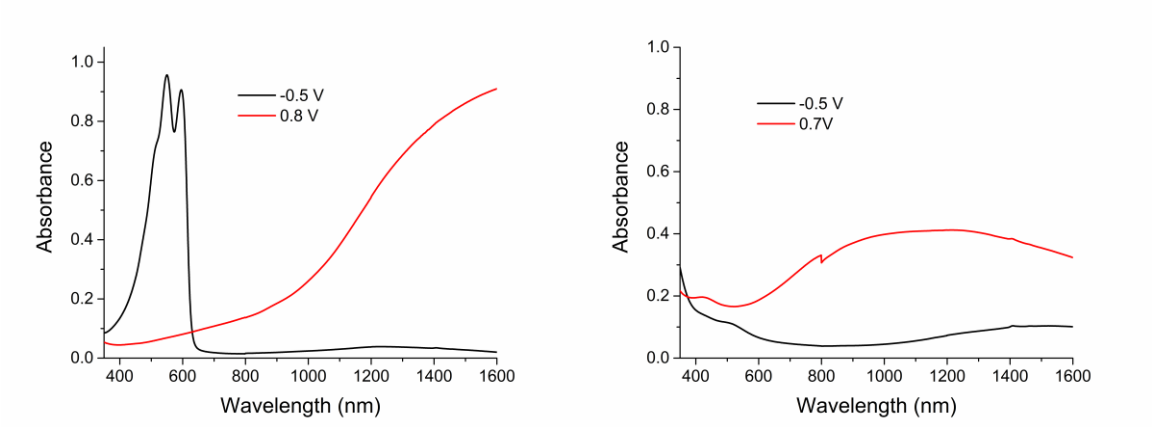

Figure 6.4.1.1. Spectroelectrochemistry of an ECP-M film irradiated for 1 month under an argon atmosphere, in physical contact with a gel electrolyte.

In the case of ECP-Magenta, no loss in contrast is observed at 550 nm, nor is the spectral profile of ECP films irradiated in this fashion altered to any appreciable degree. As is the case with ECP-Magenta, the MCCP films (represented by the one month sample shown in Figure 6.4.1.1.), are seen to show the electrochromic behavior characteristic of that material. The second point made by the spectra shown in Figure 6.4.1.1 is to reinforce the necessity for proper handling and encapsulation in the application of DOT- and DOP-based electrochromic polymers. As previously observed, had these films been encapsulated on the benchtop, the presence or absence of the gel electrolyte mixture would likely have a much lesser impact on film stability than the presence or absence of water vapor or oxygen.

The results discussed in this chapter, while arguably preliminary, serve to demonstrate the photo-stability of conjugated, electrochromic polymers provided care is taken to preclude conditions which have been observed to foster photo-oxidation. This observation is relatable to both DOT- and DOP-based conjugated polymers, and future studies would benefit from focusing on photo-stability in environments more akin to a full electrochromic device setting, as well as the examination of alternative electrochromic polymer repeat unit structures.

CHAPTER 7

PERSPECTIVE AND SUGGESTIONS FOR FUTURE RESEARCH

The materials, devices, and data discussed in this thesis are presented in an effort to demonstrate a few of the many modes of application for conjugated polymers, and those demonstrated here pertain directly to electrochromic and supercapacitive applications. More broadly however, this dissertation as a whole might be summed into three theses.

The first of these is demonstrated in Chapter 3, and is in some regards two-fold. Through synthetic control of the solubilizing groups appended to the main conjugated portion of a polymer chain, aqueous solubility and processability might be attained, as was previously demonstrated by Shi *et al* in 2012. This observation becomes more relevant in light of its utility in the modification of high surface area electrode substrates for charge storage applications, particularly due to the prevalence of electrodeposition as the means to carry out such modifications, and the difficulties faced when applying this method to large-scale and high-throughput settings. The utility of this method was demonstrated through the modification of a non-woven CNT textile substrate with ProDOT-$EDOT_2$ processed from a water solution, wherein capacitive performance was observed to nearly double on a gravimetric basis and nearly quintuple on an areal basis. While a demonstration of the application of solution processing towards the fabrication of composite CNT-polymer electrodes has been made and the capacitive performance of the resultant composite electrodes has been examined, much is left to understand regarding the physical characteristics of the composite electrodes. Imaging of both the surface and cross sections of the composite electrodes, likely through electron microscopy, will do much to inform our knowledge of the degree of electrode coverage attained through the solution processing steps taken, and this will in turn inform steps taken in the future to

optimize the solution processing technique to create a more intimate interface between the solution cast pseudocapacitive polymers employed the substrates on which they're cast.

The second of the three theses put forth in this dissertation pertains to the application of color mixing in electrochromic polymers. Materials-level strategies towards tailoring the optical properties of electrochromic materials offer a recourse to the purely synthetic, structure-property relationship driven methods more commonly applied to tune the optical and colorimetric properties of electrochromic materials. Demonstrated in Chapters 4 and 5 are two divergent routes towards the application of color-mixing in ECPs. The first, through the utilization of an electrochromic device architecture featuring physically separate and individually addressable electrochromic films, illustrated the attainability of a broad color gamut using pairs of ECP films representative of the cyan-magenta-yellow subtractive color mixing primaries. The latter, eschewing the physical separation of ECP films, demonstrates that co-processing of ECP mixtures can be used to achieve similar color-mixing effects, and that the products of this process may follow a predictable color mixing scheme, discernable through ECP mixture composition. With regards to the future of research into the application of color-mixing strategies to electrochromic polymers, the broad gamut attained in Chapter 4 and the visual homogeneity of mixed films cast in Chapter 5 suggest that discrete patterning of ECP elements is likely to produce a similarly wide gamut while displaying the same visual continuity as the co-processed films. Given sufficiently patterned electrode substrates, these discretely deposited color elements could conceivably be individually addressed, allowing for greater control over the color properties of a completed ECD.

Finally, the results presented in Chapter 6 attempt to address the persistent notion regarding the purported instability of conjugated polymers under high intensity illumination. Examined through spectroelectrochemistry and XPS following a controlled period of irradiation, photo-oxidation of conjugated polymers is indeed an enduring

challenge to the practical application of ECPs. Presented in tandem with this re-confirmation of photo-oxidative instability however is the observation that steps taken to preclude the conditions known to foster photo-oxidation (namely, the presence of atmospheric oxygen and water vapor) are effective at maintaining the chemical, and therefore functional, integrity of ECPs. Encapsulation of ECP films with a polyisobutylene rubber sealant is sufficient to limit the intrusion of atmospheric oxygen and water vapor, inhibiting photo-initiated degradation. A pair of caveats are naturally apparent in this finding however, both the range of materials involved in the study as well as the duration over which the study was carried out. As an exploratory effort, two polymer structures out of a much larger family were selected for experimentation, representative of the two major structural motifs present in the aforementioned family. While the results obtained might be generalized for structures not studied, results obtained directly from the remainder of electrochromic polymers available would best inform out understanding of photo-stability in ECPs. Further, exposure to the solar simulator used to assess photostability was limited to one month in the efforts discussed in Chapter 6. While this period of one month may be thought of as six to twelve months of "real world" light exposure, an examination of the photostability of ECPs over a much longer time frame is necessary to demonstrate suitability of ECPs for long-term, i.e. multi-year, applications.

REFERENCES

1. McNeill, R.; Siudak, R.; Wardlaw, J.; Weiss, D., Electronic Conduction in Polymers. I. The Chemical Structure of Polypyrrole. *Australian Journal of Chemistry* **1963,** *16* (6), 1056-1075.
2. Shirakawa, H.; Louis, E. J.; MacDiarmid, A. G.; Chiang, C. K.; Heeger, A. J., Synthesis of electrically conducting organic polymers: halogen derivatives of polyacetylene, (CH). *Journal of the Chemical Society, Chemical Communications* **1977,** (16), 578-580.
3. Heeger, A. J., Semiconducting and Metallic Polymers: The Fourth Generation of Polymeric Materials†. *The Journal of Physical Chemistry B* **2001,** *105* (36), 8475-8491.
4. Heeger, A. J., Nobel Lecture: Semiconducting and metallic polymers: The fourth generation of polymeric materials. *Reviews of Modern Physics* **2001,** *73* (3), 681-700.
5. Salzner, U.; Lagowski, J. B.; Pickup, P. G.; Poirier, R. A., Comparison of geometries and electronic structures of polyacetylene, polyborole, polycyclopentadiene, polypyrrole, polyfuran, polysilole, polyphosphole, polythiophene, polyselenophene and polytellurophene. *Synthetic Metals* **1998,** *96* (3), 177-189.
6. Jahn, H. A.; Teller, E., *Stability of Polyatomic Molecules in Degenerate Electronic States. I. Orbital Degeneracy*. 1937; Vol. 161, p 220-235.
7. Little, W. A., Possibility of Synthesizing an Organic Superconductor. *Physical Review* **1964,** *134* (6A), A1416-A1424.
8. Chien, J. C. W.; Karasz, F. E.; Shimamura, K., An estimate of bond length alternation in trans-polyacetylene. *Die Makromolekulare Chemie, Rapid Communications* **1982,** *3* (10), 655-659.
9. Baeriswyl, D.; Campbell, D.; Mazumdar, S., An Overview of the Theory of π-Conjugated Polymers. In *Conjugated Conducting Polymers*, Kiess, H., Ed. Springer Berlin Heidelberg: 1992; Vol. 102, pp 7-133.
10. Bredas, J. L.; Street, G. B., Polarons, bipolarons, and solitons in conducting polymers. *Accounts of Chemical Research* **1985,** *18* (10), 309-315.
11. Stafström, S.; Brédas, J. L.; Epstein, A. J.; Woo, H. S.; Tanner, D. B.; Huang, W. S.; MacDiarmid, A. G., Polaron lattice in highly conducting polyaniline: Theoretical and optical studies. *Physical Review Letters* **1987,** *59* (13), 1464-1467.
12. Beverina, L.; Pagani, G. A.; Sassi, M., Multichromophoric electrochromic polymers: colour tuning of conjugated polymers through the side chain functionalization approach. *Chemical Communications* **2014,** *50* (41), 5413-5430.
13. Bubnova, O.; Khan, Z. U.; Wang, H.; Braun, S.; Evans, D. R.; Fabretto, M.; Hojati-Talemi, P.; Dagnelund, D.; Arlin, J.-B.; Geerts, Y. H.; Desbief, S.; Breiby, D. W.; Andreasen, J. W.; Lazzaroni, R.; Chen, W. M.; Zozoulenko, I.; Fahlman, M.; Murphy, P. J.; Berggren, M.; Crispin, X., Semi-metallic polymers. *Nat Mater* **2014,** *13* (2), 190-194.
14. Garnier, F.; Tourillon, G.; Gazard, M.; Dubois, J. C., Organic conducting polymers derived from substituted thiophenes as electrochromic material. *Journal of Electroanalytical Chemistry and Interfacial Electrochemistry* **1983,** *148* (2), 299-303.

15. Mortimer, R. J., Electrochromic materials. *Chemical Society Reviews* **1997,** *26* (3), 147-156.
16. Hyodo, K., Electrochromism of conducting polymers. *Electrochimica Acta* **1994,** *39* (2), 265-272.
17. Mitchell, G. R.; Davis, F. J.; Legge, C. H., The effect of dopant molecules on the molecular order of electrically-conducting films of polypyrrole. *Synthetic Metals* **1988,** *26* (3), 247-257.
18. de Oliveira, H. P.; Sydlik, S. A.; Swager, T. M., Supercapacitors from Free-Standing Polypyrrole/Graphene Nanocomposites. *The Journal of Physical Chemistry C* **2013,** *117* (20), 10270-10276.
19. Tao, J.; Liu, N.; Ma, W.; Ding, L.; Li, L.; Su, J.; Gao, Y., Solid-State High Performance Flexible Supercapacitors Based on Polypyrrole-MnO2-Carbon Fiber Hybrid Structure. *Sci. Rep.* **2013,** *3*.
20. Lee, J. A.; Shin, M. K.; Kim, S. H.; Cho, H. U.; Spinks, G. M.; Wallace, G. G.; Lima, M. D.; Lepró, X.; Kozlov, M. E.; Baughman, R. H.; Kim, S. J., Ultrafast charge and discharge biscrolled yarn supercapacitors for textiles and microdevices. *Nat Commun* **2013,** *4*.
21. Roncali, J., Conjugated poly(thiophenes): synthesis, functionalization, and applications. *Chemical Reviews* **1992,** *92* (4), 711-738.
22. Heywang, G.; Jonas, F., Poly(alkylenedioxythiophene)s—new, very stable conducting polymers. *Advanced Materials* **1992,** *4* (2), 116-118.
23. Akoudad, S.; Roncali, J., Electrochemical synthesis of poly(3,4-ethylenedioxythiophene) from a dimer precursor. *Synthetic Metals* **1998,** *93* (2), 111-114.
24. Kumar, A.; Reynolds, J. R., Soluble Alkyl-Substituted Poly(ethylenedioxythiophenes) as Electrochromic Materials. *Macromolecules* **1996,** *29* (23), 7629-7630.
25. Sankaran, B.; Reynolds, J. R., High-Contrast Electrochromic Polymers from Alkyl-Derivatized Poly(3,4-ethylenedioxythiophenes). *Macromolecules* **1997,** *30* (9), 2582-2588.
26. Kerszulis, J. A. Reading the Rainbow: Tailoring the Proerties of Electrochromic Polymers. Georgia Institute of Technology, 2014.
27. Dyer, A. L.; Thompson, E. J.; Reynolds, J. R., Completing the Color Palette with Spray-Processable Polymer Electrochromics. *ACS Applied Materials & Interfaces* **2011,** *3* (6), 1787-1795.
28. Amb, C. M.; Dyer, A. L.; Reynolds, J. R., Navigating the Color Palette of Solution-Processable Electrochromic Polymers. *Chemistry of Materials* **2010,** *23* (3), 397-415.
29. Kerszulis, J. A.; Amb, C. M.; Dyer, A. L.; Reynolds, J. R., Follow the Yellow Brick Road: Structural Optimization of Vibrant Yellow-to-Transmissive Electrochromic Conjugated Polymers. *Macromolecules* **2014,** *47* (16), 5462-5469.
30. Amb, C. M.; Kerszulis, J. A.; Thompson, E. J.; Dyer, A. L.; Reynolds, J. R., Propylenedioxythiophene (ProDOT)-phenylene copolymers allow a yellow-to-transmissive electrochrome. *Polymer Chemistry* **2011,** *2* (4), 812-814.
31. Dyer, A. L.; Craig, M. R.; Babiarz, J. E.; Kiyak, K.; Reynolds, J. R., Orange and Red to Transmissive Electrochromic Polymers Based on Electron-Rich Dioxythiophenes. *Macromolecules* **2010,** *43* (10), 4460-4467.

32. Reeves, B. D.; Grenier, C. R. G.; Argun, A. A.; Cirpan, A.; McCarley, T. D.; Reynolds, J. R., Spray Coatable Electrochromic Dioxythiophene Polymers with High Coloration Efficiencies. *Macromolecules* **2004,** *37* (20), 7559-7569.
33. Beaujuge, P. M.; Amb, C. M.; Reynolds, J. R., Spectral Engineering in π-Conjugated Polymers with Intramolecular Donor−Acceptor Interactions. *Accounts of Chemical Research* **2010,** *43* (11), 1396-1407.
34. Beaujuge, P. M.; Vasilyeva, S. V.; Liu, D. Y.; Ellinger, S.; McCarley, T. D.; Reynolds, J. R., Structure-Performance Correlations in Spray-Processable Green Dioxythiophene-Benzothiadiazole Donor–Acceptor Polymer Electrochromes. *Chemistry of Materials* **2012,** *24* (2), 255-268.
35. Beaujuge, P. M.; Ellinger, S.; Reynolds, J. R., Spray Processable Green to Highly Transmissive Electrochromics via Chemically Polymerizable Donor–Acceptor Heterocyclic Pentamers. *Advanced Materials* **2008,** *20* (14), 2772-2776.
36. Amb, C. M.; Beaujuge, P. M.; Reynolds, J. R., Spray-Processable Blue-to-Highly Transmissive Switching Polymer Electrochromes via the Donor–Acceptor Approach. *Advanced Materials* **2010,** *22* (6), 724-728.
37. Knott, E. P.; Craig, M. R.; Liu, D. Y.; Babiarz, J. E.; Dyer, A. L.; Reynolds, J. R., A minimally coloured dioxypyrrole polymer as a counter electrode material in polymeric electrochromic window devices. *Journal of Materials Chemistry* **2012,** *22* (11), 4953-4962.
38. Shi, P.; Amb, C. M.; Knott, E. P.; Thompson, E. J.; Liu, D. Y.; Mei, J.; Dyer, A. L.; Reynolds, J. R., Broadly Absorbing Black to Transmissive Switching Electrochromic Polymers. *Advanced Materials* **2010,** *22* (44), 4949-4953.
39. Beaujuge, P. M.; Ellinger, S.; Reynolds, J. R., The donor-acceptor approach allows a black-to-transmissive switching polymeric electrochrome. *Nat Mater* **2008,** *7* (10), 795-799.
40. Niklasson, G. A.; Granqvist, C. G., Electrochromics for smart windows: thin films of tungsten oxide and nickel oxide, and devices based on these. *Journal of Materials Chemistry* **2007,** *17* (2), 127-156.
41. Corr, D.; Fay, D.; Ryan, M.; Walder, L.; Möller, M.; Asaftei, S., P-118: High Resolution Electrochromic Displays for E-Readers. *SID Symposium Digest of Technical Papers* **2005,** *36* (1), 750-751.
42. Tonar, W. L.; Forgette, J. A.; Anderson, J. S.; Bechtel, J. H.; Carter, J. W.; Stam, J. S., Electrochromic rearview mirror incorporating a third surface metal reflector and a display/signal light. Google Patents: 2002.
43. Periyat, P.; Leyland, N.; McCormack, D. E.; Colreavy, J.; Corr, D.; Pillai, S. C., Rapid microwave synthesis of mesoporous TiO2 for electrochromic displays. *Journal of Materials Chemistry* **2010,** *20* (18), 3650-3655.
44. Bonhôte, P.; Gogniat, E.; Campus, F.; Walder, L.; Grätzel, M., Nanocrystalline electrochromic displays. *Displays* **1999,** *20* (3), 137-144.
45. Dyer, A. L., *Conjugated polymer electrochromic and light-emitting devices*. 2007.
46. Aubert, P.-H.; Argun, A. A.; Cirpan, A.; Tanner, D. B.; Reynolds, J. R., Microporous Patterned Electrodes for Color-Matched Electrochromic Polymer Displays. *Chemistry of Materials* **2004,** *16* (12), 2386-2393.
47. Argun, A. A.; Aubert, P.-H.; Thompson, B. C.; Schwendeman, I.; Gaupp, C. L.; Hwang, J.; Pinto, N. J.; Tanner, D. B.; MacDiarmid, A. G.; Reynolds, J. R., Multicolored

Electrochromism in Polymers: Structures and Devices. *Chemistry of Materials* **2004,** *16* (23), 4401-4412.
48. Schwendeman, I.; Hwang, J.; Welsh, D. M.; Tanner, D. B.; Reynolds, J. R., Combined visible and infrared electrochromism using dual polymer devices. *Advanced Materials* **2001,** *13* (9), 634-637.
49. BALOUKAS, B.; Martinu, L., Metameric security devices using an active material. Google Patents: 2013.
50. Kondo, Y.; Tanabe, H.; Kudo, H.; Nakano, K.; Otake, T., Electrochromic Type E-Paper Using Poly(1H-Thieno[3,4-d]Imidazol-2(3H)-One) Derivatives by a Novel Printing Fabrication Process. *Materials* **2011,** *4* (12), 2171.
51. Remmele, J.; Shen, D. E.; Mustonen, T.; Fruehauf, N., High Performance and Long-Term Stability in Ambiently Fabricated Segmented Solid-State Polymer Electrochromic Displays. *ACS Applied Materials & Interfaces* **2015,** *7* (22), 12001-12008.
52. Reynolds, J. R.; Zong, K.; Schwendeman, I.; Sonmez, G.; Schottland, P.; Argun, A. A.; Aubert, P. H., Electrochromic polymers and polymer electrochromic devices. Google Patents: 2004.
53. Yen, H.-J.; Chen, C.-J.; Liou, G.-S., Flexible Multi-Colored Electrochromic and Volatile Polymer Memory Devices Derived from Starburst Triarylamine-Based Electroactive Polyimide. *Advanced Functional Materials* **2013,** *23* (42), 5307-5316.
54. Gesheva, K.; Ivanova, T.; Hamelmann, F., Optical Coatings of CVD-transition Metal Oxides as Functional Layers in "SMART WINDOWS" and X-ray Mirrors. *Journal of Optoelectronics and Advanced Materials* **2005,** *7* (3), 1243-1252.
55. Byker, H. J., Single-compartment, self-erasing, solution-phase electrochromic devices, solutions for use therein, and uses thereof. Google Patents: 1990.
56. Baucke, F. In *Reflecting electrochromic devices-construction, operation, and application*, proceedings of the Symposium on Electrochromic Materials, edited by M. K. Carpenter and D. A. Corrigan, Proceedings, 1990; pp 90-2.
57. Nikolou, M.; Dyer, A. L.; Steckler, T. T.; Donoghue, E. P.; Wu, Z.; Heston, N. C.; Rinzler, A. G.; Tanner, D. B.; Reynolds, J. R., Dual n- and p-Type Dopable Electrochromic Devices Employing Transparent Carbon Nanotube Electrodes. *Chemistry of Materials* **2009,** *21* (22), 5539-5547.
58. Vasilyeva, S. V.; Beaujuge, P. M.; Wang, S.; Babiarz, J. E.; Ballarotto, V. W.; Reynolds, J. R., Material strategies for black-to-transmissive window-type polymer electrochromic devices. *ACS applied materials & interfaces* **2011,** *3* (4), 1022-1032.
59. Bulloch, R. H.; Kerszulis, J. A.; Dyer, A. L.; Reynolds, J. R., Mapping the Broad CMY Subtractive Primary Color Gamut Using a Dual-Active Electrochromic Device. *ACS Applied Materials & Interfaces* **2014,** *6* (9), 6623-6630.
60. Bulloch, R. H.; Kerszulis, J. A.; Dyer, A. L.; Reynolds, J. R., An Electrochromic Painter's Palette: Color Mixing via Solution Co-Processing. *ACS Applied Materials & Interfaces* **2015,** *7* (3), 1406-1412.
61. Svensson, J.; Granqvist, C., Electrochromic coatings for "smart windows". *Solar energy materials* **1985,** *12* (6), 391-402.
62. Runner, B., Ridley Scott. *Warner Bros* **1982**.
63. Rauh, R. D., Electrochromic windows: an overview. *Electrochimica Acta* **1999,** *44* (18), 3165-3176.

64. Lee, E. S.; DiBartolomeo, D., Application issues for large-area electrochromic windows in commercial buildings. *Solar Energy Materials and Solar Cells* **2002,** *71* (4), 465-491.
65. Azens, A.; Granqvist, C., Electrochromic smart windows: energy efficiency and device aspects. *Journal of Solid State Electrochemistry* **2003,** *7* (2), 64-68.
66. Zinzi, M., Office worker preferences of electrochromic windows: a pilot study. *Building and Environment* **2006,** *41* (9), 1262-1273.
67. Baetens, R.; Jelle, B. P.; Gustavsen, A., Properties, requirements and possibilities of smart windows for dynamic daylight and solar energy control in buildings: A state-of-the-art review. *Solar Energy Materials and Solar Cells* **2010,** *94* (2), 87-105.
68. Schick, G. A.; Sun, Z., Spectroscopic characterization of sulfonyl chloride immobilization on silica. *Langmuir* **1994,** *10* (9), 3105-3110.
69. Ragone, D. V. *Review of battery systems for electrically powered vehicles*; 0148-7191; SAE Technical Paper: 1968.
70. Winter, M.; Brodd, R. J., What are batteries, fuel cells, and supercapacitors? *Chemical reviews* **2004,** *104* (10), 4245-4270.
71. Jennings, A. A.; Hise, S.; Kiedrowski, B.; Krouse, C., Urban battery litter. *Journal of Environmental Engineering* **2009,** *135* (1), 46-57.
72. Miller, J. R.; Simon, P., Electrochemical capacitors for energy management. *Science Magazine* **2008,** *321* (5889), 651-652.
73. Shown, I.; Ganguly, A.; Chen, L. C.; Chen, K. H., Conducting polymer-based flexible supercapacitor. *Energy Science & Engineering* **2015,** *3* (1), 2-26.
74. Lee, J. A.; Shin, M. K.; Kim, S. H.; Cho, H. U.; Spinks, G. M.; Wallace, G. G.; Lima, M. D.; Lepró, X.; Kozlov, M. E.; Baughman, R. H., Ultrafast charge and discharge biscrolled yarn supercapacitors for textiles and microdevices. *Nature communications* **2013,** *4*.
75. Le, V. T.; Kim, H.; Ghosh, A.; Kim, J.; Chang, J.; Vu, Q. A.; Pham, D. T.; Lee, J.-H.; Kim, S.-W.; Lee, Y. H., Coaxial fiber supercapacitor using all-carbon material electrodes. *ACS nano* **2013,** *7* (7), 5940-5947.
76. Jost, K.; Perez, C. R.; McDonough, J. K.; Presser, V.; Heon, M.; Dion, G.; Gogotsi, Y., Carbon coated textiles for flexible energy storage. *Energy & Environmental Science* **2011,** *4* (12), 5060-5067.
77. Yang, Z.; Deng, J.; Chen, X.; Ren, J.; Peng, H., A Highly Stretchable, Fiber-Shaped Supercapacitor. *Angewandte Chemie International Edition* **2013,** *52* (50), 13453-13457.
78. Conway, B. E., *Electrochemical Supercapacitors: Scientific Fundamentals and Technological Applications*. Springer US: 1999.
79. Frackowiak, E.; Beguin, F., Carbon materials for the electrochemical storage of energy in capacitors. *Carbon* **2001,** *39* (6), 937-950.
80. Jiang, H.; Lee, P. S.; Li, C., 3D carbon based nanostructures for advanced supercapacitors. *Energy & Environmental Science* **2013,** *6* (1), 41-53.
81. Pandolfo, A.; Hollenkamp, A., Carbon properties and their role in supercapacitors. *Journal of power sources* **2006,** *157* (1), 11-27.
82. Kalaji, M.; Murphy, P.; Williams, G., The study of conducting polymers for use as redox supercapacitors. *Synthetic metals* **1999,** *102* (1), 1360-1361.

83. Liu, T.; Finn, L.; Yu, M.; Wang, H.; Zhai, T.; Lu, X.; Tong, Y.; Li, Y., Polyaniline and polypyrrole pseudocapacitor electrodes with excellent cycling stability. *Nano letters* **2014,** *14* (5), 2522-2527.
84. Prasad, K. R.; Koga, K.; Miura, N., Electrochemical deposition of nanostructured indium oxide: high-performance electrode material for redox supercapacitors. *Chemistry of materials* **2004,** *16* (10), 1845-1847.
85. Zhi, M.; Xiang, C.; Li, J.; Li, M.; Wu, N., Nanostructured carbon–metal oxide composite electrodes for supercapacitors: a review. *Nanoscale* **2013,** *5* (1), 72-88.
86. Mike, J. F.; Lutkenhaus, J. L., Recent advances in conjugated polymer energy storage. *Journal of Polymer Science Part B: Polymer Physics* **2013,** *51* (7), 468-480.
87. Ramya, R.; Sivasubramanian, R.; Sangaranarayanan, M., Conducting polymers-based electrochemical supercapacitors—progress and prospects. *Electrochimica Acta* **2013,** *101*, 109-129.
88. Snook, G. A.; Kao, P.; Best, A. S., Conducting-polymer-based supercapacitor devices and electrodes. *Journal of Power Sources* **2011,** *196* (1), 1-12.
89. Frackowiak, E.; Khomenko, V.; Jurewicz, K.; Lota, K.; Beguin, F., Supercapacitors based on conducting polymers/nanotubes composites. *Journal of Power Sources* **2006,** *153* (2), 413-418.
90. Lota, K.; Khomenko, V.; Frackowiak, E., Capacitance properties of poly (3, 4-ethylenedioxythiophene)/carbon nanotubes composites. *Journal of Physics and Chemistry of Solids* **2004,** *65* (2), 295-301.
91. Hughes, M.; Shaffer, M. S.; Renouf, A. C.; Singh, C.; Chen, G. Z.; Fray, D. J.; Windle, A. H., Electrochemical capacitance of nanocomposite films formed by coating aligned arrays of carbon nanotubes with polypyrrole. *Advanced Materials* **2002,** *14* (5), 382-385.
92. Zhou, Y.; Lachman, N.; Ghaffari, M.; Xu, H.; Bhattacharya, D.; Fattahi, P.; Abidian, M. R.; Wu, S.; Gleason, K. K.; Wardle, B. L., A high performance hybrid asymmetric supercapacitor via nano-scale morphology control of graphene, conducting polymer, and carbon nanotube electrodes. *Journal of Materials Chemistry A* **2014,** *2* (26), 9964-9969.
93. Nyström, G.; Mihranyan, A.; Razaq, A.; Lindström, T.; Nyholm, L.; Strømme, M., A nanocellulose polypyrrole composite based on microfibrillated cellulose from wood. *The Journal of Physical Chemistry B* **2010,** *114* (12), 4178-4182.
94. Nyström, G.; Razaq, A.; Strømme, M.; Nyholm, L.; Mihranyan, A., Ultrafast all-polymer paper-based batteries. *Nano letters* **2009,** *9* (10), 3635-3639.
95. Park, J. H.; Park, O. O., Hybrid electrochemical capacitors based on polyaniline and activated carbon electrodes. *Journal of Power Sources* **2002,** *111* (1), 185-190.
96. Song, H. K.; Palmore, G. T. R., Redox-Active Polypyrrole: Toward Polymer-Based Batteries. *Advanced Materials* **2006,** *18* (13), 1764-1768.
97. Wang, K.; Meng, Q.; Zhang, Y.; Wei, Z.; Miao, M., High-performance two-ply yarn supercapacitors based on carbon nanotubes and polyaniline nanowire arrays. *Advanced materials* **2013,** *25* (10), 1494-1498.
98. Zhou, H.; Han, G.; Xiao, Y.; Chang, Y.; Zhai, H.-J., Facile preparation of polypyrrole/graphene oxide nanocomposites with large areal capacitance using electrochemical codeposition for supercapacitors. *Journal of Power Sources* **2014,** *263*, 259-267.

99. Benson, J.; Kovalenko, I.; Boukhalfa, S.; Lashmore, D.; Sanghadasa, M.; Yushin, G., Multifunctional CNT-Polymer Composites for Ultra-Tough Structural Supercapacitors and Desalination Devices. *Advanced Materials* **2013,** *25* (45), 6625-6632.
100. Sharma, R. K.; Zhai, L., Multiwall carbon nanotube supported poly (3, 4-ethylenedioxythiophene)/manganese oxide nano-composite electrode for super-capacitors. *Electrochimica Acta* **2009,** *54* (27), 7148-7155.
101. Shi, P.; Amb, C. M.; Dyer, A. L.; Reynolds, J. R., Fast Switching Water Processable Electrochromic Polymers. *ACS Applied Materials & Interfaces* **2012,** *4* (12), 6512-6521.
102. Pavlishchuk, V. V.; Addison, A. W., Conversion constants for redox potentials measured versus different reference electrodes in acetonitrile solutions at 25°C. *Inorganica Chimica Acta* **2000,** *298* (1), 97-102.
103. Genz, O.; Lohrengel, M. M.; Schultze, J. W., Fast Charge-Discharge Kinetics in Intrinsically Conducting Polymers — Intercalation and Film Relaxation. In *New Promising Electrochemical Systems for Rechargeable Batteries*, Barsukov, V.; Beck, F., Eds. Springer Netherlands: 1996; Vol. 6, pp 321-331.
104. Odin, C.; Nechtschein, M., Slow relaxation in conducting polymers: the case of poly(3-methylthiophene). *Synthetic Metals* **1991,** *44* (2), 177-188.
105. Liu, D. Y.; Chilton, A. D.; Shi, P.; Craig, M. R.; Miles, S. D.; Dyer, A. L.; Ballarotto, V. W.; Reynolds, J. R., In Situ Spectroscopic Analysis of Sub-Second Switching Polymer Electrochromes. *Advanced Functional Materials* **2011,** *21* (23), 4535-4542.
106. Kuehni, R. G., The early development of the Munsell system. *Color Research & Application* **2002,** *27* (1), 20-27.
107. Cleland, T. M., *A practical description of the Munsell color system: with suggestions for its use*. Munsell Color Co.: Baltimore, 1937; p 21 p.
108. *CIE Technical Report: Colorimetry*; Commission Internationale De L'eclairage: 2004.
109. Ohta, N.; Robertson, A., *Colorimetry: Fundamentals and Applications*. John Wiley & Sons: 2006.
110. Macadam, D. L., Visual Sensitivities to Color Differences in Daylight. *J. Opt. Soc. Am.* **1942,** *32* (5), 247-273 UR - http://www.osapublishing.org/abstract.cfm?URI=josa-32-5-247.
111. Berns, R. S.; Billmeyer, F. W.; Saltzman, M., *Billmeyer and Saltzman's principles of color technology*. Wiley: 2000.
112. Mortimer, R. J.; Varley, T. S., Quantification of colour stimuli through the calculation of CIE chromaticity coordinates and luminance data for application to in situ colorimetry studies of electrochromic materials. *Displays* **2011,** *32* (1), 35-44.
113. Kim, Y.; Kim, H.; Graham, S.; Dyer, A.; Reynolds, J. R., Durable polyisobutylene edge sealants for organic electronics and electrochemical devices. *Solar Energy Materials and Solar Cells* **2012,** *100* (0), 120-125.
114. ASTM Standard G173-03(2012) "Standard Tables for Reference Solar Spectral Irradiances: Direct Normal and Hemispherical on 37° Tilted Surface", ASTM International. West Conshohocken, PA, 2012.

115. Faraji, S.; Ani, F. N., The development supercapacitor from activated carbon by electroless plating—A review. *Renewable and Sustainable Energy Reviews* **2015,** *42* (0), 823-834.
116. Wang, G.; Wang, H.; Lu, X.; Ling, Y.; Yu, M.; Zhai, T.; Tong, Y.; Li, Y., Solid-State Supercapacitor Based on Activated Carbon Cloths Exhibits Excellent Rate Capability. *Advanced Materials* **2014,** *26* (17), 2676-2682.
117. Portet, C.; Taberna, P. L.; Simon, P.; Flahaut, E.; Laberty-Robert, C., High power density electrodes for Carbon supercapacitor applications. *Electrochimica Acta* **2005,** *50* (20), 4174-4181.
118. Turano, S. P.; Ready, J., Chemical vapor deposition synthesis of self-aligned carbon nanotube arrays. *Journal of electronic materials* **2006,** *35* (2), 192-194.
119. Wang, Y.; Shi, Z.; Huang, Y.; Ma, Y.; Wang, C.; Chen, M.; Chen, Y., Supercapacitor devices based on graphene materials. *The Journal of Physical Chemistry C* **2009,** *113* (30), 13103-13107.
120. Evanoff, K.; Benson, J.; Schauer, M.; Kovalenko, I.; Lashmore, D.; Ready, W. J.; Yushin, G., Ultra Strong Silicon-Coated Carbon Nanotube Nonwoven Fabric as a Multifunctional Lithium-Ion Battery Anode. *ACS Nano* **2012,** *6* (11), 9837-9845.
121. Inoue, Y.; Suzuki, Y.; Minami, Y.; Muramatsu, J.; Shimamura, Y.; Suzuki, K.; Ghemes, A.; Okada, M.; Sakakibara, S.; Mimura, H., Anisotropic carbon nanotube papers fabricated from multiwalled carbon nanotube webs. *Carbon* **2011,** *49* (7), 2437-2443.
122. Conway, B. E., *Electrochemical supercapacitors: scientific fundamentals and technological applications*. Springer Science & Business Media: 2013.
123. Hong, S.-C.; Kim, S.; Jang, W.-J.; Han, T.-H.; Hong, J.-P.; Oh, J.-S.; Hwang, T.; Lee, Y.; Lee, J.-H.; Nam, J.-D., Supercapacitor characteristics of pressurized RuO2/carbon powder as binder-free electrodes. *RSC Advances* **2014,** *4* (89), 48276-48284.
124. Lang, X.; Hirata, A.; Fujita, T.; Chen, M., Nanoporous metal/oxide hybrid electrodes for electrochemical supercapacitors. *Nat Nano* **2011,** *6* (4), 232-236.
125. Wang, Q.; Wen, Z. H.; Li, J. H., A Hybrid Supercapacitor Fabricated with a Carbon Nanotube Cathode and a TiO2–B Nanowire Anode. *Advanced Functional Materials* **2006,** *16* (16), 2141-2146.
126. Balducci, A.; Henderson, W. A.; Mastragostino, M.; Passerini, S.; Simon, P.; Soavi, F., Cycling stability of a hybrid activated carbon//poly(3-methylthiophene) supercapacitor with N-butyl-N-methylpyrrolidinium bis(trifluoromethanesulfonyl)imide ionic liquid as electrolyte. *Electrochimica Acta* **2005,** *50* (11), 2233-2237.
127. Zhao, X.; Johnston, C.; Grant, P. S., A novel hybrid supercapacitor with a carbon nanotube cathode and an iron oxide/carbon nanotube composite anode. *Journal of Materials Chemistry* **2009,** *19* (46), 8755-8760.
128. Yuan, C.; Zhang, X.; Wu, Q.; Gao, B., Effect of temperature on the hybrid supercapacitor based on NiO and activated carbon with alkaline polymer gel electrolyte. *Solid State Ionics* **2006,** *177* (13–14), 1237-1242.
129. Liu, J.; Essner, J.; Li, J., Hybrid Supercapacitor Based on Coaxially Coated Manganese Oxide on Vertically Aligned Carbon Nanofiber Arrays. *Chemistry of Materials* **2010,** *22* (17), 5022-5030.
130. Zhang, F.; Zhang, T.; Yang, X.; Zhang, L.; Leng, K.; Huang, Y.; Chen, Y., A high-performance supercapacitor-battery hybrid energy storage device based on

graphene-enhanced electrode materials with ultrahigh energy density. *Energy & Environmental Science* **2013,** *6* (5), 1623-1632.
131. Liu, D. Y.; Reynolds, J. R., Dioxythiophene-Based Polymer Electrodes for Supercapacitor Modules. *ACS Applied Materials & Interfaces* **2010,** *2* (12), 3586-3593.
132. Österholm, A. M.; Shen, D. E.; Dyer, A. L.; Reynolds, J. R., Optimization of PEDOT films in ionic liquid supercapacitors: demonstration as a power source for polymer electrochromic devices. *ACS applied materials & interfaces* **2013,** *5* (24), 13432-13440.
133. Estrada, L. A.; Liu, D. Y.; Salazar, D. H.; Dyer, A. L.; Reynolds, J. R., Poly[Bis-EDOT-Isoindigo]: An Electroactive Polymer Applied to Electrochemical Supercapacitors. *Macromolecules* **2012,** *45* (20), 8211-8220.
134. Beaujuge, P. M.; Amb, C. M.; Reynolds, J. R., A Side-Chain Defunctionalization Approach Yields a Polymer Electrochrome Spray-Processable from Water. *Advanced Materials* **2010,** *22* (47), 5383-5387.
135. Zhou, Y.; Qin, Z.-Y.; Li, L.; Zhang, Y.; Wei, Y.-L.; Wang, L.-F.; Zhu, M.-F., Polyaniline/multi-walled carbon nanotube composites with core–shell structures as supercapacitor electrode materials. *Electrochimica Acta* **2010,** *55* (12), 3904-3908.
136. Dyer, A. L.; Bulloch, R. H.; Zhou, Y.; Kippelen, B.; Reynolds, J. R.; Zhang, F., A Vertically Integrated Solar-Powered Electrochromic Window for Energy Efficient Buildings. *Advanced Materials* **2014,** *26* (28), 4895-4900.
137. Schwendeman, I.; Hickman, R.; Sönmez, G.; Schottland, P.; Zong, K.; Welsh, D. M.; Reynolds, J. R., Enhanced Contrast Dual Polymer Electrochromic Devices. *Chemistry of Materials* **2002,** *14* (7), 3118-3122.
138. Unur, E.; Beaujuge, P. M.; Ellinger, S.; Jung, J.-H.; Reynolds, J. R., Black to Transmissive Switching in a Pseudo Three-Electrode Electrochromic Device. *Chemistry of Materials* **2009,** *21* (21), 5145-5153.
139. Hwang, J.; Tanner, D.; Schwendeman, I.; Reynolds, J., Optical properties of nondegenerate ground-state polymers: Three dioxythiophene-based conjugated polymers. *Physical Review B* **2003,** *67* (11), 115205.
140. Peres, M. R., *The Focal Encyclopedia of Photography*. Taylor & Francis: 2013.
141. Lübbe, E., *Farbe im Kopf: Farbsysteme in der Realität*. Hansen-Schmidt: 2008.
142. Munsell, A. H., A Pigment Color System and Notation. *The American Journal of Psychology* **1912,** *23* (2), 236-244.
143. Mortimer, R. J.; Graham, K. R.; Grenier, C. R. G.; Reynolds, J. R., Influence of the Film Thickness and Morphology on the Colorimetric Properties of Spray-Coated Electrochromic Disubstituted 3,4-Propylenedioxythiophene Polymers. *ACS Applied Materials & Interfaces* **2009,** *1* (10), 2269-2276.
144. Benson, D. K.; Branz, H. M., Design goals and challenges for a photovoltaic-powered electrochromic window covering. *Solar energy materials and solar cells* **1995,** *39* (2), 203-211.
145. Bechinger, C.; Ferrere, S.; Zaban, A.; Sprague, J.; Gregg, B. A., Photoelectrochromic windows and displays. *Nature* **1996,** *383* (6601), 608-610.
146. Ahn, K.-S.; Yoo, S. J.; Kang, M.-S.; Lee, J.-W.; Sung, Y.-E., Tandem dye-sensitized solar cell-powered electrochromic devices for the photovoltaic-powered smart window. *Journal of Power Sources* **2007,** *168* (2), 533-536.

147. Deb, S. K.; Lee, S.-H.; Tracy, C. E.; Pitts, J. R.; Gregg, B. A.; Branz, H. M., Stand-alone photovoltaic-powered electrochromic smart window. *Electrochimica Acta* **2001,** *46* (13), 2125-2130.
148. Jensen, J.; Dam, H. F.; Reynolds, J. R.; Dyer, A. L.; Krebs, F. C., Manufacture and demonstration of organic photovoltaic-powered electrochromic displays using roll coating methods and printable electrolytes. *Journal of Polymer Science Part B: Polymer Physics* **2012,** *50* (8), 536-545.
149. Adhikary, P.; Venkatesan, S.; Maharjan, P. P.; Galipeau, D.; Qiao, Q., Enhanced performance of PDPP3T/solar cells using high boiling solvent and UV-ozone treatment. *Electron Devices, IEEE Transactions on* **2013,** *60* (5), 1763-1768.
150. Bijleveld, J. C.; Zoombelt, A. P.; Mathijssen, S. G.; Wienk, M. M.; Turbiez, M.; de Leeuw, D. M.; Janssen, R. A., Poly (diketopyrrolopyrrole− terthiophene) for ambipolar logic and photovoltaics. *Journal of the American Chemical Society* **2009,** *131* (46), 16616-16617.
151. Zhou, Y.; Fuentes-Hernandez, C.; Shim, J.; Meyer, J.; Giordano, A. J.; Li, H.; Winget, P.; Papadopoulos, T.; Cheun, H.; Kim, J., A universal method to produce low–work function electrodes for organic electronics. *Science* **2012,** *336* (6079), 327-332.
152. Beaujuge, P. M.; Reynolds, J. R., Color Control in π-Conjugated Organic Polymers for Use in Electrochromic Devices. *Chemical Reviews* **2010,** *110* (1), 268-320.
153. Overheim, R. D.; Wagner, D. L., *Light and Color*. Wiley: 1982.
154. Monk, P. M. S.; Mortimer, R. J.; Rosseinsky, D. R., *Electrochromism and Electrochromic Devices*. Cambridge University Press: 2007.
155. Mahy, M.; Van Eycken, L.; Oosterlinck, A., Evaluation of Uniform Color Spaces Developed after the Adoption of CIELAB and CIELUV. *Color Research & Application* **1994,** *19* (2), 105-121.
156. Schanda, J., *Colorimetry: Understanding the CIE System*. Wiley: 2007.
157. Österholm, A. M.; Shen, D. E.; Kerszulis, J. A.; Bulloch, R. H.; Kuepfert, M.; Dyer, A. L.; Reynolds, J. R., Four Shades of Brown: Tuning of Electrochromic Polymer Blends Toward High-Contrast Eyewear. *ACS Applied Materials & Interfaces* **2015,** *7* (3), 1413-1421.
158. Kim, Y.; Kim, H.; Graham, S.; Dyer, A.; Reynolds, J. R., Durable polyisobutylene edge sealants for organic electronics and electrochemical devices. *Solar Energy Materials and Solar Cells* **2012,** *100*, 120-125.
159. Day, M.; Wiles, D., Photochemical degradation of poly (ethylene terephthalate). III. Determination of decomposition products and reaction mechanism. *Journal of Applied Polymer Science* **1972,** *16* (1), 203-215.
160. Gijsman, P.; Meijers, G.; Vitarelli, G., Comparison of the UV-degradation chemistry of polypropylene, polyethylene, polyamide 6 and polybutylene terephthalate. *Polymer Degradation and Stability* **1999,** *65* (3), 433-441.
161. Abdou, M. S.; Holdcroft, S., Mechanisms of photodegradation of poly (3-alkylthiophenes) in solution. *Macromolecules* **1993,** *26* (11), 2954-2962.
162. Holdcroft, S., A photochemical study of poly (3-hexylthiophene). *Macromolecules* **1991,** *24* (17), 4834-4838.
163. Jensen, J.; Madsen, M. V.; Krebs, F. C., Photochemical stability of electrochromic polymers and devices. *Journal of Materials Chemistry C* **2013,** *1* (32), 4826-4835.

164. Marciniak, S.; Crispin, X.; Uvdal, K.; Trzcinski, M.; Birgerson, J.; Groenendaal, L.; Louwet, F.; Salaneck, W. R., Light induced damage in poly (3, 4-ethylenedioxythiophene) and its derivatives studied by photoelectron spectroscopy. *Synthetic metals* **2004,** *141* (1), 67-73.
165. Kang, E.; Neoh, K.; Zhang, X.; Tan, K.; Liaw, D., Surface modification of electroactive polymer films by ozone treatment. *Surface and interface analysis* **1996,** *24* (1), 51-58.
166. Hu, R.; Shao, D.; Wang, X., Graphene oxide/polypyrrole composites for highly selective enrichment of U (VI) from aqueous solutions. *Polymer Chemistry* **2014,** *5* (21), 6207-6215.
167. Spanninga, S. A.; Martin, D. C.; Chen, Z., X-ray photoelectron spectroscopy study of counterion incorporation in poly (3, 4-ethylenedioxythiophene). *The Journal of Physical Chemistry C* **2009,** *113* (14), 5585-5592.
168. Manceau, M.; Gaume, J.; Rivaton, A.; Gardette, J.-L.; Monier, G.; Bideux, L., Further insights into the photodegradation of poly (3-hexylthiophene) by means of X-ray photoelectron spectroscopy. *Thin Solid Films* **2010,** *518* (23), 7113-7118.
169. Mahat, M. M.; Mawad, D.; Nelson, G. W.; Fearn, S.; Palgrave, R. G.; Payne, D. J.; Stevens, M. M., Elucidating the deprotonation of polyaniline films by X-ray photoelectron spectroscopy. *Journal of Materials Chemistry C* **2015,** *3* (27), 7180-7186.
170. Louette, P.; Bodino, F.; Pireaux, J.-J., Poly (pyrrole)(PPY) XPS Reference Core Level and Energy Loss Spectra. *Surface Science Spectra* **2005,** *12* (1), 84-89.

VITA

Rayford H. Bulloch

Rayford H. Bulloch was born in Melbourne, Florida. After attending public schools in Port St. John and Merritt Island, Florida, he began his undergraduate education at Florida State University in Tallahassee, Florida, where he received a B.S. in Chemistry in 2010, with several anomalous minors. Following the bright colors in research, he moved to Gainesville, Florida to pursue a doctoral degree at the University of Florida under the advisement of Dr. John Reynolds. While working under the direction of Dr. Reynolds, he was abruptly transplanted to Atlanta, Georgia and the Georgia Institute of Technology in the winter of 2012. He plans to graduate in the fall of 2015 with a doctoral degree from the Georgia Institute of Technology.